



COLLISIONAL BROADENING OF SPECTRAL LINES  
IN THE  $X \rightarrow b$  SYSTEM OF  $O_2$  AND THE FIRST  
VIBRATIONAL BAND OF  $NO$  BY THE NOBLE GASES

THESIS

John Joseph Cornicelli, Captain, USAF

AFIT/ENP/GAP/97D-01

**DISTRIBUTION STATEMENT A**

Approved for public release;  
Distribution Unlimited

DEPARTMENT OF THE AIR FORCE  
AIR UNIVERSITY  
**AIR FORCE INSTITUTE OF TECHNOLOGY**

DTIC QUALITY INSPECTED 3

Wright-Patterson Air Force Base, Ohio

19980120 123

AFIT/ENP/GAP/97D-01

COLLISIONAL BROADENING OF SPECTRAL LINES  
IN THE  $X \rightarrow b$  SYSTEM OF  $O_2$  AND THE FIRST  
VIBRATIONAL BAND OF NO BY THE NOBLE GASES

THESIS

John Joseph Cornicelli, Captain, USAF

AFIT/ENP/GAP/97D-01

DTIC QUALITY INSPECTED 3

AFIT/ENP/GAP/97D-01

The views expressed in this thesis are those of the author and do not reflect the official policy or position of the Department of Defense or the U. S. Government.

AFIT/GAP/ENP/97D-01

COLLISIONAL BROADENING OF SPECTRAL LINES IN THE  $X \rightarrow b$  SYSTEM OF  
 $O_2$  AND THE FIRST VIBRATIONAL BAND OF NO BY THE NOBLE GASES

THESIS

Presented to the Faculty of the School of Engineering

of the Air Force Institute of Technology

Air University

In Partial Fulfillment of the

Requirements for the Degree of

Master of Science in Applied Physics

John Joseph Cornicelli, B.S.

Captain, United States Air Force

December 1997

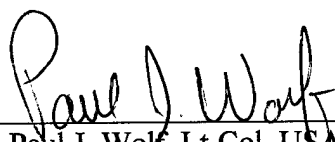
Approved for public release; distribution unlimited

COLLISIONAL BROADENING OF SPECTRAL LINES IN THE  $X \rightarrow b$  SYSTEM OF  
 $O_2$  AND THE FIRST VIBRATIONAL BAND OF NO BY THE NOBLE GASES

John Joseph Cornicelli, B.S.

Captain, United States Air Force

Approved:



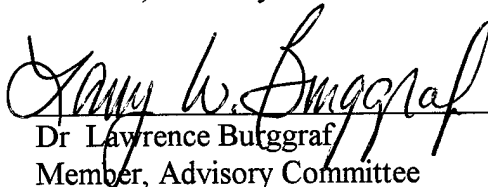
Paul J. Wolf, Lt Col, USAF  
Chairman, Advisory Committee

24 Nov-97  
Date



Glen A. Perram, Lt Col, USAF  
Member, Advisory Committee

24 Nov 97  
Date



Dr. Lawrence Buttgraf  
Member, Advisory Committee

24 Nov 97  
Date

### **Acknowledgments**

I would like to express my sincere appreciation to Lt Col Paul Wolf, my thesis advisor for all his patience and expertise as well as his willingness to do wrench turning with us. I would also like to thank Dr Lawrence Burggraf for all of his help in matters theoretical as well as patience in explaining quantum mechanics to me and Lt Col Glen Perram for his assistance, be it in experimental or theoretical spectroscopic matters. I would also like to thank the laboratory technician crew, Jim Reynolds, Belinda Johnson and Greg Smith for their patience and assistance. I would especially like to thank my laboratory partner Rob Pope for all of his help with things experimental, theoretical and for letting me share space with him and break his equipment. He took time out from his own studies to help me out. I would also like to express my appreciation to Tom Niday for his assistance in data analysis. Without his help, we would have a lot of data in a pile and no results (or thesis). Without all of these folks' help, we would not have even gotten started.

I would definitely not even have gotten this far without the loving support given me by my wife Nathalie, my daughter Marianne and our families. Nathalie, instead of the laboratory, now has possession of her husband, and Marianne has her daddy back.

## Table of Contents

Acknowledgments . . . . .	iii
List of Figures . . . . .	vi
List of Tables . . . . .	ix
Abstract . . . . .	x
I. Introduction . . . . .	1
Purpose . . . . .	1
Problem . . . . .	3
Theory and Background . . . . .	4
Line Broadening . . . . .	4
Spectroscopy . . . . .	9
Historical Background . . . . .	23
II. Experimental . . . . .	29
Apparatus . . . . .	29
Data Analysis . . . . .	44
III. Results and Discussion . . . . .	48
O <sub>2</sub> Study . . . . .	48
Spectrum Production . . . . .	48
Curve Fitting Using Peak Fit . . . . .	52
$\gamma_0$ Determination . . . . .	57
$\gamma_0$ vs. J'' Pattern Study . . . . .	57
NO Study . . . . .	60
Spectrum Production . . . . .	60
Curve Fitting Using Peak Fit . . . . .	60
$\gamma_0$ Determination . . . . .	61
$\gamma_0$ vs. J'' Pattern Study . . . . .	73
IV. Conclusion and Recommendation . . . . .	75
O <sub>2</sub> Study . . . . .	75
NO Study . . . . .	78

Appendix A: Fourier Transform Spectroscopy Theory	.	.	.	87
Appendix B: Results Graphs	.	.	.	92
Bibliography	.	.	.	116
Vita	.	.	.	119

## List of Figures

<u>Figure</u>	<u>Page</u>
1-1 Comparison of Lorentzian and Gaussian line profiles . . . . .	7
1-2 Normalized Voigt profiles . . . . .	8
1-3 O <sub>2</sub> energy diagram . . . . .	12
1-4 Hund's case (b) coupling . . . . .	13
1-5 Spectrum of X to b $v''=0 \rightarrow v'=0$ transition in O <sub>2</sub> . . . . .	14
1-6 O <sub>2</sub> X $\rightarrow$ b electronic transition setup using election rules . . . . .	15
1-7 NO energy level diagram . . . . .	18
1-8 Hund's case (a) coupling . . . . .	19
1-9 Spectral line comparison for the states of NO . . . . .	20
1-10 Spectrum of $v''=1 \rightarrow v'=0$ transition in NO . . . . .	21
1-11 O <sub>2</sub> Self Broadening by research group . . . . .	26
2-1 Spectrometer diagram . . . . .	29
2-2 Boltzmann distribution of O <sub>2</sub> rotational populations . . . . .	36
2-3 Boltzmann distribution of O <sub>2</sub> rotational cross sections . . . . .	37
2-4 Pressures of e-fold absorptions of O <sub>2</sub> spectral lines . . . . .	38
2-5 O <sub>2</sub> multipass cell and gas system. . . . .	39
2-6 Boltzmann distribution of NO rotational populations . . . . .	40
2-7 Boltzmann distribution of NO rotational cross sections . . . . .	41
2-8 Pressures of e-fold absorptions of NO spectral lines . . . . .	42
2-9 No cell and gas system . . . . .	43

3-1	Unresolvable O <sub>2</sub> peak and fit attempt.	. . . . .	49
3-2	Raw O <sub>2</sub> spectrum . . . . .	. . . . .	50
3-3	O <sub>2</sub> study filter background spectra . . . . .	. . . . .	51
3-4	Example of a fitted O <sub>2</sub> peak . . . . .	. . . . .	53
3-5	Residuals for Figure 3-4 . . . . .	. . . . .	54
3-6	Misalignment feature in spectra . . . . .	. . . . .	56
3-7	Example of $\gamma_0$ determination plot for O <sub>2</sub> . . . . .	. . . . .	58
3-8	Unresolvable NO lines . . . . .	. . . . .	62
3-9	NO Q-Branch . . . . .	. . . . .	63
3-10	Raw NO spectrum . . . . .	. . . . .	64
3-11	Curve fit of unresolved 3/2 state doublet line(s) of NO . . . . .	. . . . .	65
3-12	Residuals for Figure 3-11 . . . . .	. . . . .	66
3-13	Curve fit of resolved 1/2 state doublet lines of NO . . . . .	. . . . .	68
3-14	Residuals for Figure 3-13 . . . . .	. . . . .	69
3-15	Example of $\gamma_0$ determination plot for NO . . . . .	. . . . .	71
4-1	NO broadened by CO spectrum, one spectrum. . . . .	. . . . .	80
4-2	NO broadened by CO spectrum, 3 coadded spectra . . . . .	. . . . .	81
4-3	$\sigma$ vs. J' O <sub>2</sub> broadening . . . . .	. . . . .	82
4-4	$\sigma$ vs. polarizability, O <sub>2</sub> broadening . . . . .	. . . . .	83
4-5	$\sigma$ vs. reduced mass, O <sub>2</sub> broadening . . . . .	. . . . .	84
4-6	Comparison of single spectrum and 3 coadded spectra, R-branch . . . . .	. . . . .	85
4-7	Comparison of single spectrum and 3 coadded spectra, Q-branch . . . . .	. . . . .	86

A-1: Spectrum production process using individual monochromatic sources	88
A-2: Spectrum production process using three monochromatic sources at once	89
A-3: Interferograms and spectra produced using infrared continuum source	91
Results graphs listed in Appendix B . . . . .	92

## List of Tables

<u>Table</u>	<u>Page</u>
1-1    Selection rules for Hund's case (b) coupling . . . .	13
1-2    Line positions for $X \rightarrow b \ v''=0 \rightarrow v'=0$ transition in $O_2$ . .	14
1-3    Selection rules for Hund's case (a) coupling . . . .	19
1-4    Line positions for first vibrational transition of NO . . .	22
3-1    Numeric data for curve fit of $O_2$ line . . . . .	55
3-2    Numeric data accompanying $\gamma_0$ determination plot for $O_2$ . .	59
3-3    Numeric data for curve fit of NO 3/2 state line . . . .	67
3-4    Numeric data for curve fit of NO 1/2 state line . . . .	70
3-5    Numeric data accompanying $\gamma_0$ determination plot for NO . .	72

### **Abstract**

Collisional broadening of the rotational spectral lines of the  $X \rightarrow b$  system of  $O_2$  and the first vibrational band of NO by the noble gases is examined by Fourier transform spectroscopy. Peaks of the individual rotational lines are modeled with a Voigt function, from which Lorentzian half widths are extracted. Lorentzian widths are plotted vs. pressure of foreign gas, from which the pressure broadening coefficients and pressure broadening cross sections are calculated. The pressure broadening coefficients are compared to theoretical values determined by past research for  $O_2$ . NO coefficients are compared to similar research using  $N_2$  as collision partner.  $O_2$  broadening coefficients/cross sections were found to increase with decreasing rotational quantum number. Also, a linear dependence is found between cross section and both polarizability of the collision partner and reduced mass of the collision pair.

# **Collisional Broadening of Spectral Lines in the $X \rightarrow b$ System of $O_2$ and the First Vibrational Band of NO by the noble gases.**

## **I. Introduction**

### **Purpose**

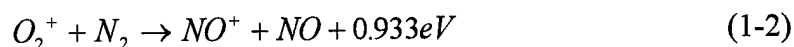
Absorption spectral line broadening has been discussed in literature for quite a while. We study radiative heat balance of planetary atmospheres, as well as remotely measure the temperature, pressure and density of atmospheric constituents. We also need to measure the working cavity temperature of military lasers to optimize output and efficiency. The Chemical Oxygen Ion Laser (COIL), under development for the Airborne Laser Antiballistic Missile Defense System, is one example where optical diagnoses are necessary.

The  $O_2$  transition we are studying (often called the A-band), lies in the atmospheric transmission region of the solar spectrum. Additionally, oxygen is a relatively poor absorber. This makes it ideal for remote sensing of atmospheric conditions (Ritter, 1987). To do so, we need to accurately measure spectral line strengths, widths and changes with temperature and pressure. We can measure the broadening of the spectral lines and relate it to the temperature using the Doppler width of the line (Rees, 1989):

$$\Delta\nu_D = \nu_0 \sqrt{\frac{8k_B T \ln 2}{mc^2}} \quad (1-1)$$

where  $\Delta\nu_D$  is the Doppler line width,  $\nu_0$  is the line center frequency, and  $T$  is the environmental kinetic temperature. We will discuss more about line broadening in Chapter 1.3.

Knowledge of NO chemistry in the upper atmosphere is limited. NO is a minor, albeit important, constituent of the upper atmosphere and is important in reactions concerning stratospheric ozone. NO reactions adjust the concentration of this ozone and infrared absorption is used for remote sensing of NO concentrations (Ballard, 1988). The chemiluminescent reaction (Rees, 1989):



produces NO ions as well as neutral NO in vibrationally excited states (Billingsley, 1976). This reaction produces infrared radiation observable from the ground, and can be converted to absolute concentration of NO if we understand the emission rates and know the Einstein coefficients. To study emission rates, we must understand the spectral properties of NO, which requires knowledge of spectral line center positions, line strengths and line broadening methods (Ballard, 1988), and line shapes (Pine, 1985). To understand the line shapes, we must understand how the lines broaden.

For remote sensing of temperature in lasers, as well as for measuring flow fields (Vyrodov, 1995), NO has been considered as a "seed" gas due to its inherent stability (DiRosa, 1994). A seed gas is one that we add to our working medium, measure its spectral properties, and relate them to the environmental conditions. We can measure the broadening of the NO lines and relate it to the temperature using the Doppler width of the line (Rees, 1989).

## **Problem**

Our goal in this study is to experimentally determine the pressure broadening coefficients (PBCs) for molecular oxygen ( $O_2$ ) and nitric oxide (NO) using Fourier transform spectroscopy, both using the individual noble gases as collision partners. We then intend to plot the pressure broadening coefficients and pressure broadening cross sections as a function of rotational quantum number ( $J''$ ) and observe the pattern. The pressure broadening coefficient is expected to increase with decreasing  $J''$  (Ritter, 1987). We will also compare the pattern in the PBC vs.  $J''$  plots to other researchers' data in the case of  $O_2$ . There will be no comparison for NO since there has been no other research in this area, although we still expect the same type of pattern as with  $O_2$  (Ritter, 1989). We will also compare the effects of the different collision partners and attempt to explain them.

## Theory and Background

### Line Broadening

We often imagine spectral lines to be perfect delta functions, that is, a certain energy transition emitting (or absorbing) *one* frequency of radiation. However, spectral lines exhibit natural broadening, Doppler broadening and collisional broadening. In this study, we are concerned with collisional broadening, but we must understand natural broadening and take Doppler broadening into account in our collisional broadening calculations.

Spectral lines would be delta functions if the emitted wave were an infinite wave train. In fact, the wave pulse has a start and an end. The Heisenberg uncertainty principle states that we cannot simultaneously know the energy levels' exact values and the start and end time of a transition:

$$\Delta E \Delta t = h \quad (1-3)$$

If we relate this to frequency instead of energy,

$$\Delta \nu = \frac{1}{2\pi t} \quad (1-4)$$

we can determine the natural line width by converting frequency to wave number. Here,  $t$  is the state lifetime (Rees, 1989). The spectral *intensity* distribution of the natural line width is Lorentzian (Rees, 1989):

$$\phi_N(\nu) = \frac{\frac{\Delta \nu_N}{2\pi}}{(\nu - \nu_0)^2 + \left(\frac{\Delta \nu_N}{2}\right)^2} \quad (1-5)$$

where  $\nu_0$  is the line center frequency, and  $\Delta\nu_0$  is the line width at half maximum as shown in Figure 1-1.

Doppler broadening is due to the fact that the molecules in a gas move randomly in direction and exhibit a Boltzmann distribution of velocities. Molecules moving in different directions will absorb slightly different frequencies off line center. At our operating temperatures (and in the thermosphere, where temperatures range from 300K down to 180K) Doppler broadening becomes significant (Rees, 1989). The distribution of frequencies is Gaussian centered on the line center frequency. The full width at half maximum (FWHM) is related to the temperature by this relation: (Rees, 1989)

$$\Delta\nu_D = \nu_0 \sqrt{\frac{8k_B T \ln 2}{mc^2}} \quad (1-6)$$

where  $k$  is Boltzmann's constant,  $m$  is the mass of the absorbing or emitting species, and  $\nu_0$  is the line center in wave number (Rees, 1989). Doppler broadening exhibits a Gaussian distribution of spectral intensity, where  $M$  is the mass of  $O_2$ ,  $\nu$  is the energy in wave number units and  $\nu_D$  is the doppler width in wave number units. (Rees, 1989):

$$\phi_D(\nu) = \frac{c}{\nu_0} \sqrt{\frac{M}{2\pi k_B T}} \exp \left[ \frac{-(\nu - \nu_0)^2}{\frac{2k_B T \nu_0^2}{Mc}} \right] \quad (1-7)$$

Collisional (pressure) broadening happens in high density situations where the time between collisions is less than the time between the start and end of an emission due to a transition between energy levels. The collision interrupts the emission event. This

introduces a broadening of the line around the line center in a Lorentzian profile, with the same form as with natural broadening (Rees, 1989):

$$\phi_P(\nu) = \frac{\Delta\nu_P / 2\pi}{(\nu - \nu_0)^2 + (\Delta\nu_P / 2)^2} \quad (1-8)$$

where  $\Delta\nu_P$  is the line width due to collisions. In collisional broadening, the line width is proportional to the mean collision frequency (Rees, 1989):

$$\Delta\nu_P = f_P / 2\pi \quad (1-9)$$

Now, when we measure the width of a spectral line, we must take into account all of these broadening methods when we determine the line shape. The two Lorentzian functions add to give us another Lorentzian. Then when we superimpose the resulting Lorentzian and the Gaussian distributions, we are in effect broadening each element of the Lorentzian curve by a Gaussian function. A convolution of the two gives us our Voigt profile (Jansson, 1984):

$$\phi_V = \frac{1}{\Delta\nu_D} \sqrt{\frac{\ln 2}{\pi}} \frac{\mu}{\pi} \int_{-\infty}^{\infty} \frac{\exp(-t^2)}{\mu^2 + (\zeta - t)^2} dt \quad (1-10a)$$

$$t = \frac{x - \nu_0}{\sqrt{2\Delta\nu_P}} \quad (1-10b)$$

$$\mu = \sqrt{\ln 2} \frac{\Delta\nu_P}{\Delta\nu_D} \quad (1-10c)$$

$$\zeta = \sqrt{\ln 2} \frac{\nu - \nu_0}{\Delta\nu_D} \quad (1-10d)$$

As an example, Figure 1-2 depicts Voigt curves with different ratios of Lorentzian and Gaussian half widths using (Rees, 1989):

$$ratio = \sqrt{\ln 2} * \frac{\Delta \nu_L}{\Delta \nu_D} \quad (1-11)$$

where  $\Delta \nu_L$  is the addition of natural and collisional broadening half widths and  $\Delta \nu_D$  is the Doppler half width. In Chapter 2.2 we will cover the use of this equation in data analysis.

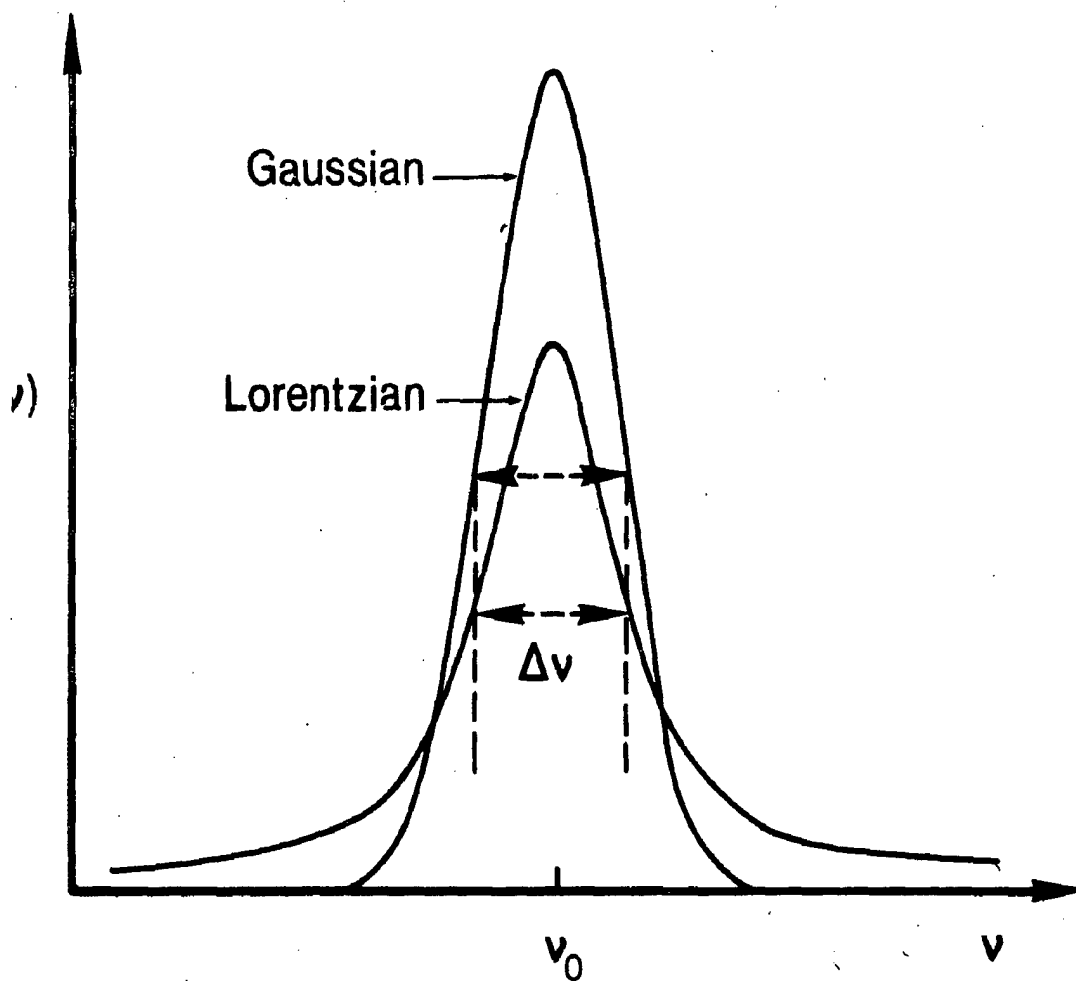


**Figure 1-1: Comparison of Lorentzian and Gaussian line profiles. The two curves have the same equivalent width, the same area, and the same half width value (Rees, 1989).**

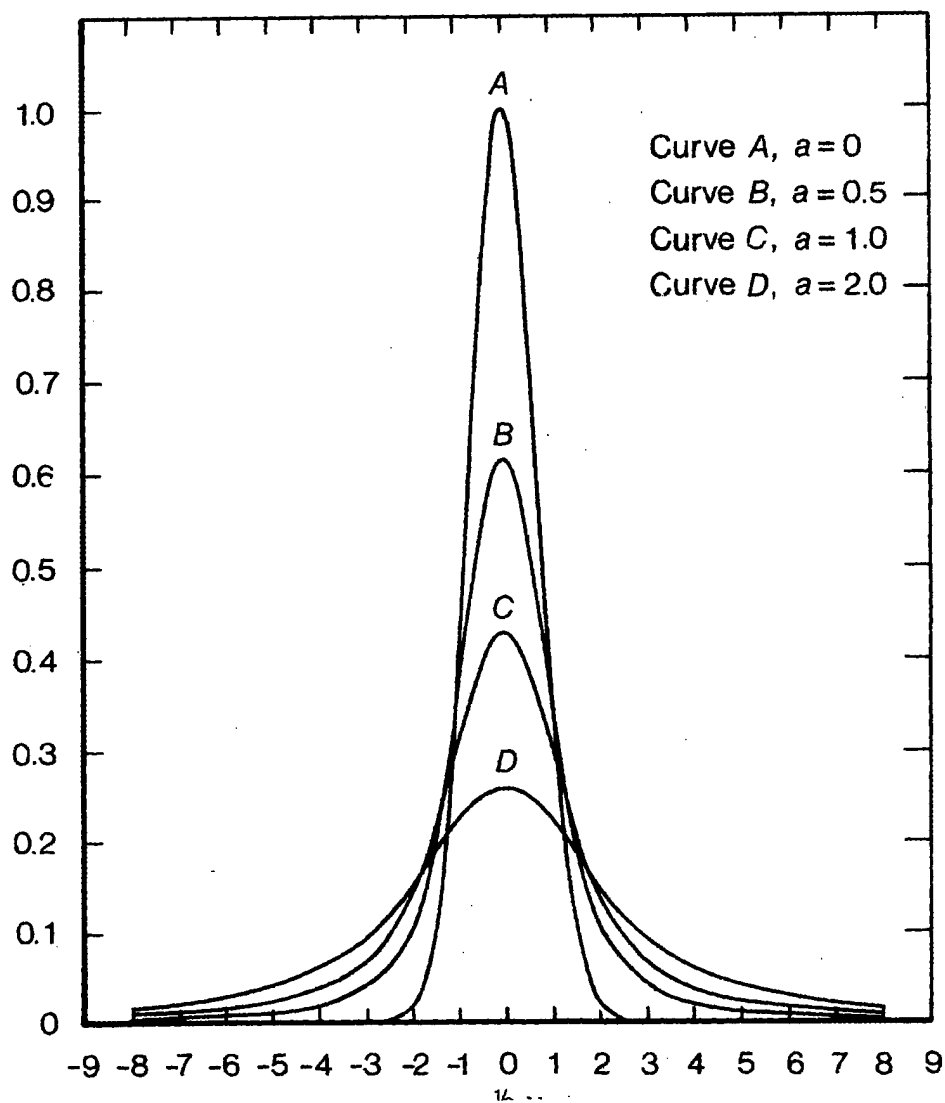


**Figure 1-2: Normalized Voigt profiles for a range of ratios of the Lorentzian to Doppler half widths. Here, the x-axis is frequency (wave number) and the y-axis is amplitude. (Rees, 1989).**

## Spectroscopy

The  $O_2$  absorption transition we are studying is the  $X \ ^3\Sigma_g^- \rightarrow b \ ^1\Sigma_g^+$  electronic transition from the ground state to the second electronically excited state (see Figure 1-3) and is centered at  $13123 \text{ cm}^{-1}$  or  $762 \text{ nm}$  (Rees, 1989). One notices from a rough measurement of the potentials' energy differences that the  $X \rightarrow b$  transition requires  $\sim 1.6 \text{ eV}$  which upon conversion gives us  $\sim 13,000 \text{ cm}^{-1}$  which is about where our transition lies (Rees, 1989).

The  $b$  state has a radiative lifetime of 7-12 s. (Kearns, 1971). This transition is the  $(v''=0) \rightarrow (v'=0)$  vibrational change. We see this transition in the upper atmosphere, and it is often called the oxygen A-band. (Kearns, 1971). Molecular oxygen has no electric dipole moment and a very small quadrupole moment, but the transition is not a quadrupole-quadrupole interaction (de Angelis et. al., 1996). The  $X \rightarrow b$  is a magnetic-dipole transition (de Angelis et. al., 1996).

The ground state of  $O_2$  has a total spin,  $S$ , of 1. This gives us an electron spin angular momentum ( $\Sigma$ ) of 1, 0, -1, which describes a spin multiplicity  $(2\Sigma + 1)$  of 3. The molecule has electron orbital angular momentum component parallel to the internuclear axis ( $\Lambda$ ) of 0 giving us the " $\Sigma$ " state. (Herzberg, 1950). Repeating this procedure for the  $b$  state (no unpaired electrons), we get  $S = 0$ ,  $\Sigma = 0$ , spin multiplicity of 1, and  $\Lambda = 0$ . Like the ground state, the  $b$  state is a  $\Sigma$  state.

Since  $O_2$  is a homonuclear diatomic molecule, any plane that cuts through the internuclear axis is a plane of symmetry (Herzberg, 1966). The eigenfunctions of the  $S$  states depend on the relative azimuths of the electrons. (Herzberg, 1966). The ground

state has two unpaired electrons, and since  $\Sigma$  states are non-degenerate, the electronic eigenfunction changes sign on reflection across these planes, giving us the  $\Sigma^-$  designation. Since the b state has no unpaired electrons, the eigenfunction will not change sign on reflection, giving us the  $\Sigma^+$  designation. The fact that  $O_2$  is homonuclear tells us that the molecule has a center of symmetry along the internuclear axis, and hence, even symmetry. This gives us the  $\Sigma_g$  designation on both states, which, in German, is "gerade" or even.

Since  $\Lambda = 0$  and  $S \neq 0$ , the spin vector  $S$  is not coupled to the internuclear axis (Herzberg, 1966). Therefore, since  $O_2$  is a homonuclear molecule, it follows Hund's case (b) coupling (See Table 1-1 and Figure 1-4). Now, we calculate  $K$ , the total angular momentum including molecule rotation but excluding spin (Herzberg, 1966), using:

$$K = \Lambda, \Lambda + 1, \Lambda + 2, \Lambda + 3, \dots \quad (1-12)$$

Here,  $\Lambda = 0$  which, according to Figure 1-4, makes  $K$  perpendicular to the internuclear axis and identical to  $N$  (Herzberg, 1966).  $K$  becomes  $0, 1, 2, 3, \dots$ . Now we can calculate  $J$ , the total angular momentum including spin by adding  $K$  and  $S$  vectorially like this (Herzberg, 1966):

$$J = (K + S), (K + S - 1), (K + S - 2), \dots, |K - S| \quad (1-13)$$

which gives us integer values  $0, 1, 2, 3, 4, \dots$

For an absorption, the lower (start) level is  $J''$  and the higher (end) level is  $J'$ . So, for example, the line at  $13098 \text{ cm}^{-1}$ , which we label as  $J'' = 7$  is the rotational energy change from quantum number 7 in the X state to quantum number 6 in the b state. Since  $\Delta J = -1$ , this is a P-branch line. The line at  $13140 \text{ cm}^{-1}$  is an R-branch line with quantum number change from 7 to 8 ( $\Delta J = +1$  for the R-branch). This is due to the Hund's case (b)

selection rules that govern the transition. Using the rules  $\Delta J = -1$  for the P-branch and  $\Delta J = +1$  for the R-branch, we can predict that the first P-branch line will be the  $J'' = 2 \rightarrow J' = 1$  line and the first R-Branch line will be the  $J'' = 1 \rightarrow J' = 2$  line. Note that the quantum number  $0 \rightarrow 0$  rotational transition is not in the spectrum. There will be no Q-Branch since  $\Delta J = 0$  is not allowed. (Burch et. al., 1969 and Hertzberg, 1966)

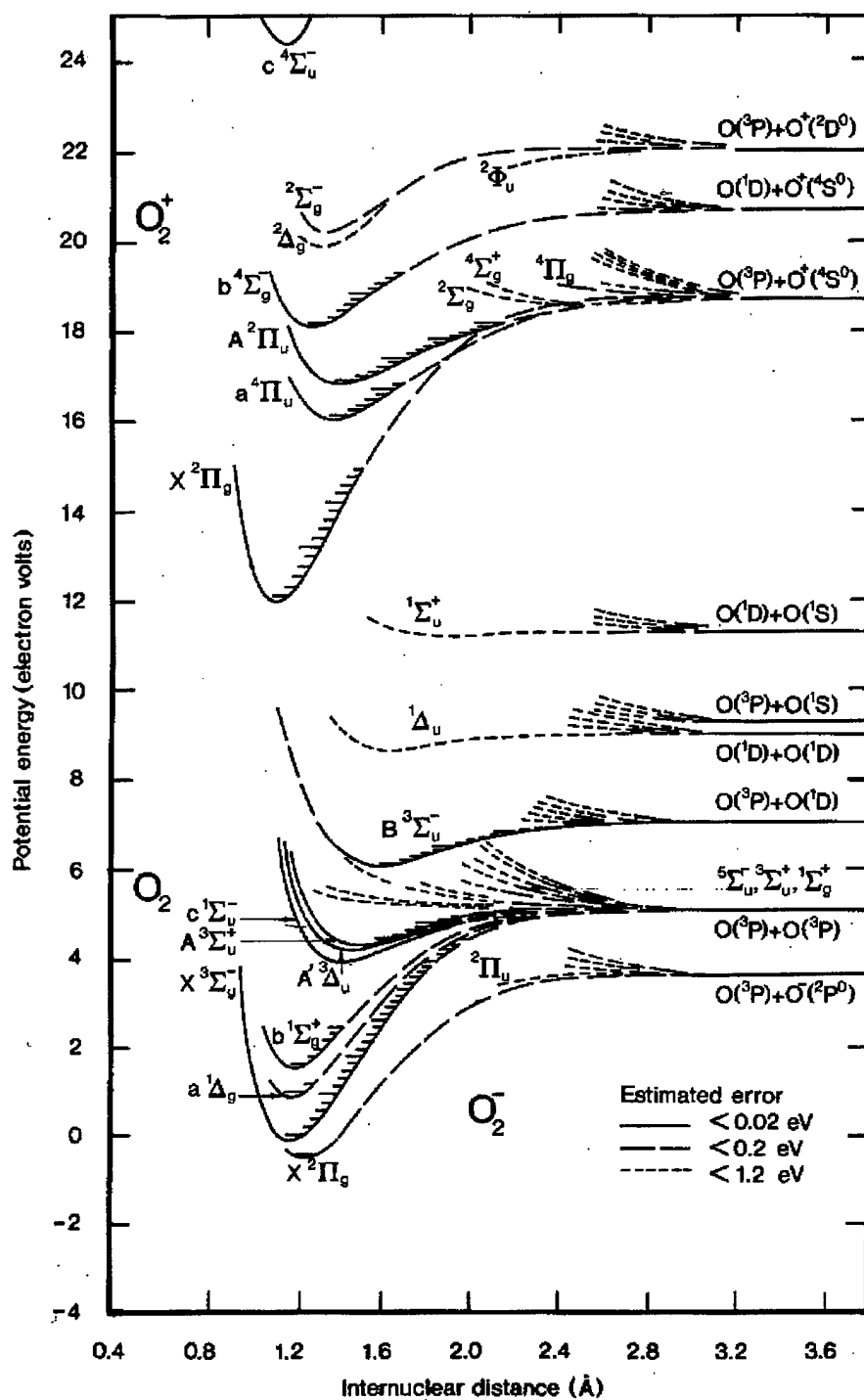
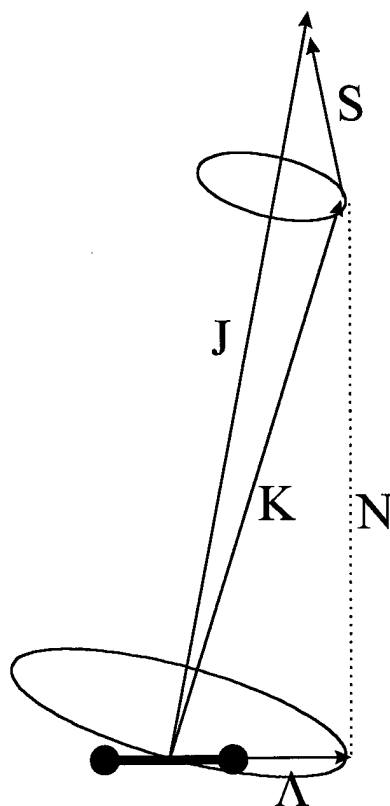


Figure 1-3:  $O_2$  energy diagram (Rees, 1989).

**Table 1-1: Magnetic dipole selection rules for a homonuclear diatomic molecule obeying Hund's case (b) coupling. (Hertzberg, 1966)**

Total angular momentum.	$\Delta J = \pm 1$ but $\Delta J = 0$ forbidden
Total angular momentum excluding spin	$\Delta K = 0, \pm 1$ but $\Delta K = 0$ forbidden for $\Sigma$ to $\Sigma$ transitions
Electronic orbital angular momentum	$\Delta \Lambda = 0, \pm 1$ but $\Delta \Lambda = 0$ only for singlet/triplet transitions
Electronic wave function symmetry	$(+ \rightarrow +), (- \rightarrow -),$ no $(+ \rightarrow -),$ no $(- \rightarrow +)$
Like nuclear charge symmetry	$(g \rightarrow g), (u \rightarrow u),$ no $(g \rightarrow u),$ no $(u \rightarrow g)$
Identical nuclei symmetry	$(s \rightarrow s), (a \rightarrow a),$ no $(s \rightarrow a),$ no $(a \rightarrow s)$



**Figure 1-4: Hund's case (b) coupling**

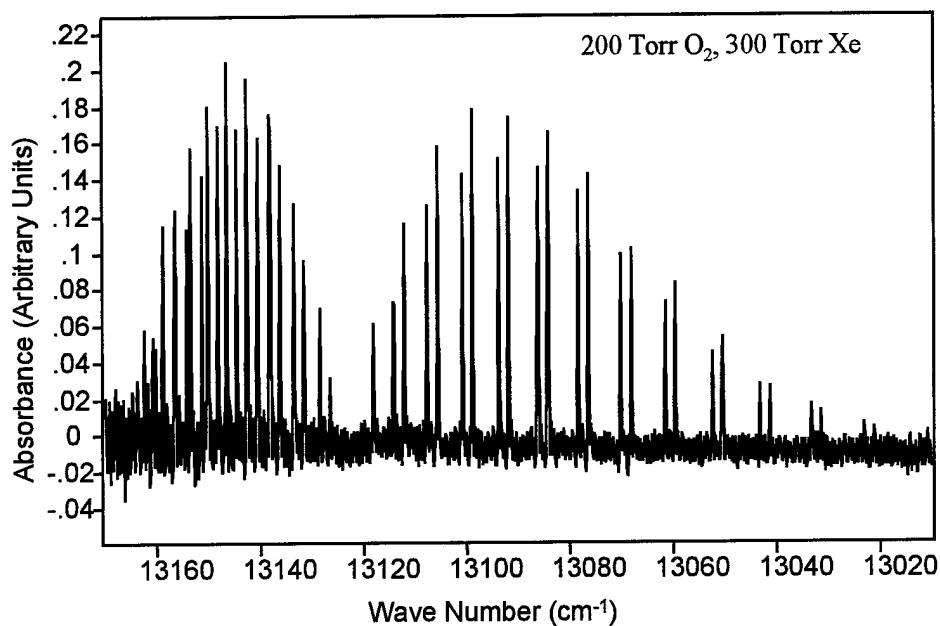
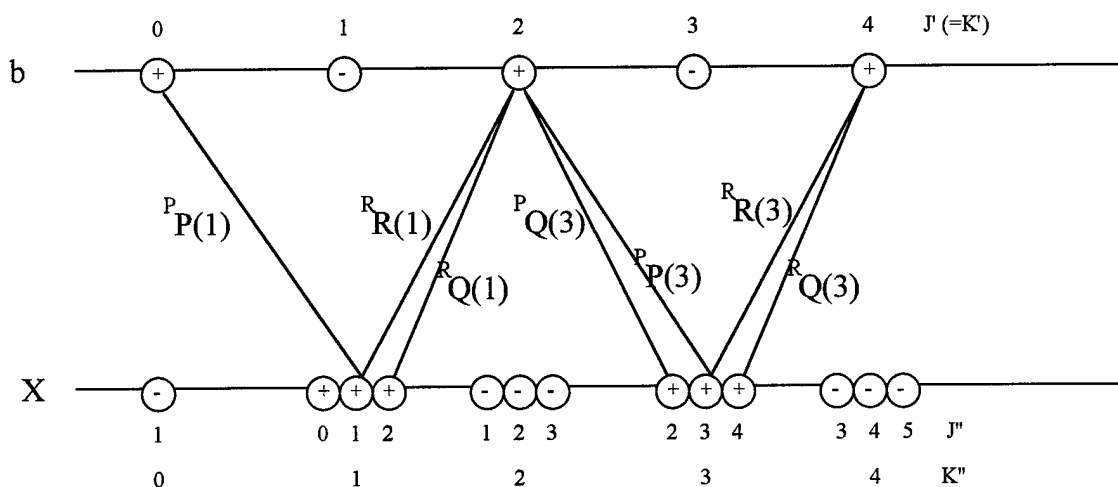


Figure 1-5: Spectrum of X to b  $v''=0 \rightarrow v'=0$  transition in  $O_2$ .

Table 1-2: Line positions for X to b  $v''=0 \rightarrow v'=0$  transition in  $O_2$  (Burch, 1969).

P-Branch: $\Delta J = -1$			R-Branch: $\Delta J = +1$		
$J''$	$J'$	$\nu(\text{cm}^{-1})$	$J''$	$J'$	$\nu(\text{cm}^{-1})$
1	0	13118	1	2	13126
2	1	13114	2	3	13128
3	2	13112	3	4	13131
4	3	13107	4	5	13133
5	4	13105	5	6	13136
6	5	13100	6	7	13138
7	6	13098	7	8	13140
8	7	13093	8	9	13142
9	8	13091	9	10	13144
10	9	13086	10	11	13146
11	10	13084	11	12	13148
12	11	13078	12	13	13150
13	12	13076	13	14	13151
14	13	13069	14	15	13153
15	14	13068	15	16	13154
16	15	13061	16	17	13156.2
17	16	13059	17	19	13156.6
18	17	13052	19	18	13158.6
19	18	13050	18	21	13158.7
20	19	13042	21	20	13160.3
21	20	13041	20	21	13160.8

Figure 1-6 illustrates the transitions according to the selection rules. Note that, in reality,  $O_2$  has four branches. What we call the P-branch in this study is made up of  $^P P$  and  $^P Q$  and what we call the R-branch is made up of  $^R R$  and  $^R Q$ . This is why the R-branch lines start overlapping. Note  $(- \rightarrow -)$  transitions are not allowed due to nuclear spin.  $K''$  is the total angular momentum quantum number. (Pope, 1997)



**Figure 1-6:  $O_2$   $X \rightarrow b$  electronic transition setup using selection rules (Herzberg, 1950)**

With molecules that follow Hund's case (b), like  $O_2$ , we expect  $\Lambda$ -doubling of the spectral lines which is due to the interaction of the nuclear rotation and  $L$ , the orbital angular momentum. Remember,  $\Lambda$  is the orbital angular momentum component along the internuclear axis. However we expect no  $L$ -doubling of the lines with  $O_2$  since  $L$  is perpendicular to the internuclear axis in  $\Sigma$  states (Herzberg, 1966).

The NO absorption spectrum we are studying is the first vibrational transition, designated " $(v''=0) \rightarrow (v'=1)$ ," of the ground state (see Figure 1-7) This transition is centered at  $\sim 1880 \text{ cm}^{-1}$ , which puts it in the infrared. Like with  $O_2$ , we can calculate the

energy requirement for the transition of .23 eV. As with O<sub>2</sub>, we wish to categorize the states studied.

NO has a total spin (S) of 1/2. The electron spin angular momentum,  $\Sigma$ , is then 1/2 or -1/2. This gives it a spin multiplicity ( $2\Sigma + 1$ ) of 2. The electron orbital angular momentum parallel to the internuclear axis,  $\Lambda$ , is 1 giving us a "II" state (Herzberg, 1966). The electron orbital angular momentum and the spin angular momentum add to give us the total electron angular momentum,  $\Omega$ , which can be parallel or antiparallel ( $\Omega = \Lambda \pm \Sigma$ ) giving us 1/2 and 3/2. To calculate our J values which designate total angular momentum including electron spin, we use  $\Omega$ ,  $\Omega + 1$ ,  $\Omega + 2$ ,  $\Omega + 3$ .....So we have for the two states 1/2, 3/2, 5/2...for  $^2\Pi_{1/2}$  and 3/2, 5/2, 7/2...for  $^2\Pi_{3/2}$ .

The NO rotational transition we are studying can be explained based on a Hund's case (a) description (Herzberg, 1966). Figure 1-8 and Table 1-3 show the coupling scheme. In transitions where  $\Delta J = 0$  are allowed we expect a Q-branch, as well as P and R-branches using  $\Delta J = -1$  and  $\Delta J = 1$ , respectively. From the J values we calculated we expect the first line of the P-branch to be  $J'' = 2.5$  for the 3/2 state and  $J'' = 1.5$  for the 1/2 state. The Q-branch should have its first lines at  $J'' = 1.5$  for the 3/2 state and  $J'' = .5$  for the 1/2 state. And, lastly, we expect the first line for the R-branch to be  $J'' = 1.5$  for the 3/2 state and  $J'' = .5$  for the 1/2 state. This pattern can be seen in Figure 1-9. This verifies the data found in Spencer, et. al, 1994. The spectrum and center frequencies of all the lines are listed in Figure 1-10 and Table 1-2.

With a closer look at Figure 1-10, one will notice that the spectral lines of the 1/2 and 3/2 states are split in two. This is the  $\Lambda$ -doubling discussed in the O<sub>2</sub> section and is

due to the interaction of the nuclear rotation and  $L$ , the orbital angular momentum. In this  $\Pi$ -state,  $L$  is not constrained to be perpendicular to the internuclear axis, so  $\Lambda$  is not 0. We expect the splitting to increase with increasing  $J$ . The two components are labeled e and f and have slightly different energies on the order of  $0.01 \text{ cm}^{-1}$  for the  $\Omega = 1/2$  state and  $.001 \text{ cm}^{-1}$  for the  $\Omega = 3/2$  state (Herzberg, 1966). As we will see later, this means we can resolve the  $1/2$  state lines and not the  $3/2$  state lines. This gives us two lines to analyze for each  $J''$  for each state ( $1/2$  and  $3/2$ ). This will be discussed in Chapter 2.

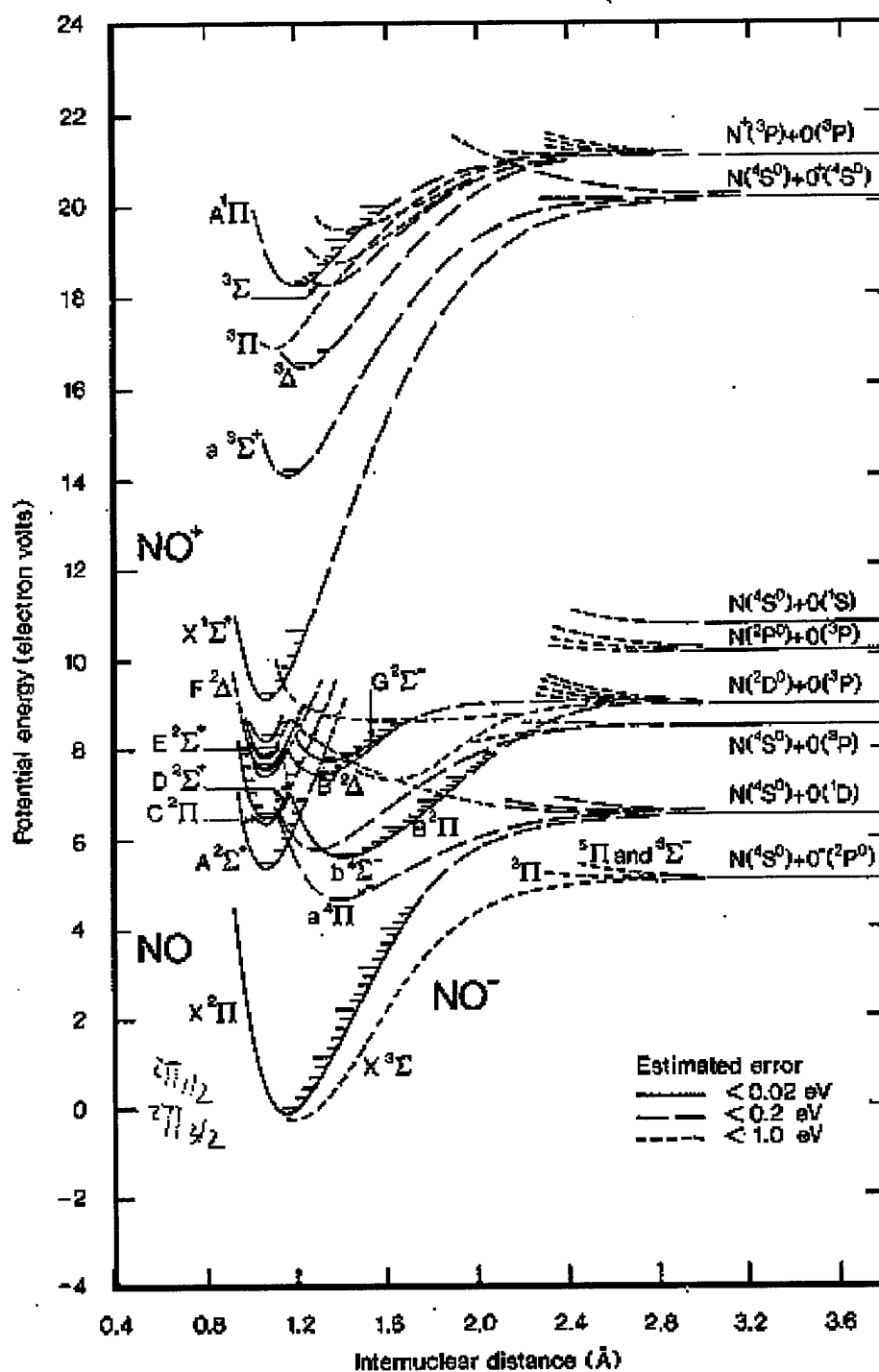
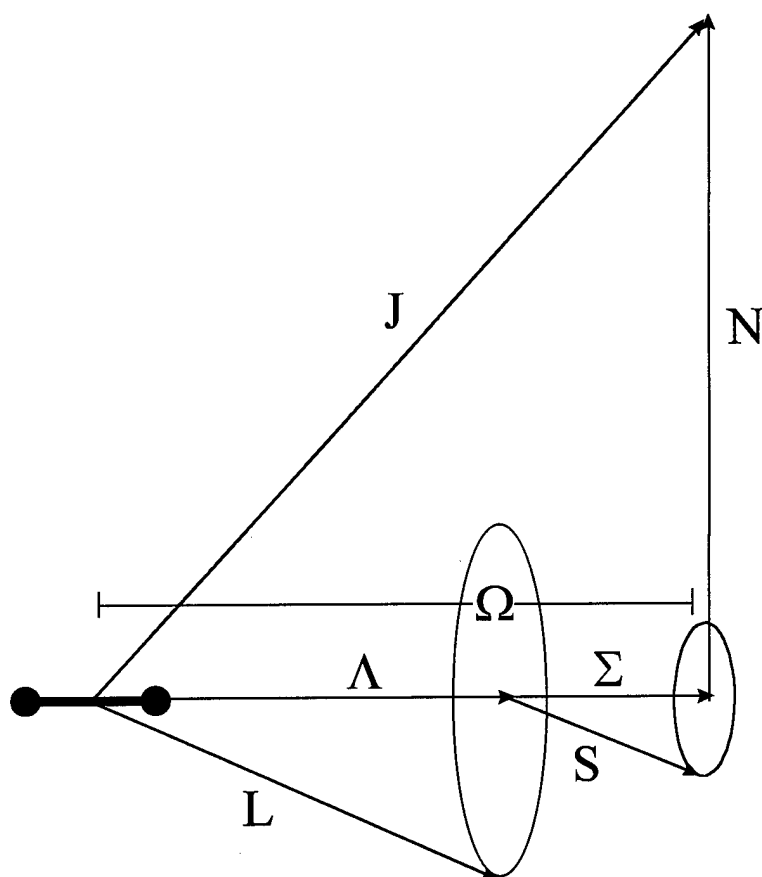


Figure 1-7: NO energy level diagram (Rees, 1989)

**Table 1-3: Selection rules for a heteronuclear diatomic molecule obeying Hund's case (a) coupling. (Herzberg, 1966)**

Total angular momentum.	$\Delta J = 0, \pm 1$ but no $J'' = 0 \rightarrow J = 0$
Total angular momentum excluding spin	$\Delta K = 0, \pm 1$ but $\Delta K = 0$ forbidden for $\Sigma \rightarrow \Sigma$ transitions
Electronic orbital angular momentum	$\Delta \Lambda = 0, \pm 1$ but $\Delta \Lambda = 0$ only singlet/triplet transitions
Electronic wave function symmetry	$(+ \rightarrow +)$ , $(- \rightarrow -)$ , no $(+ \rightarrow -)$ , no $(- \rightarrow +)$
Like nuclear charge symmetry	$(g \rightarrow g)$ , $(u \rightarrow u)$ , no $(g \rightarrow u)$ , no $(u \rightarrow g)$
Identical nuclei symmetry	$(s \rightarrow s)$ , $(a \rightarrow a)$ , no $(s \rightarrow a)$ , no $(a \rightarrow s)$



**Figure 1-8: Hund's case (a) coupling (Herzberg, 1966)**

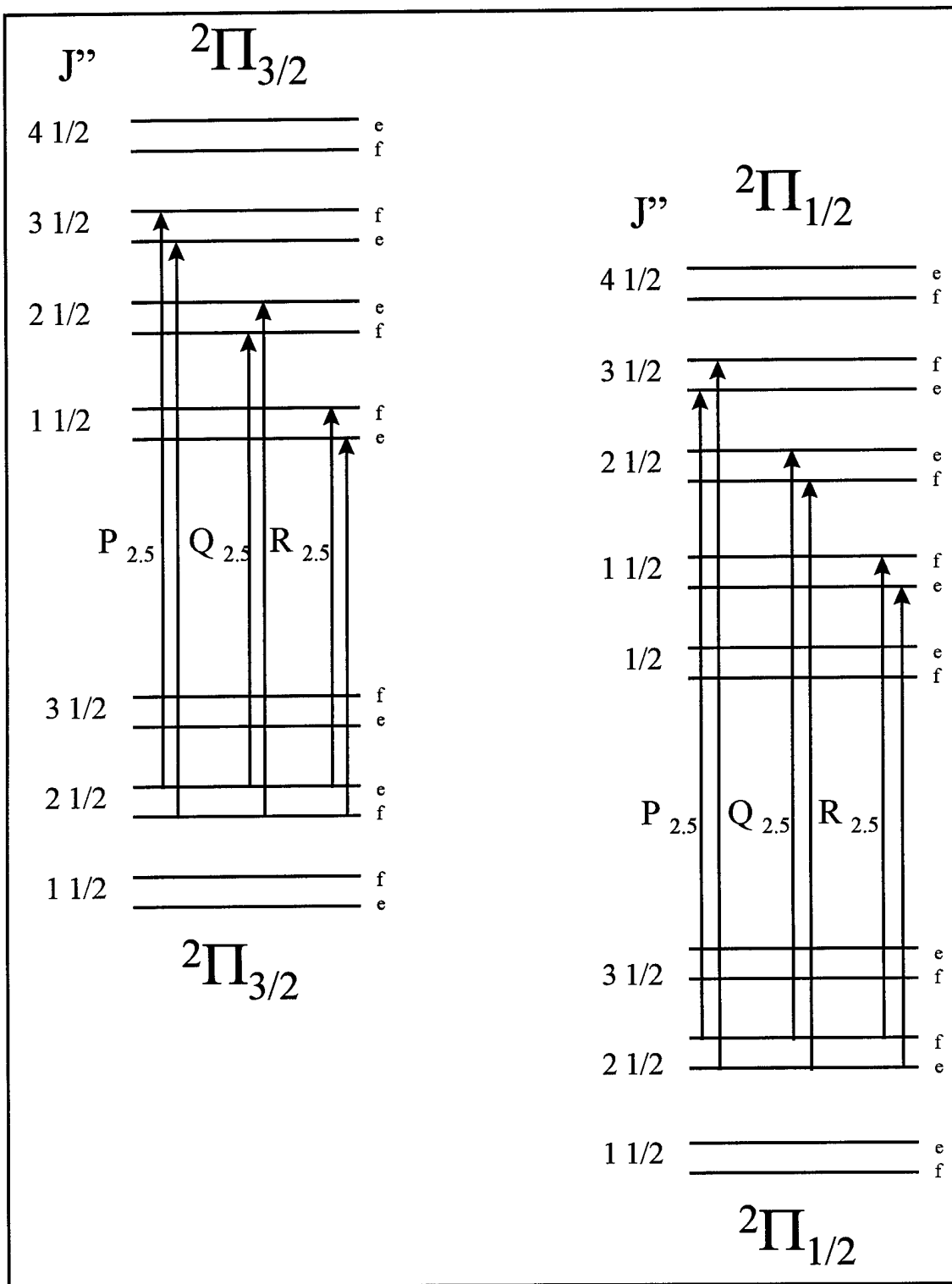


Figure 1-9: Spectral line comparison for the states of NO (Herzberg, 1966)

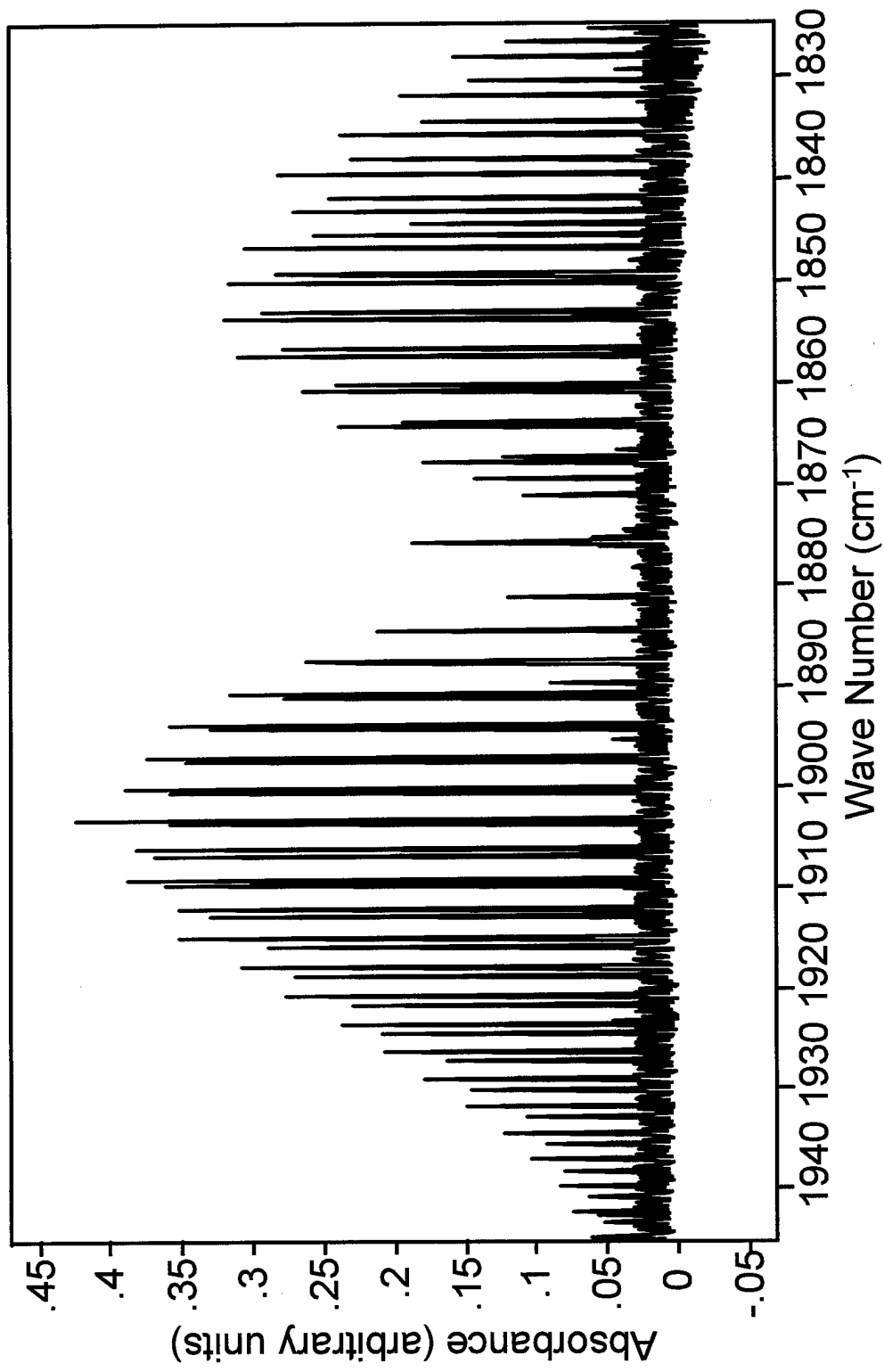


Figure 1-10: Spectrum of  $v''=1 \rightarrow v'=0$  transition in NO (500 mTorr NO, 40 Torr He).

**Table 1-4: Line center locations of  $v''=0 \rightarrow v'=1$  transition in NO.  
(Spencer, 1994).**

P-Branch			Q-branch			R-branch		
state	J''	$v(\text{cm}^{-1})$	state	J''	$v(\text{cm}^{-1})$	state	J''	$v(\text{cm}^{-1})$
3/2	18.5	1806.6539	3/2	5.5	1875.2351	3/2	0.5	no line
1/2	18.5	1808.6946	1/2	5.5		1/2	0.5	1881.0349
3/2	17.5	1810.6865	3/2	4.5	1875.4336	3/2	1.5	1884.2932
1/2	17.5	1812.6344	1/2	4.5		1/2	1.5	1884.3232
3/2	16.5	1814.6871	3/2	3.5	1875.5963	3/2	2.5	1887.5174
1/2	16.5	1816.5406	1/2	3.5	1875.772	1/2	2.5	1887.6363
3/2	15.5	1818.6553	3/2	2.5	1875.7226	3/2	3.5	1890.7072
1/2	15.5	1820.4129	1/2	2.5	1875.904	1/2	3.5	1890.9124
3/2	14.5	1822.5911	3/2	1.5	1875.8129	3/2	4.5	1893.8627
1/2	14.5	1824.2516	1/2	1.5	1876.001	1/2	4.5	1894.1515
3/2	13.5	1826.4941	3/2	0.5		3/2	5.5	1896.9839
1/2	13.5	1828.0563	1/2	0.5		1/2	5.5	1897.3531
3/2	12.5	1830.3644				3/2	6.5	1900.0706
1/2	12.5	1831.8271				1/2	6.5	1900.5171
3/2	11.5	1834.2016				3/2	7.5	1903.1228
1/2	11.5	1835.5639				1/2	7.5	1903.6434
3/2	10.5	1838.0055				3/2	8.5	1906.1405
1/2	10.5	1839.2666				1/2	8.5	1906.7318
3/2	9.5	1844.7759				3/2	9.5	1909.1234
1/2	9.5	1842.9352				1/2	9.5	1909.7821
3/2	8.5	1845.5127				3/2	10.5	1912.0716
1/2	8.5	1846.5697				1/2	10.5	1912.7939
3/2	7.5	1849.2155				3/2	11.5	1914.9848
1/2	7.5	1850.1701				1/2	11.5	1915.7674
3/2	6.5	1852.8842				3/2	12.5	1917.8631
1/2	6.5	1853.7363				1/2	12.5	1918.7021
3/2	5.5	1856.5185				3/2	13.5	1920.7061
1/2	5.5	1857.2682				1/2	13.5	1921.5983
3/2	4.5	1860.1181				3/2	14.5	1923.5139
1/2	4.5	1860.7661				1/2	14.5	1924.4554
3/2	3.5	1863.6827				3/2	15.5	1926.2862
1/2	3.5	1864.2296				1/2	15.5	1927.2735
3/2	2.5	1867.2122				3/2	16.5	1929.0229
1/2	2.5	1867.6592				1/2	16.5	1930.0526
3/2	1.5	no line				3/2	17.5	1931.7238
1/2	1.5	1871.0543				1/2	17.5	1932.7925
						3/2	18.5	1934.3888
						1/2	18.5	1935.4931

## Historical Background

### O<sub>2</sub> Study

No previous experimental work has been done on noble gas broadening of O<sub>2</sub> X → b spectral lines. However, work has been done on line strength measurement, width and shape measurement for O<sub>2</sub> self broadening and N<sub>2</sub> broadening of O<sub>2</sub>. Theoretical work has been done on noble gas broadening, which gives us a basis for comparison with our experimental data.

Burch and Gryvnak (1969) carried out a series of experiments to measure the strengths, widths and shapes of the oxygen A-band lines using a grating spectrometer with an incandescent source and photomultiplier detector. They accurately mapped out the P- and R-branches out to J' = 30. Their half width measurements were done by calculating the integrated absorptance from the spectra and backing out the half width from that, although they noticed that problems arose using too high or too low pressure of O<sub>2</sub>. Too low of a pressure over weighted the Doppler broadening by increasing the mean free path of the molecules to where a Lorentzian profile no longer was valid. Too high of a pressure introduced pressure broadening which we now know can broaden the lines so much that they become unresolvable. In the end they were able to compare O<sub>2</sub> and N<sub>2</sub> broadening and found that N<sub>2</sub> broadened lines were  $1.06 \pm .03$  times wider than the self broadened lines. See Figure 1-11 for results of this study compared to other researchers discussed here.

An additional self broadening study was carried out by J. H. Miller, et. al. (1974) using a scanning grating spectrometer. Instead of using integrated absorptance to

determine the half widths of the lines, they used an iterative procedure whose initial value came from direct measurement of the widths of the digitized spectra. As we will see later, this is similar to our strategy. They used an alternate method of width determination for low pressures which took into account the Doppler width of the lines and used a Voigt profile. As we will see later, we incorporated Doppler widths into our data analysis and used a Voigt profile for all of our lines at all pressures. As with Burch et. al., they attempted N<sub>2</sub> broadening measurements, but found *no* difference in the broadening coefficients. See Figure 1-11 for results of this study compared to other researchers.

Other research on O<sub>2</sub> self broadening was done by Ritter and Wilkerson (1987). Their goal was to measure strengths, widths, and line shapes, and to calculate broadening coefficients. Improvements to spectroscopic analysis using a tunable dye laser allowed researchers to increase the resolution of spectra, where past researchers had to rely on white light sources and scanning grating spectrometers. Using the laser's narrow bandwidth ( $<.0001\text{ cm}^{-1}$ ) the resolution increased to smaller than the Doppler width (.015) by an order of magnitude. Ritter and Wilkerson used a Voigt profile for their curve fitting algorithm. They found that use of the Doppler width was necessary, and took this requirement further by increasing the Doppler width share of the width by 4% to reduce the fit residuals. Their hypothesis is that the increase in Doppler width is the result of Dicke narrowing of the lines, which we will not explore in this study.

Ritter (1986) also completed a study of noble gas broadening which is directly related to this study in that his calculated values have never been experimentally verified. His Ph.D. dissertation covers his O<sub>2</sub> self broadening work and his theoretical noble gas

broadening work. The above paper he submitted covered only self broadening, and he has not published the noble gas work. He measured the broadening of a few lines and then used the mass of the foreign gas atom to modify the Galatry profile he used to fit the curves and calculate the widths and pressure broadening coefficients for the rest of the lines. We will compare our work to Ritter's since his is the only other data available. See Appendix A for diagrams of Ritter's noble gas broadening data compared with ours.

Pope (1997) completed an O<sub>2</sub> self broadening study using the same method of data collection and analysis used in our study. His values for the pressure broadening coefficients match the Miller group's self broadening data. Since we are using much of the procedure used by Miller et. al., this is a good sign. Pope's data is shown compared to other researchers in Figure 1-11.

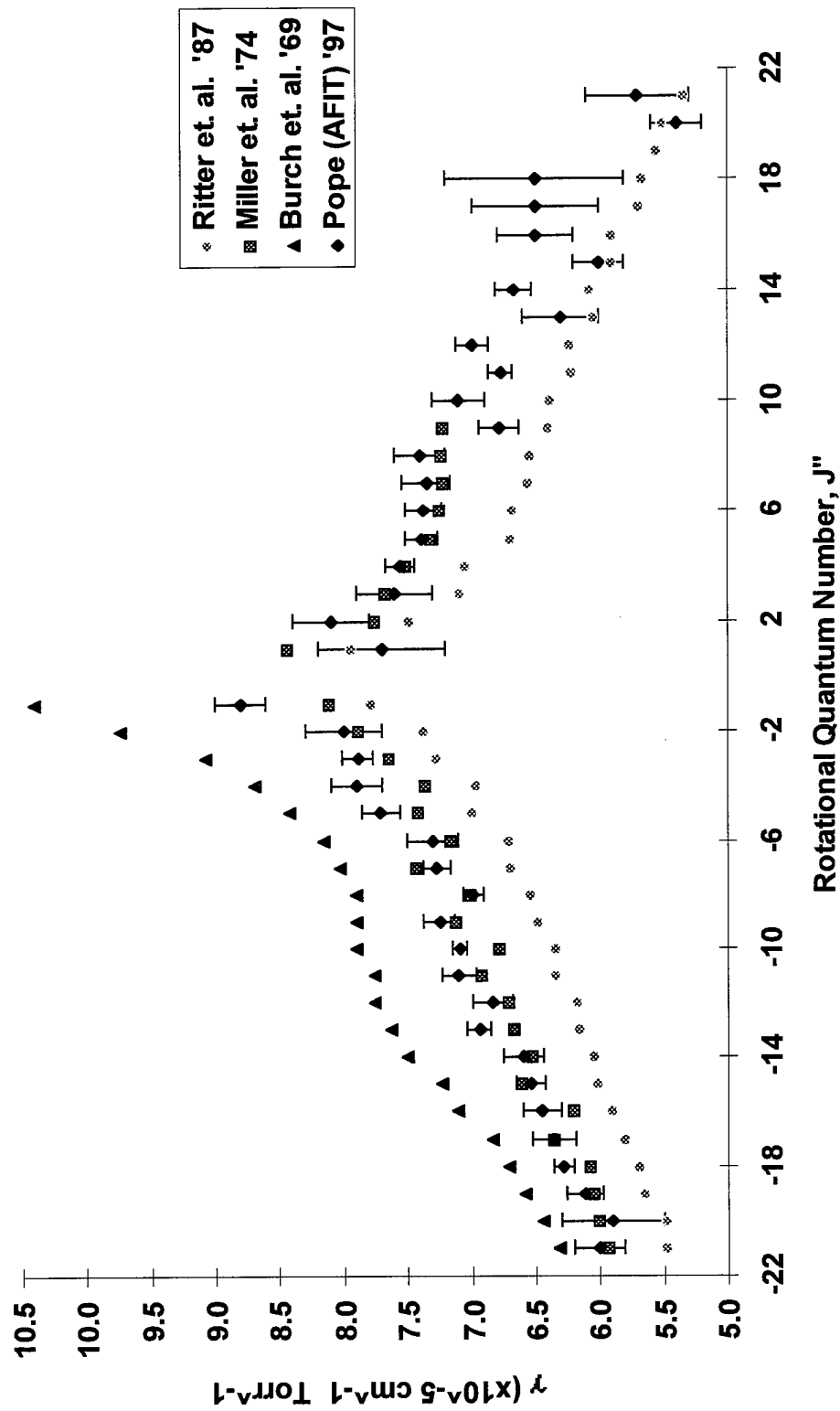


Figure 1-11: O<sub>2</sub> Self broadening by research group.

## NO Study

Considerable amounts of work have been done on broadening in the A-X , fundamental vibrational ( $v''=1 \rightarrow v'=0$ ) and second vibrational ( $v''=2 \rightarrow v'=1$ ) bands of NO using many different collision partners. In particular we are interested in the fundamental band, but methods used in other studies are also of interest.

As far as the A  $\rightarrow$  X band of NO, self broadening as well as foreign broadening using N<sub>2</sub>, argon, and helium was studied in depth by A. O. Vydrov et. al. (1994). He used a laser-induced fluorescence technique yielding broadening coefficients and line shape parameters. The second overtone was studied by Pine and Maki (1985) using tunable infrared laser system and they recorded line shape parameters for self and N<sub>2</sub> broadening.

For our study, we were interested in broadening of the fundamental band. Only self broadening and foreign broadening using N<sub>2</sub>, O<sub>2</sub>, and H<sub>2</sub>O at room temperature has been previously examined. A studies of relevance to us is the self and N<sub>2</sub> broadening study by Ballard and Johnston (1988). This is significant in that the experimental method, as with ours, is Fourier transform spectroscopy. They measured broadening by N<sub>2</sub> and NO and compared line widths to J'', but did not report broadening coefficients. The Ballard group is working on noble gas broadening with the goal of producing broadening coefficients. For coefficients for which to compare our work, the only study done so far is by Spencer et. al. (1994). They produced an expansive study of the NO fundamental band where they measured line shapes, widths and pressure broadening coefficients. They used Fourier transform spectroscopy with a similar setup to ours for gas handling and

pressure measurement. They chose to use long path lengths through the gas cell of 150 cm compared to our 11 cm cell, with NO pressures on the order of 10 mTorr compared to 500 mTorr in our study. What is significant is their data analysis scheme. They were not able to resolve the  $\Lambda$ -doubled  $3/2$  state lines but were able to resolve the  $1/2$  state lines. They assumed that the  $\Lambda$ -doubled lines must be equal and they locked the distance between the line centers for the fits. They used theoretical data provided by A. G. Maki and J. S. Wells for the line center distance data, but did not support the  $\Lambda$ -doublet intensity equality. As we will see later, this differs from our method.

Also of interest is a temperature dependent study of  $N_2$  broadening of the fundamental band by M. N. Spencer et. al. in 1997. This study used the same setup as with their previously mentioned study, but they used cryogenically cooled cells to vary the temperature to atmospheric levels. We used this study as a reference for follow on work to ours.

## II. Experimental

### Apparatus

#### General Design

For our study, we used the Bomem DA8-002 Fourier transform spectrometer for both  $O_2$  and  $NO$ . It is basically a Michelson interferometer with one beam path mirror on a movable track whose output beam is absorbed by the sample gas in the beam path. See Figure 2-1.

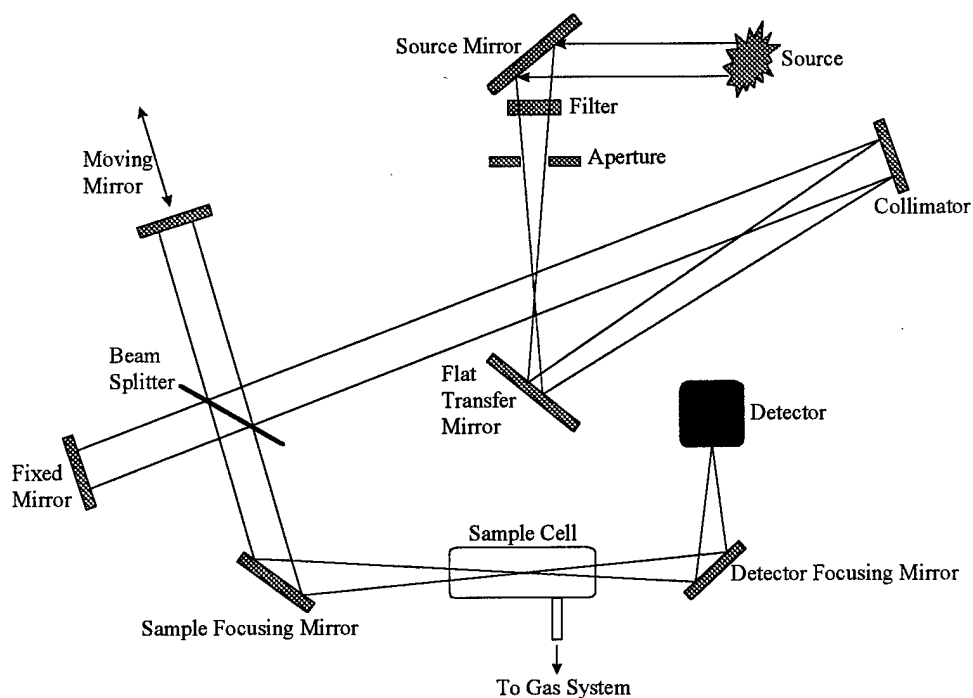


**Figure 2-1: Spectrometer diagram (Bomem Spectrometer System Manual,  
Revision 3.2)**

This section will cover how we used the spectrometer, not the theory of its operation, so see Appendix A for the theory behind Fourier transform spectroscopy. For the O<sub>2</sub> study we used a quartz halogen visible light source whose output is between 2500 and 25,000 cm<sup>-1</sup>. We used a filter centered at 766.5 nm with a wavelength range of  $\pm 10$  nm which gave us a beam with wave number between 12850 and 13350 cm<sup>-1</sup>. Our beam splitter was quartz visible with a range of 4000 to 25,000 cm<sup>-1</sup>. Our detector was an amplified silicon avalanche type with range 9000 to 22000 cm<sup>-1</sup>.

Next we had to choose our cell length and working pressure. We used Beer's Law:

$$I = I_0 \exp(-kx) \quad (2-1)$$

and rearranged it using the definition of absorption coefficient (Equation 2-2) and the ideal gas law (Equation 2-3):

$$k = n\sigma \quad (2-2)$$

$$n = \frac{P}{k_B T} \quad (2-3)$$

to get:

$$\frac{I}{I_0} = \exp\left[-\frac{P\sigma_{ABS}x}{k_B T}\right] \quad (2-4)$$

where x is the length of the cell, k is the absorption coefficient, and P is the pressure in Pascal. (Rees, 1989)  $\sigma_{ABS}$  is the absorption cross section which we had to find using the Einstein A-coefficient and the line shape partition function (g) (Verdeyen, 1982). The

Einstein  $A_{21}$  coefficient is the inverse of the state lifetime,  $\tau$ .  $\tau$  turns out to be 9 seconds (Kearns, 1971). To calculate  $\sigma$ :

$$\sigma(\nu_D) = \frac{A_{21}\lambda^2}{8\pi n^2} g(\nu) \quad (2-5)$$

Here,  $n$  is the index of refraction ( $\sim 1$ ). We compute the line shape partition using (Verdeyen, 1982):

$$g(\nu_D) = \frac{1}{\nu_D} \sqrt{\frac{mc^2}{2\pi k_B T}} \quad (2-6)$$

We calculated  $g$  to be  $1 \times 10^{-9}$ s. This gives us a cross section ( $\sigma_{ABS}$ ) of  $2.54 \times 10^{-20} \text{ cm}^2$ . This is the cross section for the entire band. Now we must factor in rotation of the molecule to calculate the cross section for each line. This is done by multiplying the absorption cross section by the fraction of the population in each rotational level:

$$\sigma_\nu = \sigma_{ABS} f_J \quad (2-7)$$

The *relative* populations of each rotational level is given by the multiplicity multiplied by the Boltzmann factor:

$$\frac{N(J'')}{N(0)} = (2J'' + 1) \text{Exp} \left[ \frac{-E_{J''}}{k_B T} \right] \quad (2-8)$$

where

$$E_J = B(J'')(J''+1) \quad (2-9)$$

and  $B$  is the rotational constant which is known for each molecule (Herzberg, 1966). For  $O_2$ ,  $B$  is  $1.40041 \text{ cm}^{-1}$  which gives us  $E_J$  of  $154.05 \text{ cm}^{-1}$  for the  $J''=10$  line. To get the fraction of the population in each rotational level, we must divide the multiplicity and Boltzmann factor by the rotational partition function,  $Q_{ROT}$ :

$$Q_{ROT} = \frac{k_B T}{hcB} \quad (2-10)$$

$$f_J = \frac{(2J+1) \exp\left[\frac{-E_J}{k_B T}\right]}{\frac{k_B T}{hcB}} \quad (2-11)$$

where  $h$  is Planck's constant,  $c$  is the speed of light and  $B$  is the same rotational constant. For the  $J'=10$  line, we find  $f_J$  to be 0.0775 (unitless). Now we adjust our cross section using equation 2-7. For the  $J'=10$  line we get  $\sigma_v$  of  $1.97 \times 10^{-21} \text{ cm}^2$ . See Figures 2-2 and 2-3. Notice how both the fractional populations and cross sections exhibit a Boltzmann distribution with  $J'$ . The peak absorption at this temperature is at the  $J'=10$  line, but at higher temperatures, we expect this peak to shift to higher  $J'$ .

We would like a usable absorption, and one e-fold is a good number to start with. Going back to our Beer's Law equation, and using one e-fold,

$$P = \frac{k_B T}{\sigma x} \quad (2-12)$$

we get a pressure of 155 Torr of  $O_2$  for a 10 m cell at the  $J'=10$  line. See Figure 2-4 for a plot of pressure needed for an e-fold absorption vs.  $J'$ . Notice how it exhibits an inverse Boltzmann distribution. We used these as a start and ran a few spectra at different pressures of  $O_2$  with no broadening gas. We found that with this particular spectrometer and cell we needed 200 Torr to give us a 50% absorption for most lines. Figure 2-5 is a diagram of the 10m multipass cell. We set the mirror to move 0.5 cm/s and used the spectrometer's detector gain and software gain "4" feature to increase intensity on the

detector. To increase signal-to-noise ratio, we used 100 scans (coadds) of the movable mirror for the lower pressures of broadening gas and 400 scans for the higher pressures. We used trial and error to determine the best procedure. We used a 1000 Torr Baratron head with an MKS digital display to monitor the pressure in the cell and gas manifold. The gases were stored in bottles connected to the manifold via high vacuum fittings, valves and lines.

For the NO study we used an infrared source whose output is between 200 and 10000  $\text{cm}^{-1}$ . We used a filter centered at 5.2  $\mu\text{m}$  with a transmission wave number range of 1750-2200  $\text{cm}^{-1}$ . Our beam splitter this time was calcium fluoride ( $\text{CaF}_2$ ) with a transmission range of 1200 to 8500  $\text{cm}^{-1}$ . Our detector was a liquid nitrogen cooled MCT type with a sensitivity range of 800 to 5000  $\text{cm}^{-1}$ . Again, these were chosen to be centered on our transition at 1880  $\text{cm}^{-1}$ .

With NO we used the same type of calculations as with  $\text{O}_2$ , only we used the  $A_{10}$  Einstein A-coefficient as 10.78 (Verdeyen, 1982). We calculated 120.15 for the rotational partition function value (Q), and  $7 \times 10^{-9}$ s for the line shape partition function value (g). This gives us a cross section ( $\sigma_{\text{ABS}}$ )  $9.062 \times 10^{-16} \text{ cm}^2$ , which is much larger than  $\text{O}_2$ , hence the shorter cell. Using the same formulas for rotational energy distribution and Beer's law we arrive at cross sections on the order of  $7 \times 10^{-17} \text{ cm}^2$ , and working pressures of tenths of Torr of NO with an 11cm cell. Figures 2-6,2-7 and 2-8 show the distributions of fractional populations, cross sections and pressures for NO. Note the same Boltzmann distributions as with  $\text{O}_2$ . Figure 2-9 is a diagram of the NO cell.

Mirror speed was set at 0.5 cm/s and used the spectrometer's software gain "4" feature to increase intensity on the detector. To increase signal-to-noise ratio, we used 32 scans (coadds) of the movable mirror for the low pressure broadening and 100 scans for the higher pressures. NO broadening increases fast with increasing pressure so we had to keep SNR down. We used a 1000 Torr Baratron head with an MKS digital display to monitor the pressure in the cell and gas manifold.

Now that we had working pressures of gas, we planned our study with representative points of broadening gas pressure and collected the data. For O<sub>2</sub> we chose broadening gas pressures from 100 to 400 Torr at 50 Torr increments with an O<sub>2</sub> pressure of 200 Torr. For NO we chose broadening gas pressures of 10, 25, 40, and 55 Torr with an NO pressure of 0.5 Torr. For the O<sub>2</sub> study we used all of the noble gases except helium and radon as collision partners (Rob Pope used helium as part of his self-broadening study), and we included nitrogen to make things interesting. For the NO study we used all of the noble gases except radon. These broadening gas pressures were chosen by trial and error by observing the spectra and determining if the broadening was too high or low for accurate measurement by our curve fitting program. For purity control we chose broadening gases of research quality 5.0 or greater (better than 99.997%) purity, used high purity regulators, and used high vacuum lines and fittings. Any losses or gains of pressure were noted and those spectra were discarded and repeated. After we collected the data we examined it for anomalies, such as abnormally low signal to noise ratio, uneven spectrum baseline, warped or asymmetrical peaks, etc. We fixed low signal to noise ratio spectra by running the measurement with 100 scans (coadds) of the

spectrometer for the higher pressures. To ensure zero baselines, we ran 100 scan measurements with the cell at vacuum, at low resolution before each gas measurement. This allowed us to choose the best background spectrum to match the envelope of each measurement spectrum.

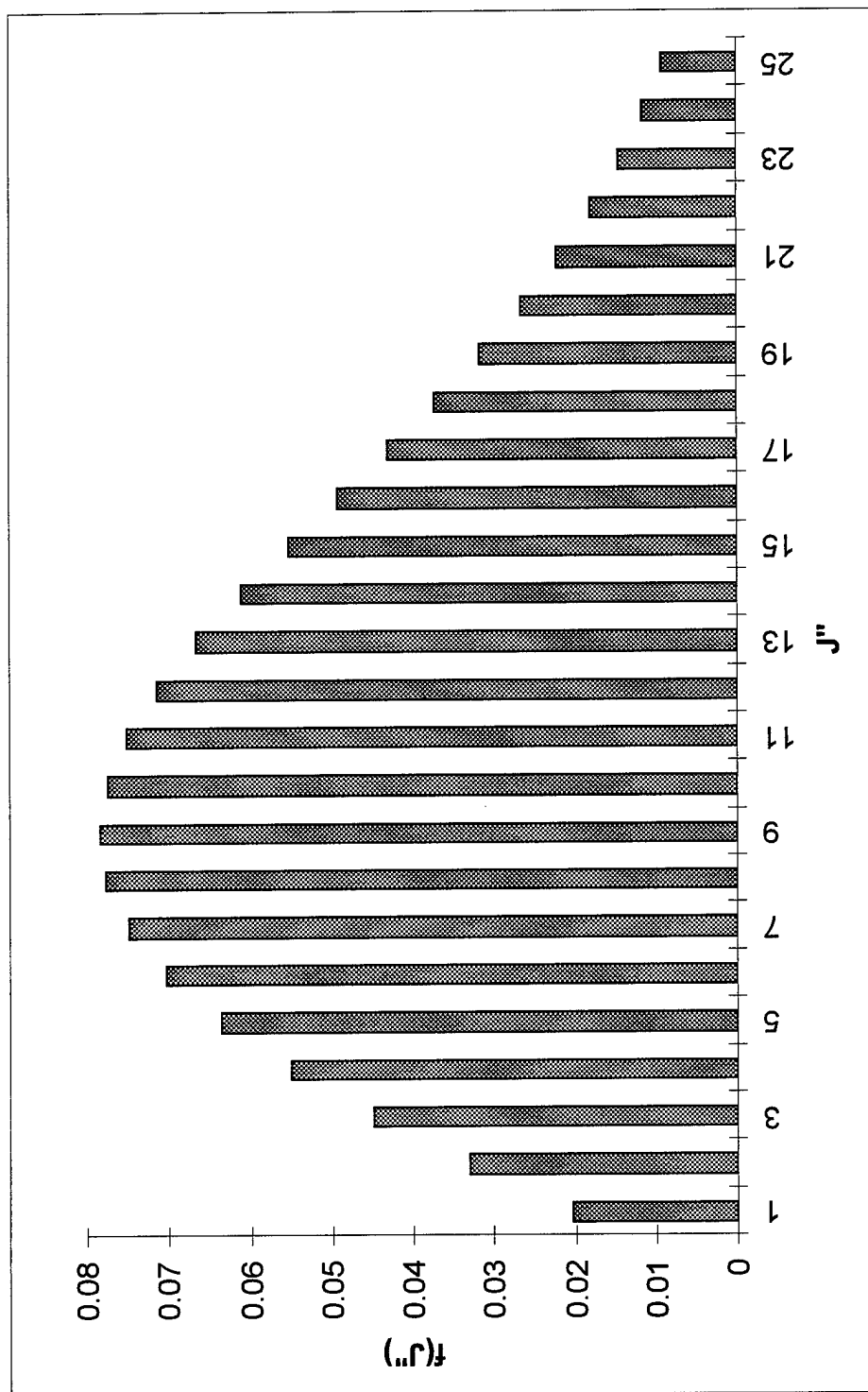


Figure 2-2: Boltzmann distribution of fractional populations in  $O_2$  rotational levels.

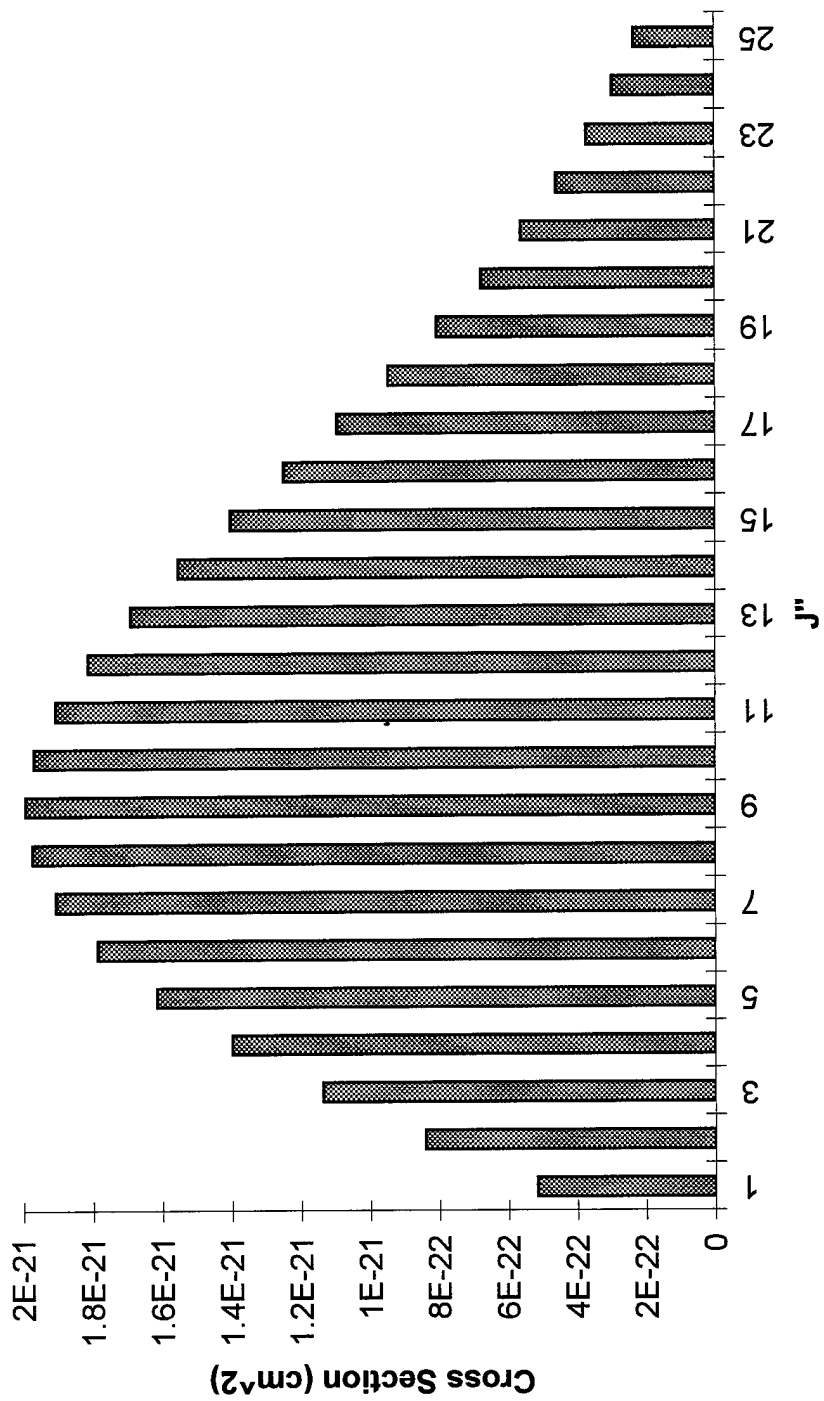


Figure 2-3: Boltzmann distribution of cross sections for  $O_2$ .

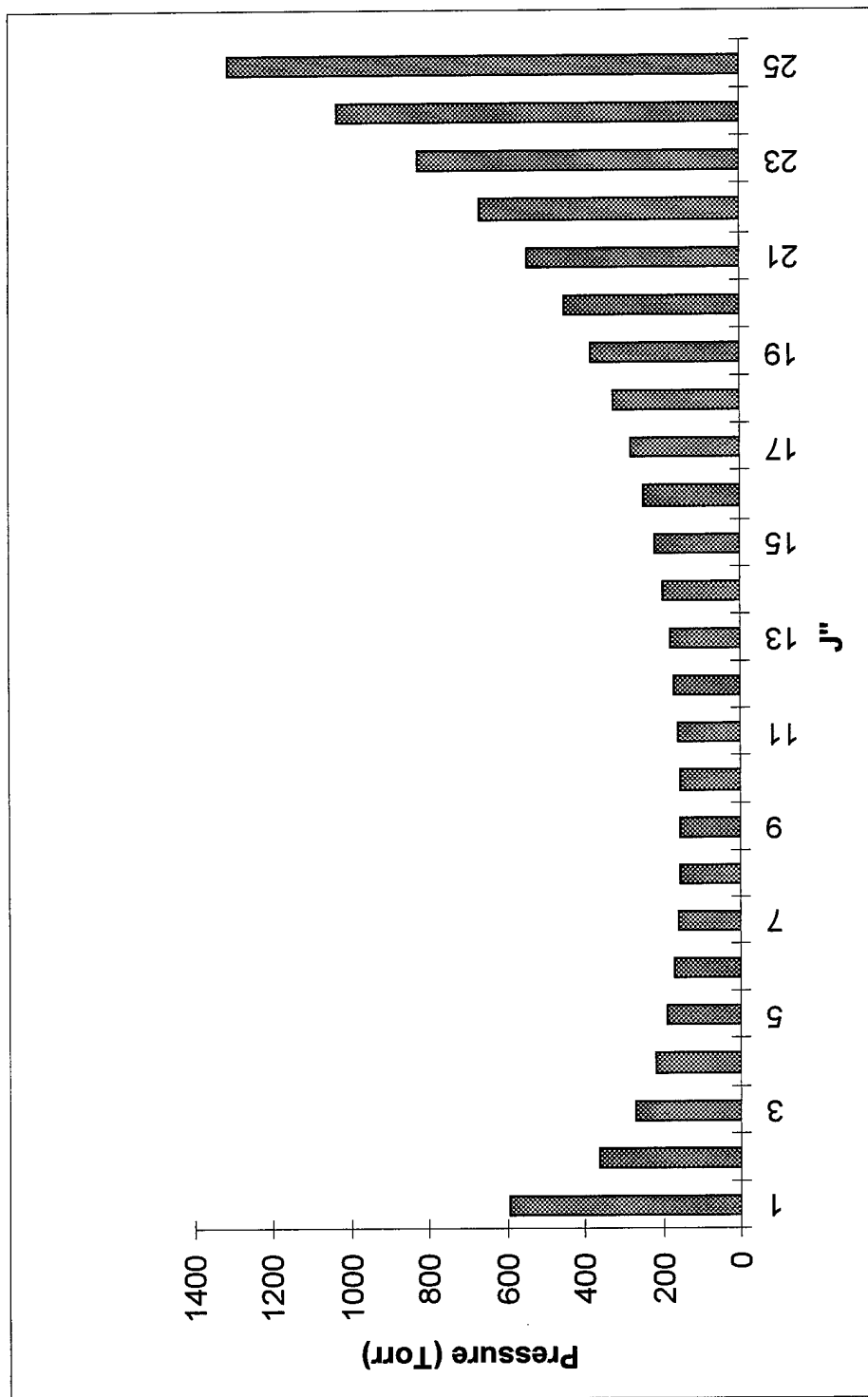


Figure 2-4: Pressures for one e-fold absorption for the spectral lines of O<sub>2</sub>.

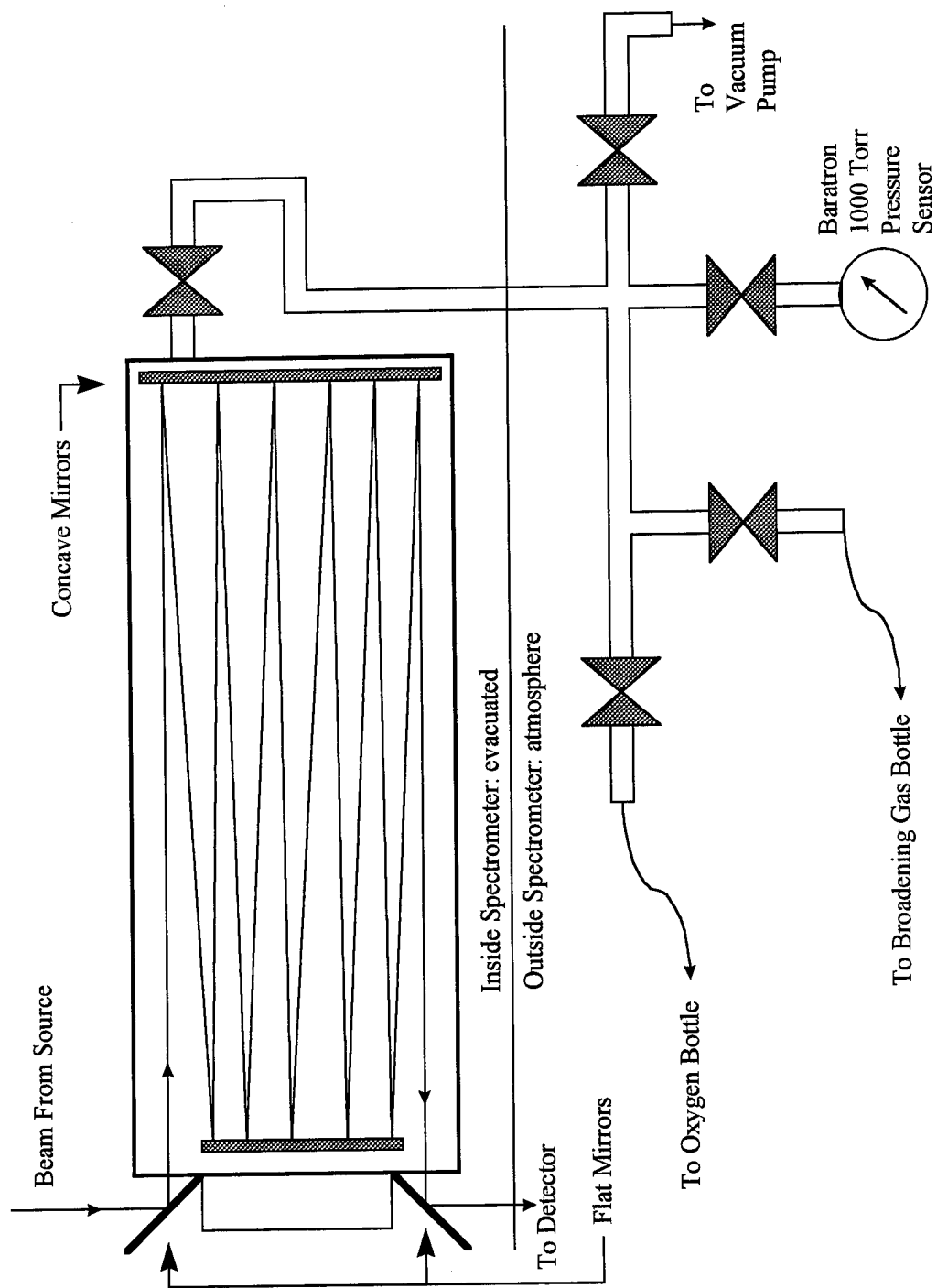


Figure 2-5:  $O_2$  multipass cell and gas system.

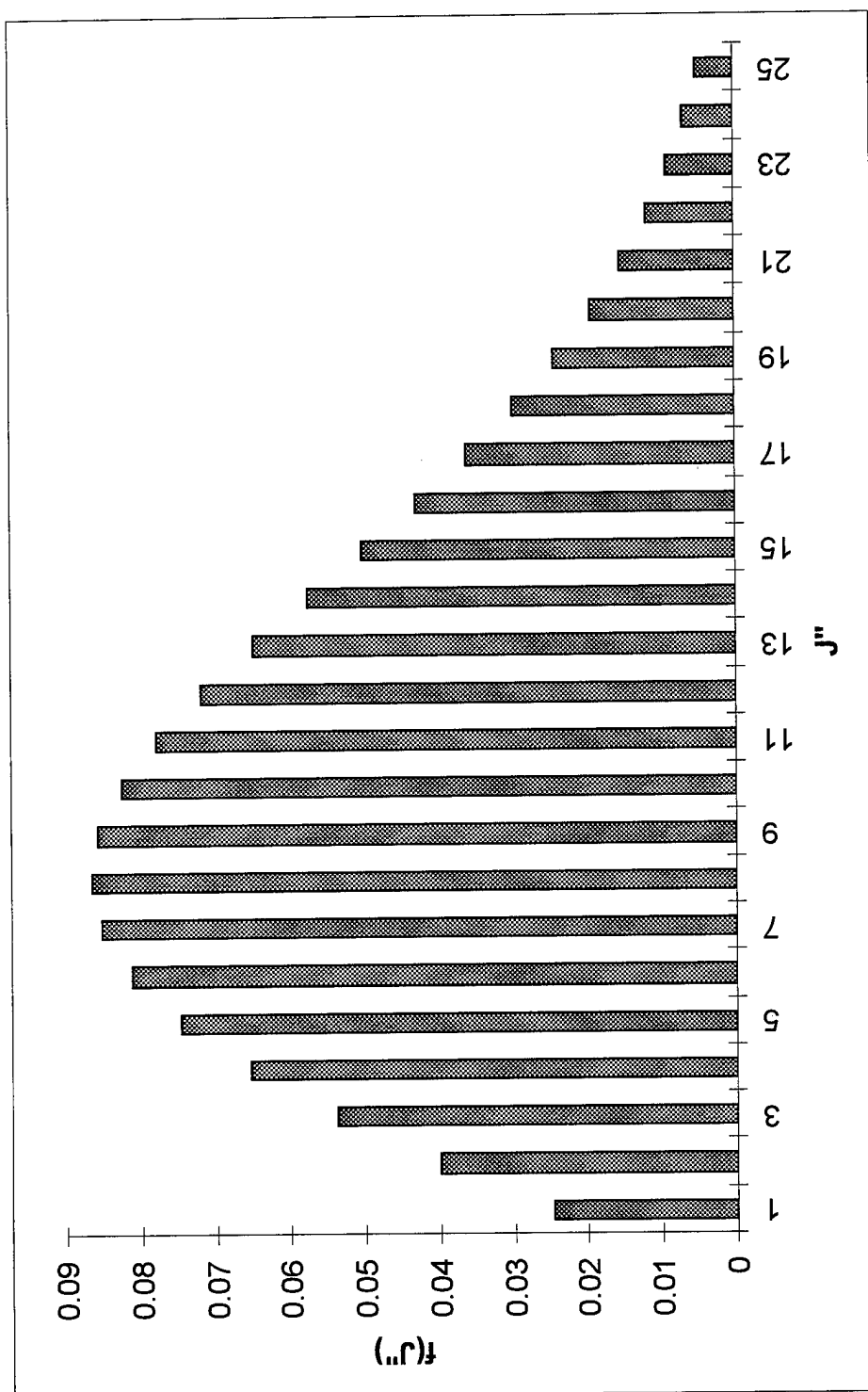


Figure 2-6: Boltzmann distribution of fractional populations in NO rotational levels.

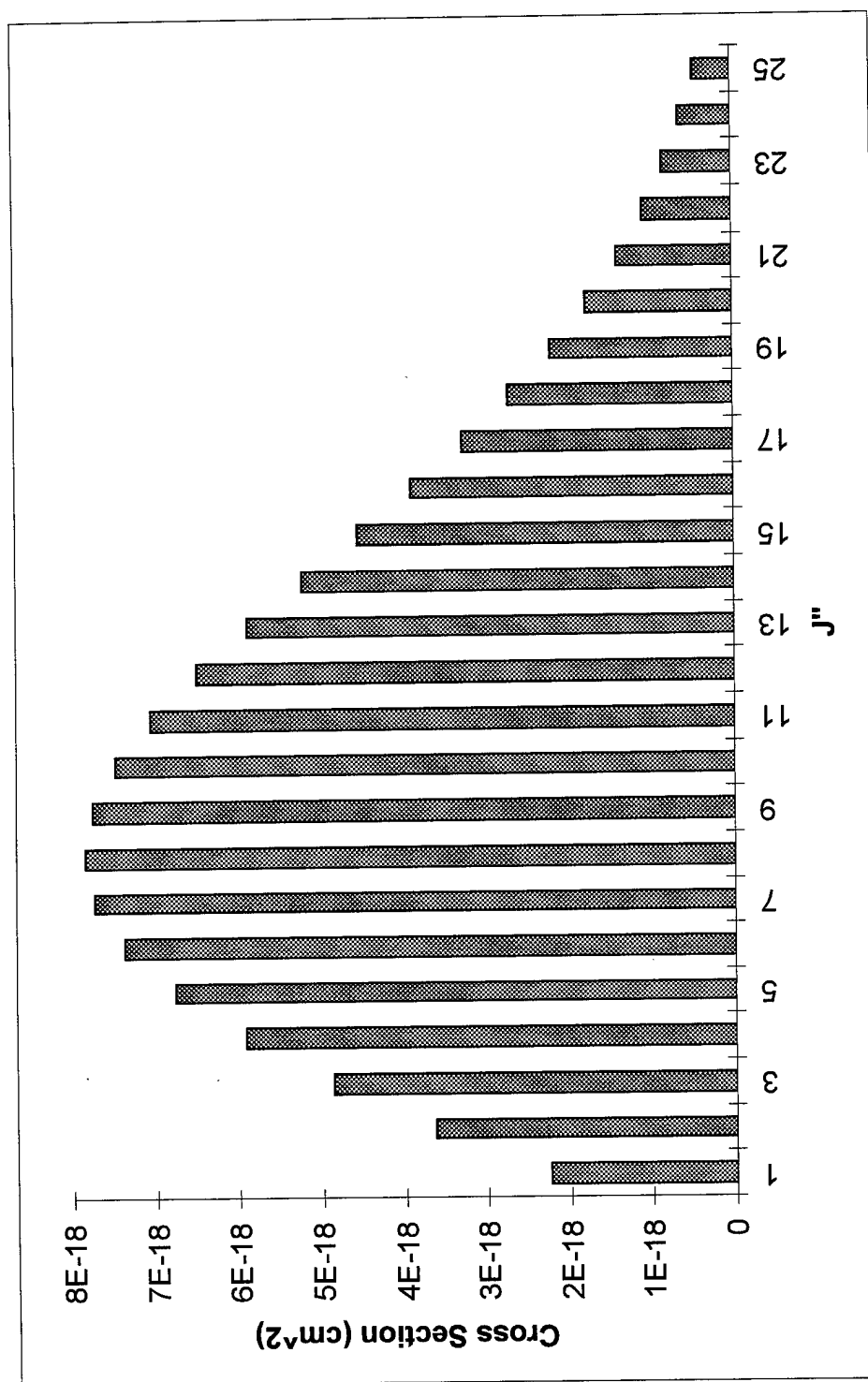


Figure 2-7: Boltzmann distribution of cross sections for NO.

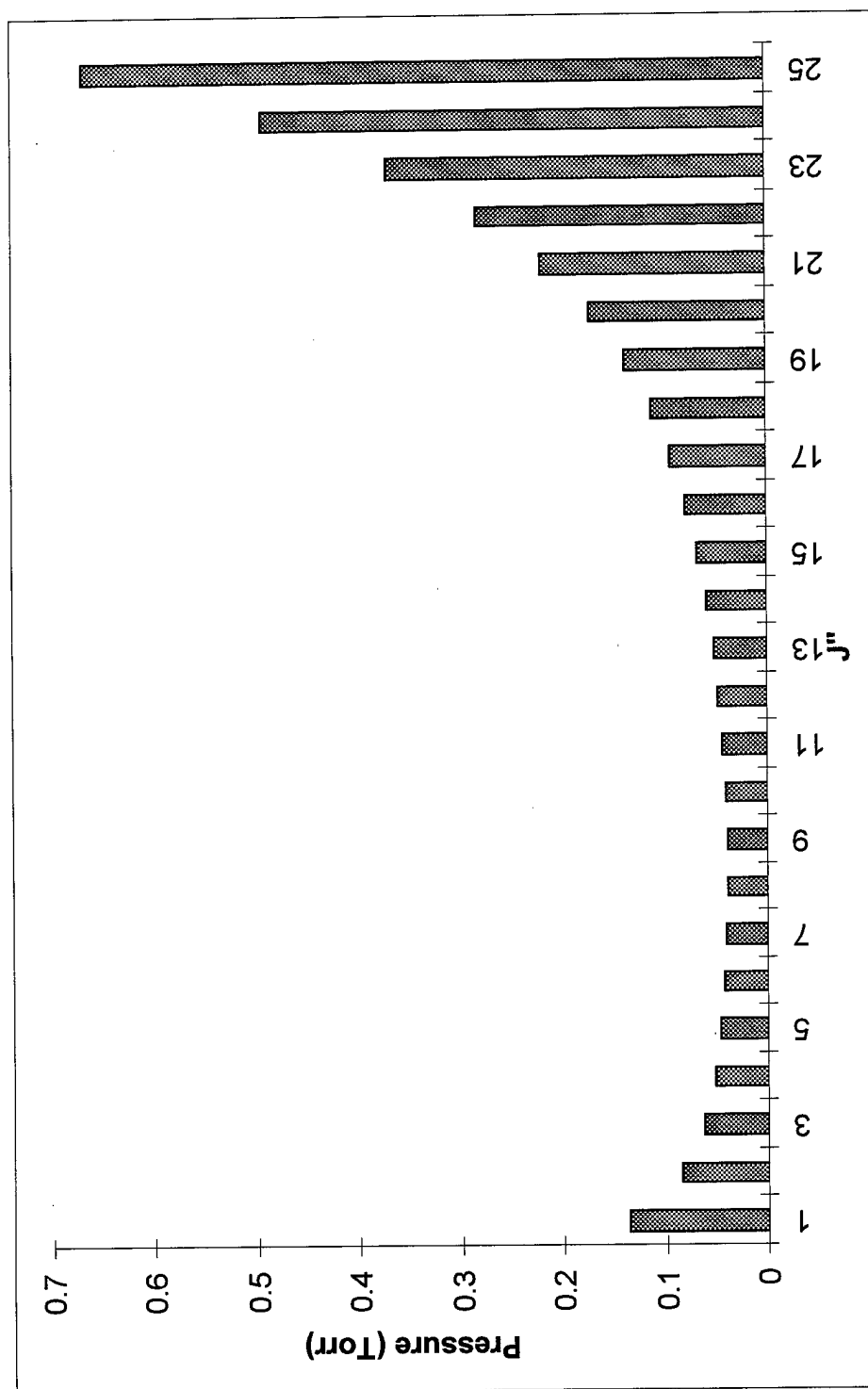
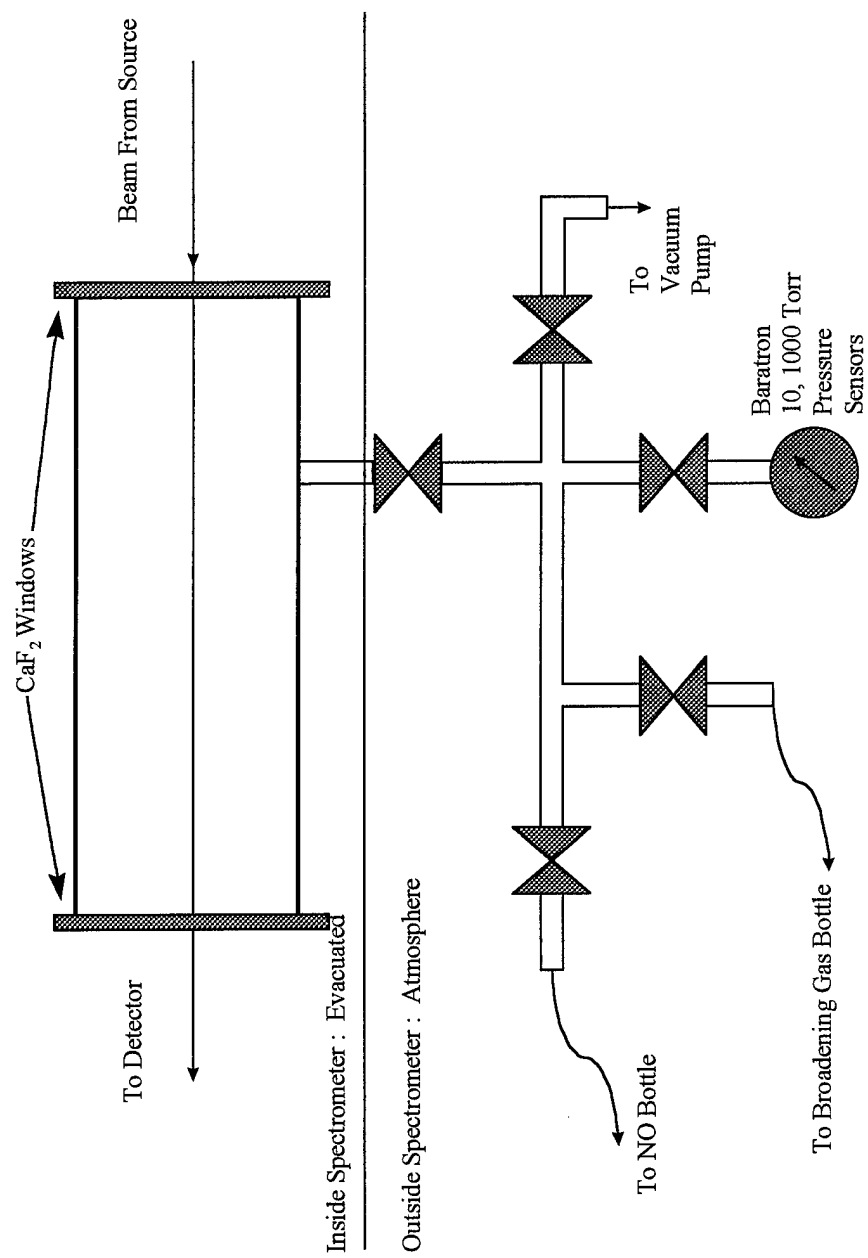


Figure 2-8: Pressures for one e-fold absorption for the spectral lines of NO.



**Figure 2-9: NO cell and gas system.**

## Data Analysis

After collecting the data (spectra) we needed to measure the Lorentzian half width at half maximum (HWHM) of all of the lines, sorted by rotational quantum number,  $J''$ . Then we had to plot HWHM against pressure for each line. By measuring the slope of this plot, we get the pressure broadening coefficients (PBC) for each line (Spencer, 1994). We then needed to plot PBC vs  $J''$  for each broadening gas and compare the pattern to other researchers' data in the case of  $O_2$  (Spencer, 1994). For NO we just note the pattern and see if it makes sense with what we expect from quantum mechanics.

The raw spectra produced by the Bomem are actually transmission data, which we had to convert to absorption data using the Bomem software (Bomem system manual). This procedure is called "Absorption" and it subtracts out the background (filter) data and converts the data file to one which can be imported into our curve fitting program. We also need the data to be in terms of wave number (Peak Fit Manual), which is what the Bomem does anyway.

To measure Lorentzian HWHM, we used a curve fitting program called Peak Fit. The curve fitter uses the Voigt profile discussed in Chapter 1 (Jansson, 1984). We can rearrange Jansson's equation to match the equation used by Peak Fit if we assign parameters,  $a_1$ ,  $a_2$ ,  $a_3$ , and  $a_0$  as follows:

$$a_1 = \nu_0 \quad (2-13)$$

$$a_2 = \frac{\Delta \nu_D}{\sqrt{2 \ln 2}} \quad (2-14)$$

$$a_3 = \Delta \nu_P \quad (2-15)$$

$$a_0 = \frac{\alpha_0}{\pi\sqrt{2}} \frac{a_3}{a_2} \quad (2-16)$$

So we get, for the rearranged Jansson's equation:

$$y = \frac{a_0}{a_2\sqrt{2\pi}} \int_{-\infty}^{\infty} \frac{\exp(-t^2)dt}{\frac{a_3^2}{2a_2^2} + \left[ \frac{x-a_1}{a_2\sqrt{2}} - t \right]^2} \quad (2-17)$$

where  $a_0$  is the area under the curve,  $a_1$  is the line center in  $\text{cm}^{-1}$ ,  $a_2$  is the Gaussian width (Doppler width half width standard deviation), and  $a_3$  is the Lorentzian HWHM. Note that parameter  $a_0$  includes parameters  $a_2$  and  $a_3$ . " $\alpha_0$ " is the actual area under the Voigt curve. When we adjust Peak Fit's "area" parameter, we are actually adjusting an algebraic shortcut including the real area (Peak Fit Manual and Jansson, 1984). To make Peak Fit's equation more understandable, we removed this shortcut:

$$y = \frac{a_3\alpha_0}{a_2^2 2\pi\sqrt{\pi}} \int_{-\infty}^{\infty} \frac{\exp(-t^2)dt}{\frac{a_3^2}{2a_2^2} + \left[ \frac{x-a_1}{a_2\sqrt{2}} - t \right]^2} \quad (2-18)$$

This matches Jansson's equation more closely, although Peak Fit uses the shortcut.

When fitting the curves, we first let the program fit the two hidden baseline parameters while holding the four above mentioned parameters constant. We then hold the Doppler HWSD constant and let the other parameters vary as the program iterates. We calculated Doppler FWHM for the band center of our  $\text{O}_2$  spectra ( $13100 \text{ cm}^{-1}$ ), using the procedure mentioned in Chapter 1 to be  $.0281 \text{ cm}^{-1}$ . This gives us a Doppler HWHM of  $0.0140 \text{ cm}^{-1}$ . We use the half width standard deviation in our analysis (Bevington, 1992):

$$\sigma = \frac{\Delta\omega_d}{2\sqrt{2\ln 2}} \quad (2-19)$$

which gives us a value of  $0.0119 \text{ cm}^{-1}$ . This is consistent with the value Pope used for his self broadening study, and since we chose to use his self-broadening data point for our “zero pressure” point, we can be consistent in our analysis. Using the same procedure for NO at the band center  $1880 \text{ cm}^{-1}$ , we calculated a Doppler FWHM of  $0.0042 \text{ cm}^{-1}$ , a HWHM of  $0.0021 \text{ cm}^{-1}$ , and a HWSD of  $0.0009 \text{ cm}^{-1}$ . Examples of fitted peaks, residuals and numeric output for O<sub>2</sub> and NO are in Chapter 4. We were able to observe the quality of the fit using the numerical data output and residuals with each fit. We looked for patterns in the residuals which would have signaled a fitting algorithm problem. For example negative residuals in peak center, positive residuals in wings would mean the peak is more Lorentzian than a true Voigt curve. Positive in the center and negative in the wings tells us that our line is more Gaussian than Voigt (Pope, private conversations). A high  $r^2$  value close to unity meant a good fit as well as a low standard error in the Lorentzian width (Wolf, private conversations). We were able to extract the Lorentzian width and the standard error from the data for our next step. We sorted the fitted peaks according to J’ number and branch in preparation for the next step.

After we curve fit all the peaks the next step was to calculate the pressure broadening coefficients for each J’ line. We used a program called Table Curve to plot Lorentzian HWHM vs. rotational quantum number. We then used a least squares fit to a straight line over our points (Bevington, 1992). First, we had to assign weights to the points using:

$$Weight = \frac{1}{error^2} \quad (2-20)$$

using the standard error in the peak width (Bevington, 1992). Usually, the sum of the weights are normalized to unity, but Table Curve allows us to avoid that last calculation with an internal normalization procedure. Examples of these plots, the residuals and numeric data can be found in Chapter 4 with the results discussion. Again, we were able to monitor the fit quality with the numerical output data. A high  $r^2$  meant a good fit. Using the residuals, we were able to watch for points which were more than 2 standard deviations away from the fit line, which would signal bad data..

Using functions built into Table Curve, we were able to extract the slopes of the lines (parameter B) which gave us the pressure broadening coefficients for each  $J''$  and the standard error which we used for the error bars (Spencer, 1994). We then plotted the pressure broadening coefficients vs.  $J''$  and observed the pattern. We also converted  $\gamma_0$  to cross section,  $\sigma$ , and plotted these vs.  $J''$  and observed the pattern. We also compared  $\sigma$  to polarizability and reduced mass of the collision pair for each line.

### **III. Results and Discussion**

#### **O<sub>2</sub> Study**

##### **Spectrum Production**

We inspected the spectra to determine whether or not they were usable. The line centers were in the proper places (Burch, 1969), and the signal to noise ratio was acceptable in that the line peaks were more than an order of magnitude greater than the noise level. In the edges of the branches,  $J'' > 17$  in the P- and R-branches, and less than  $J'' = 2$  in the R-branch, the signal to noise ratio was too low for a usable fit. The peaks there were often asymmetrical due to low SNR and often were not resolvable from the noise. We didn't expect good fits to these peaks, but attempts were made, as shown in Figure 3-1. Data runs with 100 scans reduced this problem somewhat and allowed us to resolve peaks at  $J'' > 15$  in both branches. In general, the signal to noise ratio was greater by a factor of 2 in the P-branch than in the R-branch due to the spectrum location with respect to the filter curve. Figure 3-2 shows this effect. Notice how the R-branch rides on the downswing of the curve where intensity from the source was decreased by the filter. We could not eliminate the filter without saturating the detector, and we were limited by time so we couldn't repeat the experiment with another filter centered in the R-branch. So we had to accept this problem in the R-branch. When we used the Bomem software's "Absorption" feature to convert the spectra from transmission to absorption data, we had no problems. We kept the baselines around zero by using the filter background file that matched the spectrum. See (Figure 3-3) for an example of a baseline curve.

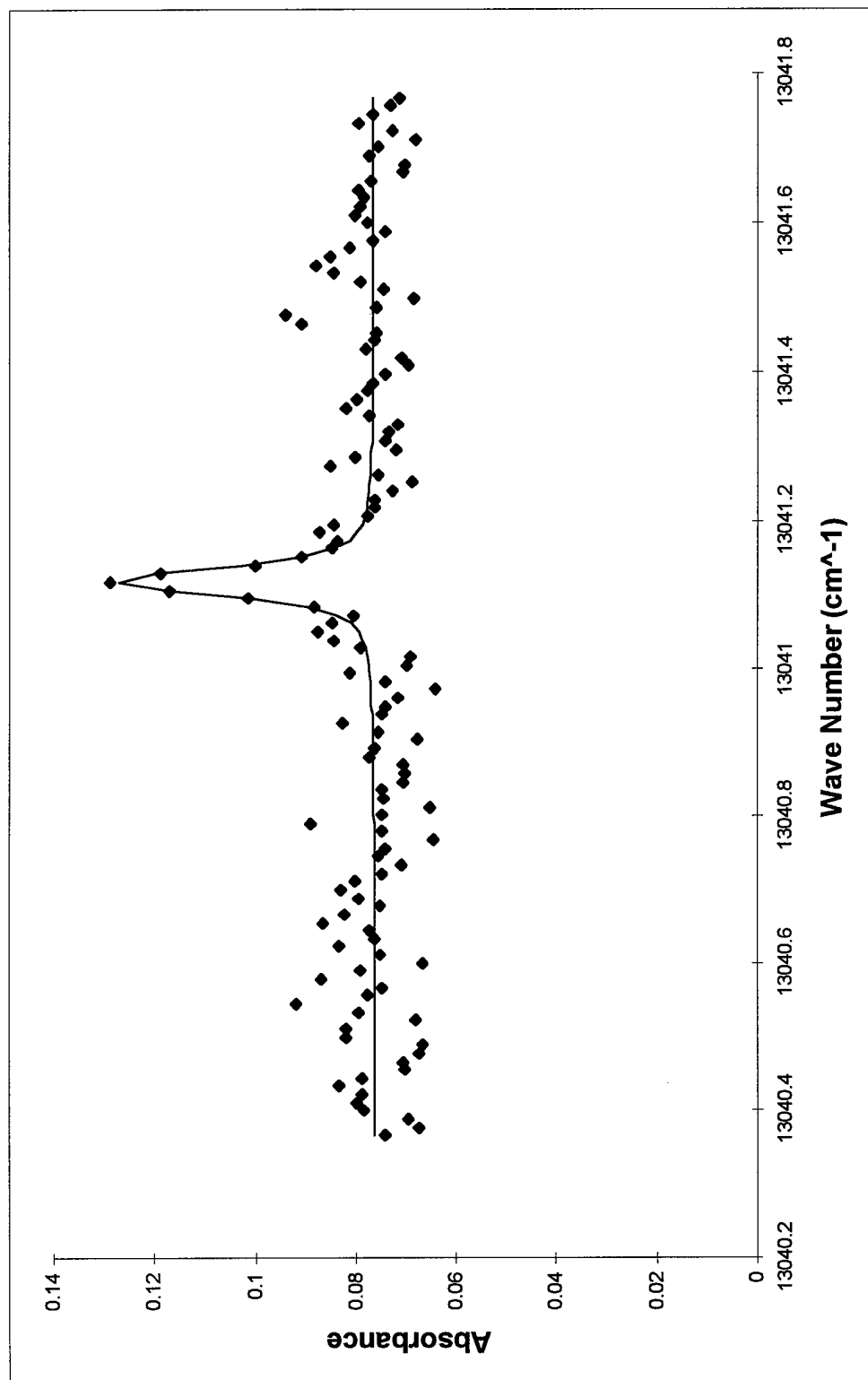


Figure 3-1: O<sub>2</sub> line with low signal to noise ratio and Peak Fit attempt.

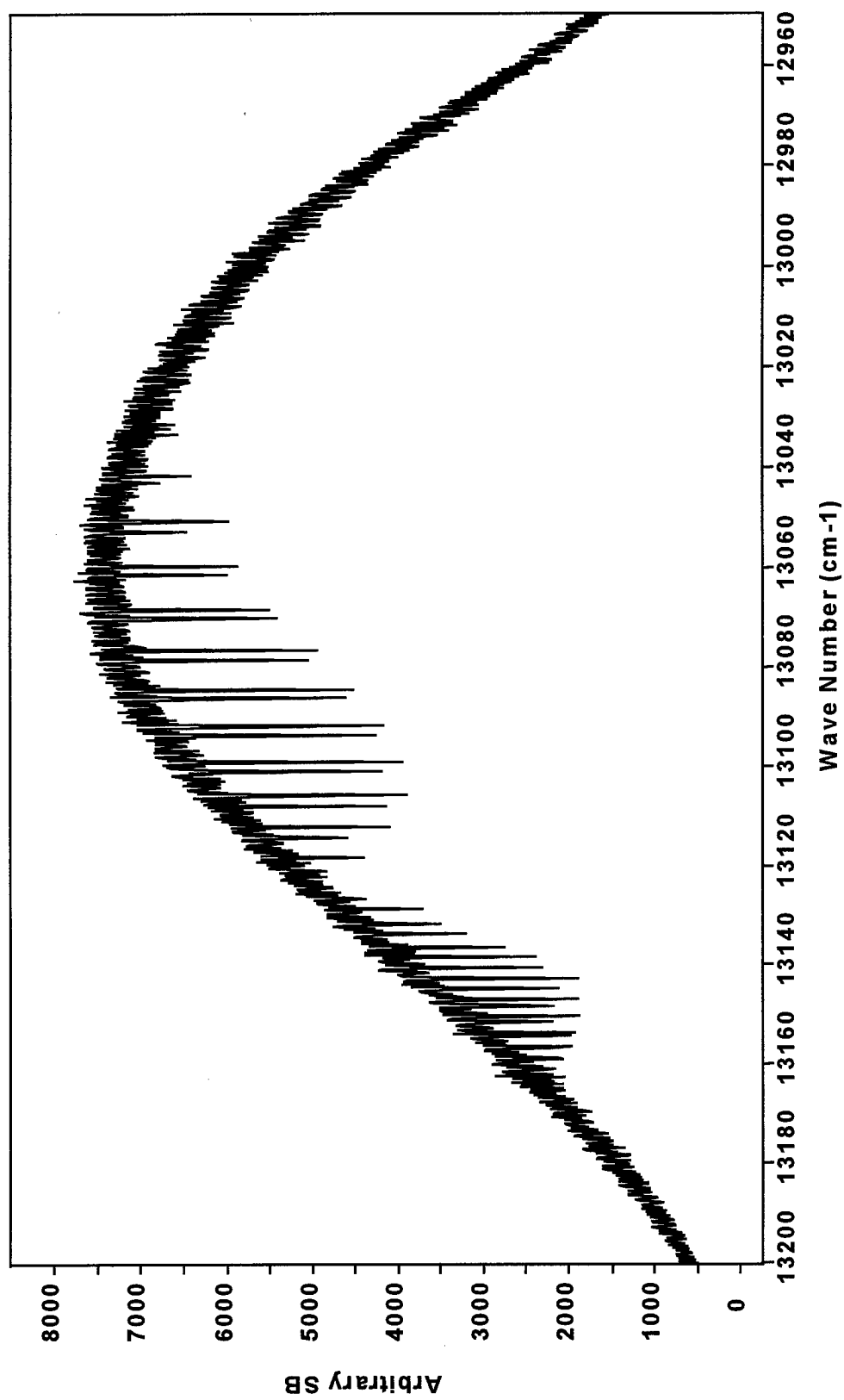


Figure 3-2: Raw  $O_2$  spectrum (output from spectrometer).

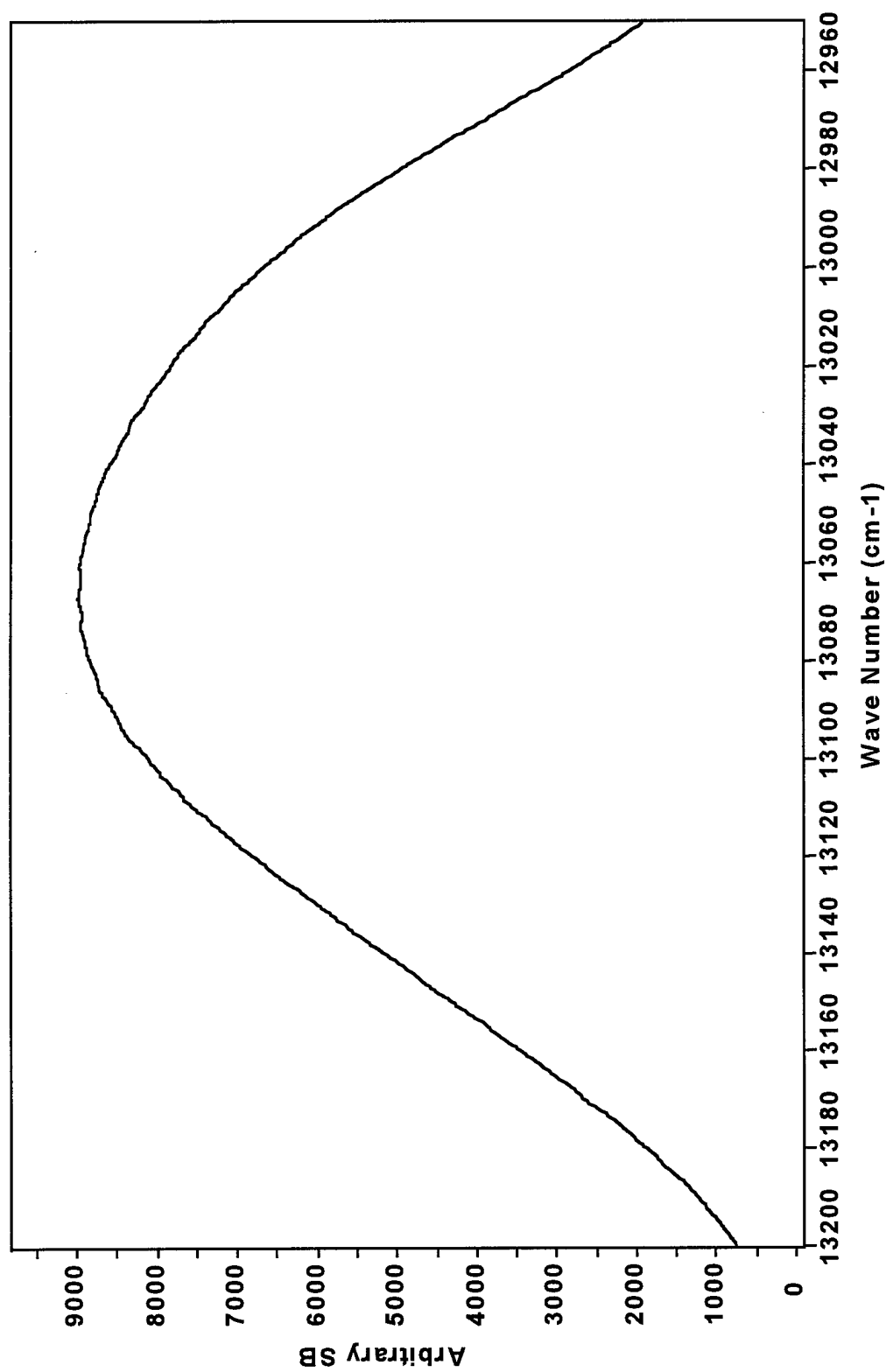


Figure 3-3: O<sub>2</sub> study filter background trace.

## **Peak Fitting**

Using the method discussed in Chapter 2, we fit the data with Voigt curves. As it turned out, the curve fitting software corrects for non-zero baseline anyway using two baseline parameters. For the peaks where  $J'' < 17$  in the P-branch and  $J'' < 15$  in the R-branch, fits were generally good with  $r^2$  greater than .960 in most cases. Where  $J'' < 13$  and  $J'' > 2$  in both branches,  $r^2$  were generally greater than .980 in both branches and in the center 7 lines of each branch, the  $r^2$  were generally greater than .990. Deviations from this trend were greater with the heavier broadeners like xenon and nitrogen. We inspected the residuals during each fitting session for each peak and we did not notice any patterns which would signal a fitting function problem (Pope, private conversations). See Figure 3-4, 3-5, and Table 3-1 for an example of a fitted peak, residuals and numeric data output.

We did, however, notice a feature on either side of the peaks which we attributed to the slight misalignment of the spectrometer (Pope, private conversations and Eliades, private conversations). This feature was a small positive peak above and a small negative peak below in energy to the peaks themselves. See Figure 3-6 for an example. Time constraints prevented us from exploring this problem further, and this feature did not affect the fit. It did, however, increase the residuals on either side of the peak where the baseline should be zero and probably caused our  $r^2$  values to be slightly higher. This probably led to slightly larger error bars on our data points, but as will be shown later, our data has not been affected.

We then extracted the Lorentzian half width at half maximum for each peak and plotted them vs. pressure of broadening gas to determine  $\gamma_0$ .

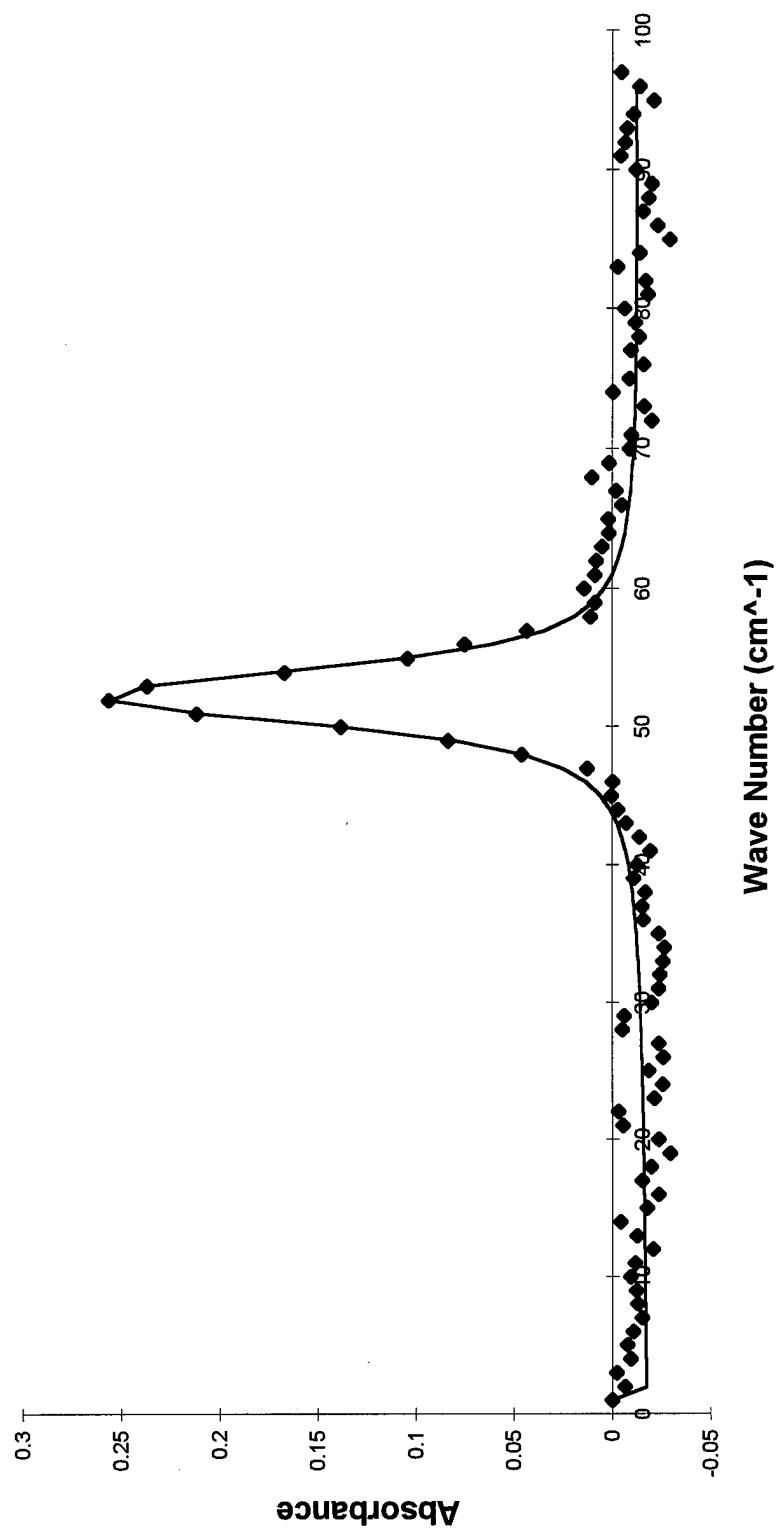


Figure 3-4: Example of a fitted O<sub>2</sub> peak at J''= 9 in the P-branch (200 Torr O<sub>2</sub>, 200 Torr Kr).

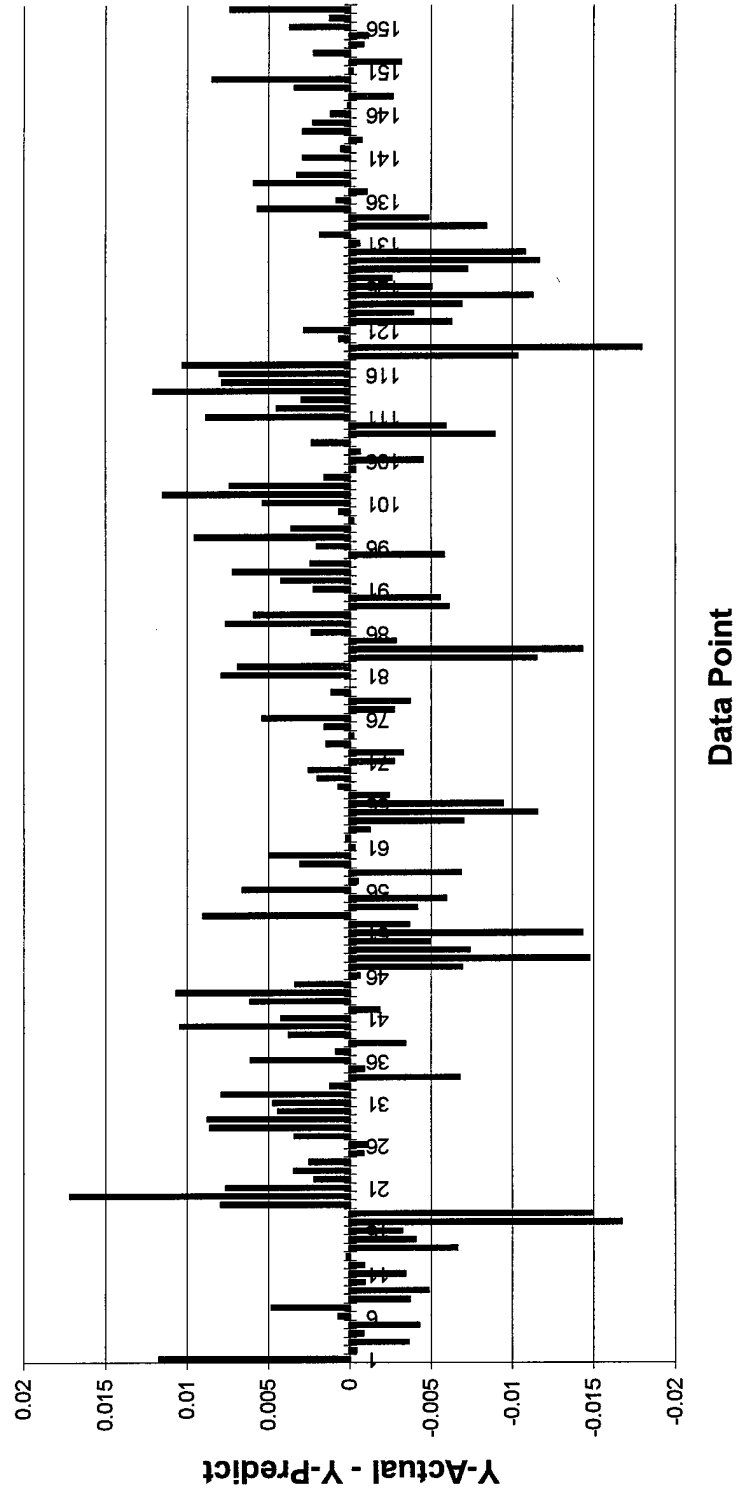


Figure 3-5: Residuals for Figure 3-4.

**Table 3-1: Numeric output for curve fit of Figure 3-4**

<u>Fitted Parameters</u>					
r <sup>2</sup>	Coef Det	DF	Adj r <sup>2</sup>	Fit Std Err	F-value
0.97228002	0.97136818		0.00633341	1341.62128	
Peak Type	a0	a1	a2	a3	
1 Voigt Area G/L	0.02192464	13091.7031	0.01189051	0.02638213	
B Linear Bg	42.1652823	-0.0032245			
<u>Measured Values</u>					
Peak Type	Amplitude	Center	FWHM	Asym50	FW Base
Asym10					
1 Voigt Area G/L	0.22852398	13091.7031	0.06545989	0.99831899	0.19511031
0.99937457					
Peak Type	Anlytc Area	% Area	Int Area	% Area	Centroid
Moment2					
1 Voigt Area G/L	0.02192464	100.000000	0.02150610	100.000000	
13091.7035	0.02533635				
Total	0.02192464	100.000000	0.02150610	100.000000	
<u>Parameter Statistics</u>					
Peak 1 Voigt Area G/L					
Parm	Value	Std Error	t-value	95% Confidence Limits	
Area	0.02192464	0.00018359	119.418725	0.02156193	0.02228734
Ctr	13091.7031	0.00022992	5.6941e+07	13091.7027	13091.7036
Wid	0.01189051				
Wid2	0.02638213	0.00035580	74.1490969	0.02567921	0.02708504
<u>Baseline Linear Bg</u>					
Parm	Value	Std Error	t-value	95% Confidence Limits	
a0	42.1652823	5.10650157	8.25717602	32.0769272	52.2536373
a1	-0.0032245	0.00039006	-8.2667757	-0.0039951	-0.0024539

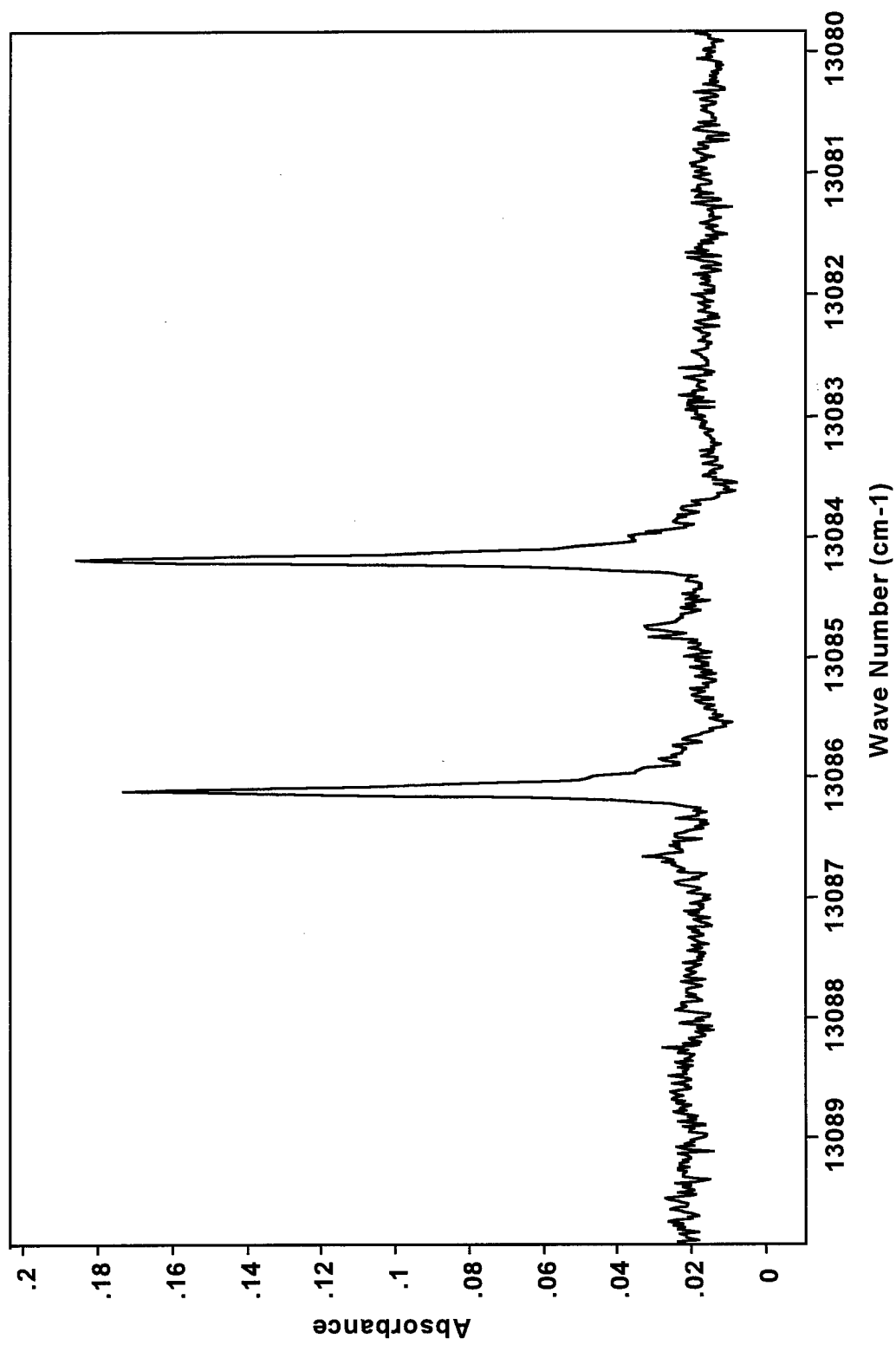


Figure 3-6: (Misalignment?) feature in O<sub>2</sub> spectrum lines  $J'' = 10, 11$  in the P-branch (200 Torr O<sub>2</sub>, 400 Torr N<sub>2</sub>).

### **$\gamma_0$ Determination**

$\gamma_0$  determination went well in that the peaks in the good range of each branch had linear least squares fits better than 0.960 in most cases. The edges of the branches were unreliable due to the original signal to noise problem at the branch ends. In the better parts of the branches, the deviations of the fits were most often less than one standard deviation from the data. An example of a  $\gamma_0$  determination plot is in Figure 3-7. The software made it easy to extract and plot the slope of the linear fit, which gave us  $\gamma_0$ , since the slope is a parameter of the fit. We then plot  $\gamma_0$  vs.  $J''$ .

### **$\gamma_0$ vs. $J''$ Pattern Study**

We examined the pattern of  $\gamma_0$  vs.  $J''$  and compared the pattern to other research. Theory states that  $\gamma_0$  should increase with decreasing  $J''$  (Burch, 1969, and Ritter, 1987) and our data followed this pattern. The work of Ritter, et. al. (1987) was the only noble gas broadening data to compare to, and as discussed in Chapter 1, it was mostly theoretical and partially experimental. We then compared our pattern to Ritter's. His data fits well with ours but our data is much more precise. Our data neatly overlays his and we got increasing  $\gamma_0$  with increasing reduced mass of broadener, except for helium. We do not know why helium does not fit this trend. We did notice a smoother adherence to the pattern in the P-branch, in that the data were not as scattered above and below the theoretical  $\gamma_0$  line. All of the  $\gamma_0$  vs.  $J''$  plots are in Appendix B.

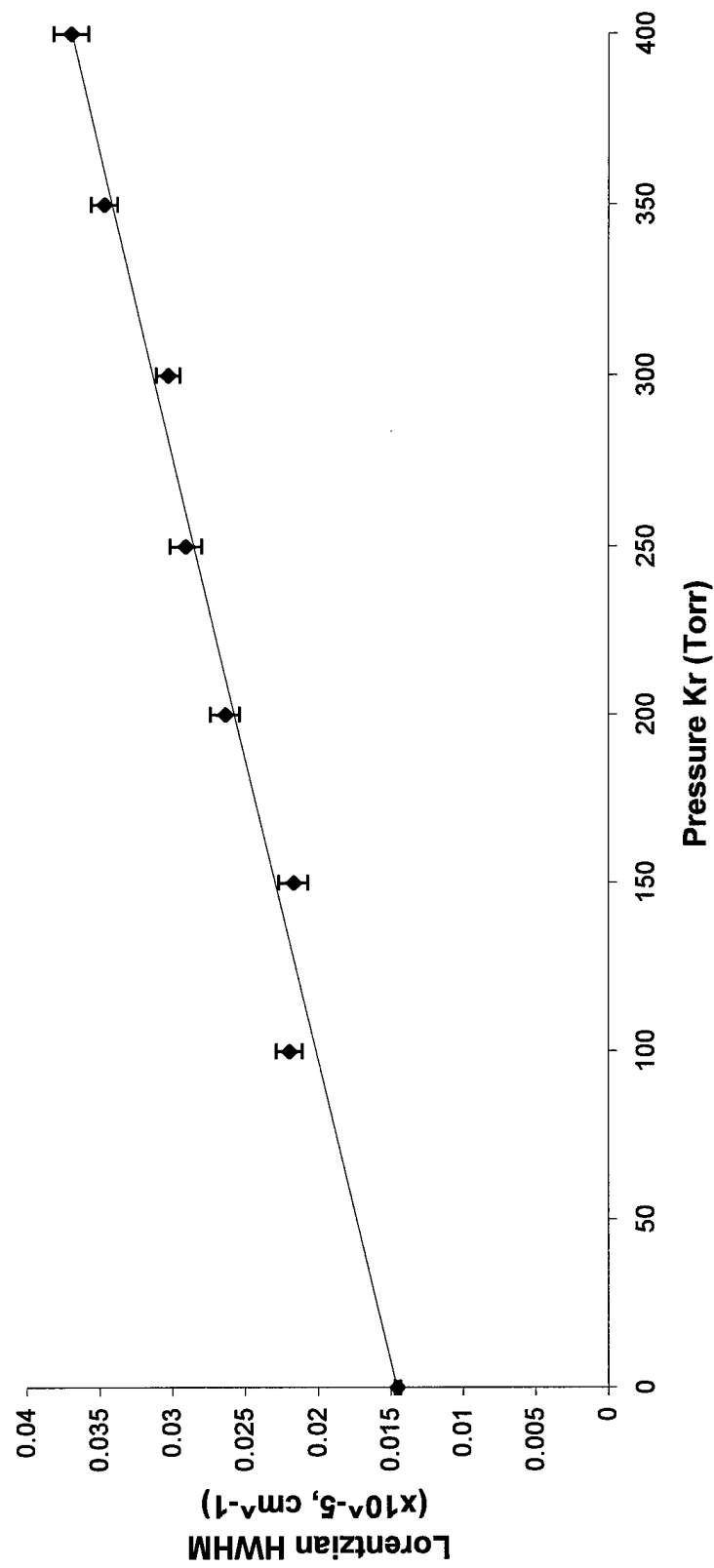


Figure 3-7: Example of Pressure Broadening Coefficient determination for the  $J'=9$  line of  $\text{O}_2$  in the P-branch (200 Torr  $\text{O}_2$ , 200 Torr Kr).

**Table 3-2: Numerical output accompanying O<sub>2</sub> Pressure Broadening Coefficient determination plot.**

Description: Oxygen Broadened With Krypton J = -9 (P-Branch)						
Rank 1 Eqn 8160 [Line Robust None, Gaussian Errors] y=a+bx						
r^2	Coef Det	DF	Adj r^2	Fit Std Err	F-value	
0.9935770575	0.9910078805	0.0005940455	928.15128717			
Parm	Value	Std Error	t-value	95% Confidence Limits		P> t
a	0.014542606	0.000234882	61.91448221	0.01396787	0.015117341	0.00000
b	5.61088e-05	1.84171e-06	30.46557544	5.16023e-05	6.06154e-05	0.00000
Area Xmin-Xmax Area Precision						
10.305749984	0					
Function min	X-Value	Function max	X-Value			
0.0145426056	1.073612e-10	0.0369861444	400			
1st Deriv min	X-Value	1st Deriv max	X-Value			
5.610885e-05	97.882266076	5.610885e-05	24.960226003			
2nd Deriv min	X-Value	2nd Deriv max	X-Value			
-5.42101e-12	38.569973566	5.421011e-12	58.043112471			
Procedure Minimization Iterations						
LevMarqdt	Least Squares		6			
r^2	Coef Det	DF	Adj r^2	Fit Std Err		
0.9935770575	0.9910078805	0.0005940455				
Source	Sum of Squares	DF	Mean Square	F Statistic	P>F	
Regr	0.00032753535	1	0.00032753535	928.151	0.00000	
Error	2.1173403e-06	6	3.5289004e-07			
Total	0.00032965269	7				
Date	Time	File Source				
Sep 16, 1997	9:34:58 AM	c:\cornice\analysis\o2kr\p branch\o2kr jn9b.prn				

## **NO Study**

### **Spectrum Production**

Now, let's consider the NO experiment. As with O<sub>2</sub> we inspected the spectra for usability. The centers were in the correct places (Spencer, 1984) and the signal to noise ratio was good. For both the 1/2 and 3/2 state, the peak intensities were more than an order of magnitude greater than the noise except where  $J'' > 18.5$  in the P-branch and  $J'' > 14.5$  in the R-branch (See Figure 3-8). The Q-branch lines were of usable signal to noise ratio for  $J'' < 6.5$  for the 3/2 state. All of the 1/2 state lines in the Q-branch were not resolvable over the noise (see Figure 3-9). The reduced intensity problem we had with the O<sub>2</sub> R-branch was not evident with NO as the spectrum was centered well on the filter curve. See Figure 3-10 for an example of this raw NO spectrum.

### **Peak Fitting**

Here is where our experiment with NO begins to produce substandard results. We knew from the fact that all of our lines were  $\Lambda$ -doubled, and that we would have to fit two very closely spaced lines for the 1/2 state. The individual e and f lines of the 3/2 state were not resolvable. So we attempted to fit the 1/2 state lines with two Voigt curves, and fit the 3/2 state lines with one Voigt as an unresolved doublet. The 3/2 state lines were not able to be fitted this way and  $r^2$  values were rarely better than 0.800 (See Figure 3-11, 3-12 and Table 3-2). We concluded that we would concentrate solely on the 1/2 state. See Figure 3-13, 3-14 and Table 3-3 for an example of a fitted NO doublet of the 1/2 state. Fits here were better, although not to the same quality as with O<sub>2</sub>. Our  $r^2$  values were on the orders of 0.920 for the best part of the spectra and 0.880 for the edges of the

P- and R-branches. The Q-branch was not resolvable for the  $1/2$  state. We concluded that we were probably not fitting the curves with the proper function for the  $1/2$  state as well. When we examined the  $3/2$  state fits themselves we noticed a difference between the e and f  $\Lambda$ -double line widths inconsistent with Spencer's  $N_2$  data. We concluded that the curve fitting of the double peaks was not proper in that the  $\Lambda$ -doublets' Lorentzian widths were being allowed to vary. We did not think we should lock them at the time since this would prevent the fit from accurately representing the actual data. Time constraints prevented us from examining other functions or curve fitting algorithms, so we pressed on to see what kind of  $\gamma_0$  values we would get.

#### $\gamma_0$ Determination

$\gamma_0$  determination went better than expected in that the peaks in the good range of each branch had linear least squares fits better than .960 in the very center of the branches. Outside the branch centers, the  $r^2$  dropped into the .900 -.950 range and in the edges of the branches the fits were unreliable due to the original signal to noise problem at the branch ends. In the best parts of the branches, the deviations of the fits were most often less than one standard deviation from the data. An example of a  $\gamma_0$  determination plot is in Figure 3-15. We then plot  $\gamma_0$  vs.  $J''$  and studied the pattern. We also converted  $\gamma_0$  to a cross section,  $\sigma$ , plotted it vs.  $J''$  and studied the pattern. We proceeded by comparing cross section to polarizability for each line and cross section to reduced mass of the collision pair for each line.

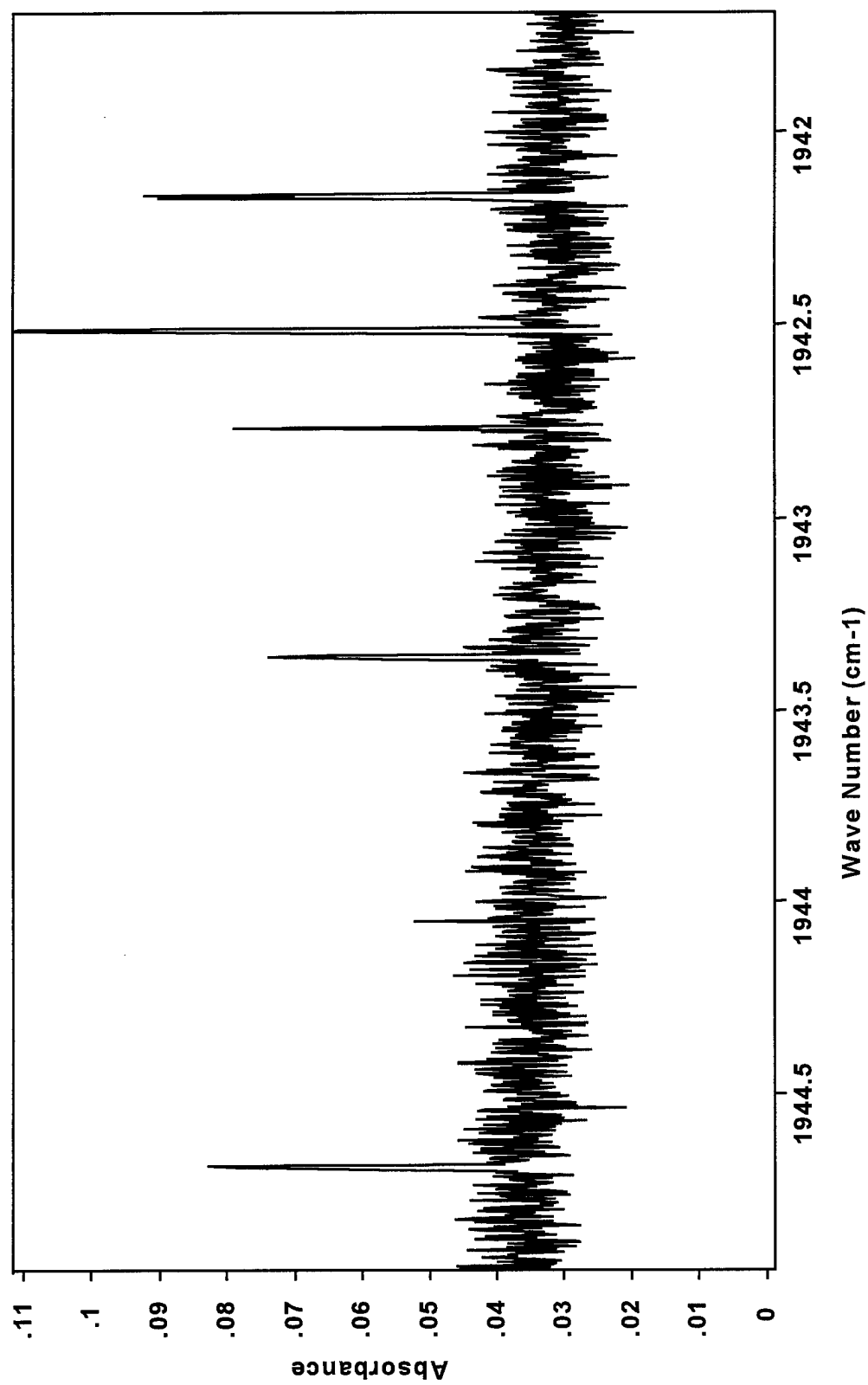


Figure 3-8: Unresolvable NO lines at  $J'' = 21.5$  in the P-branch (500mTorr NO, 10 Torr Xe).

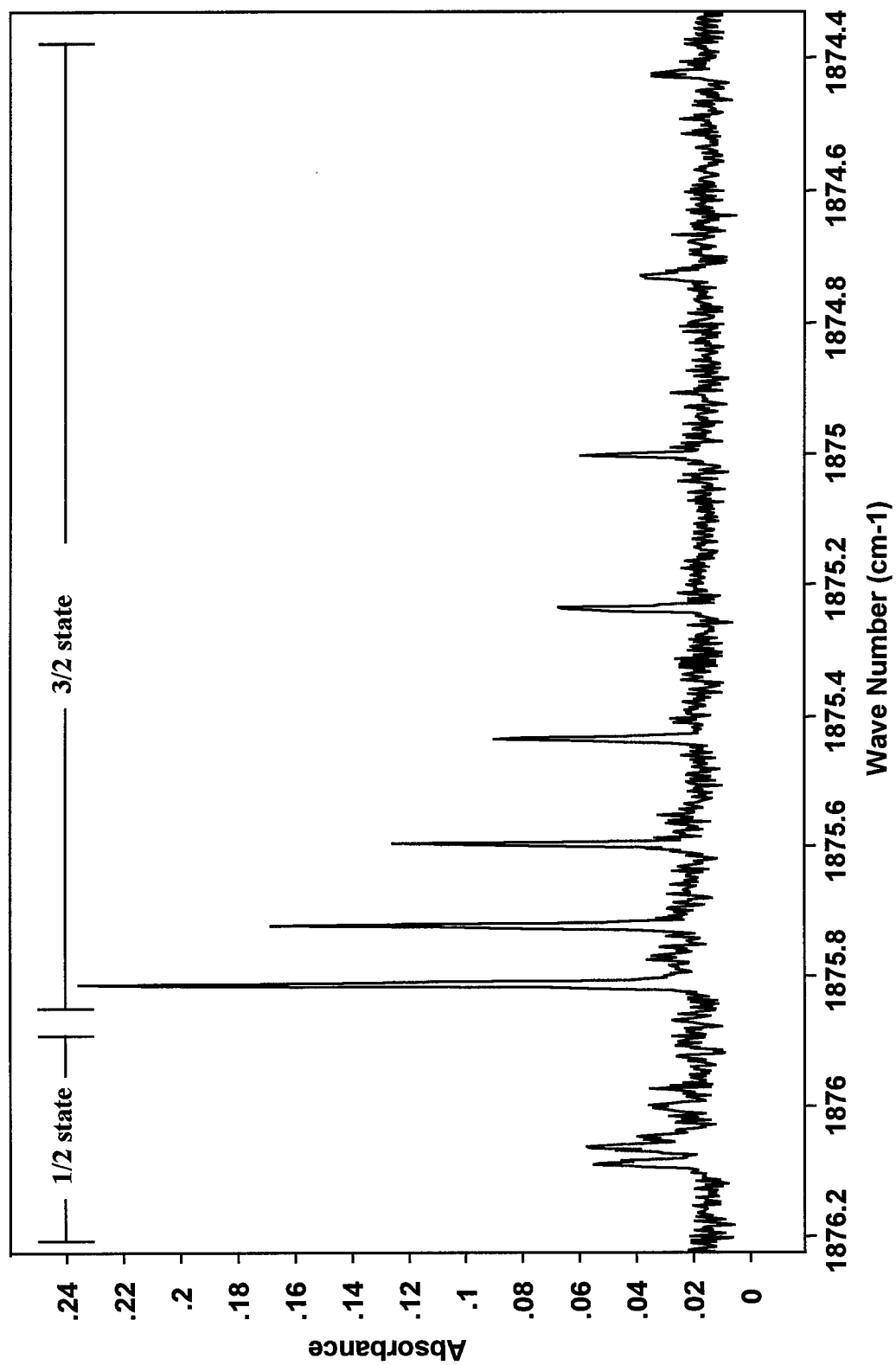


Figure 3-9: NO Q-branch (500 mTorr NO, 10 Torr Xe)

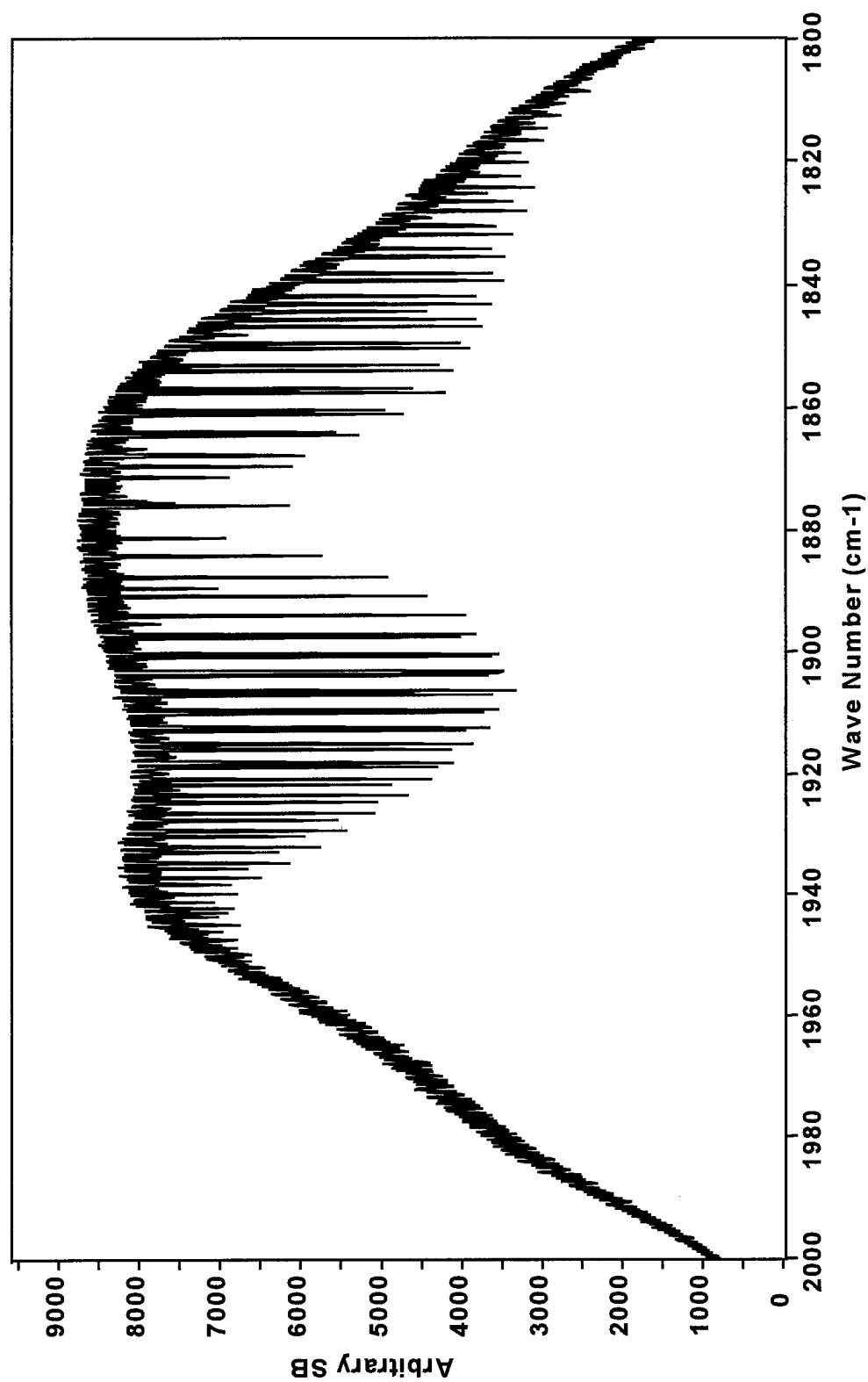


Figure 3-10: Raw NO spectrum (500 mTorr NO, 40 Torr Ar).

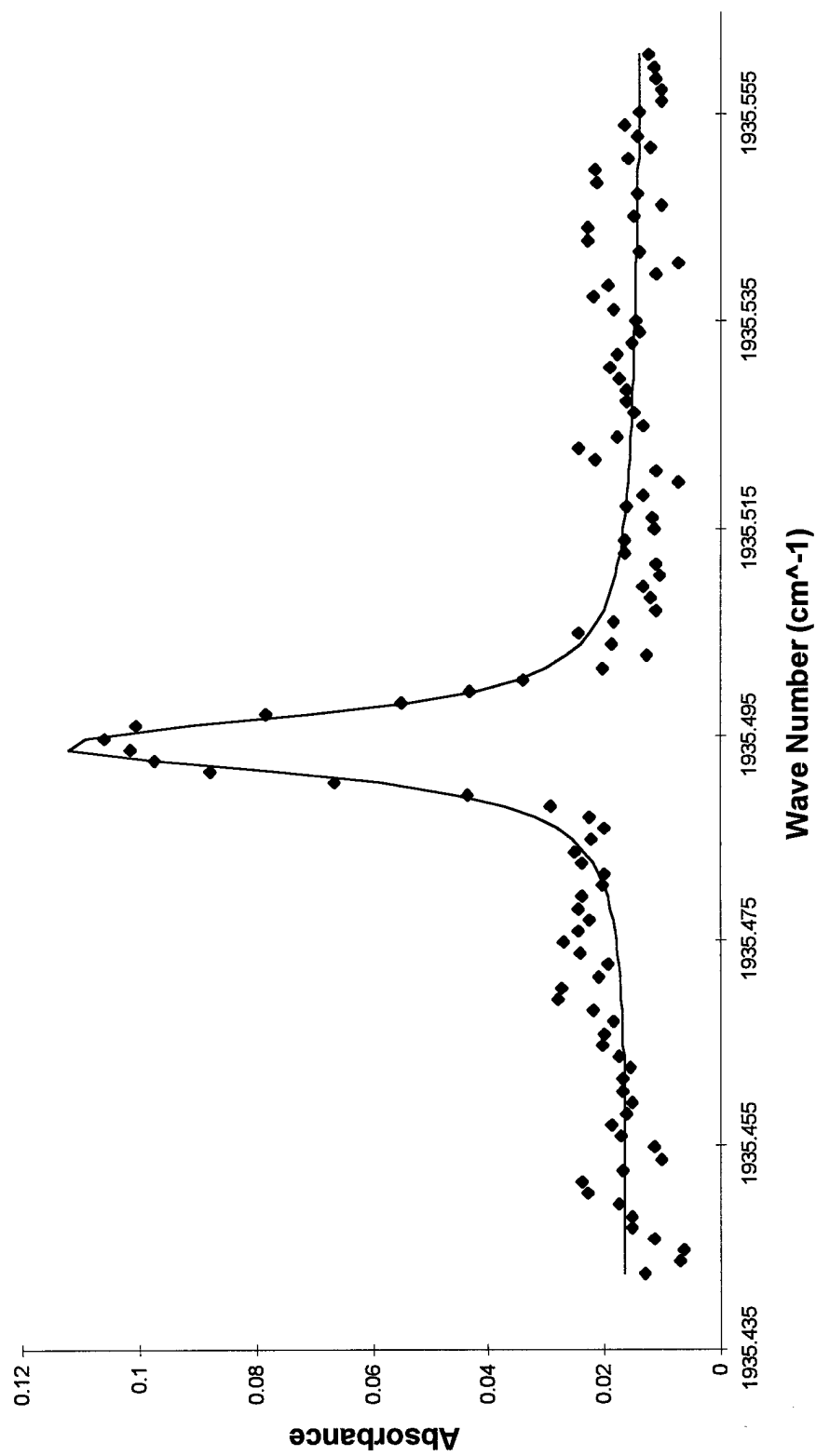
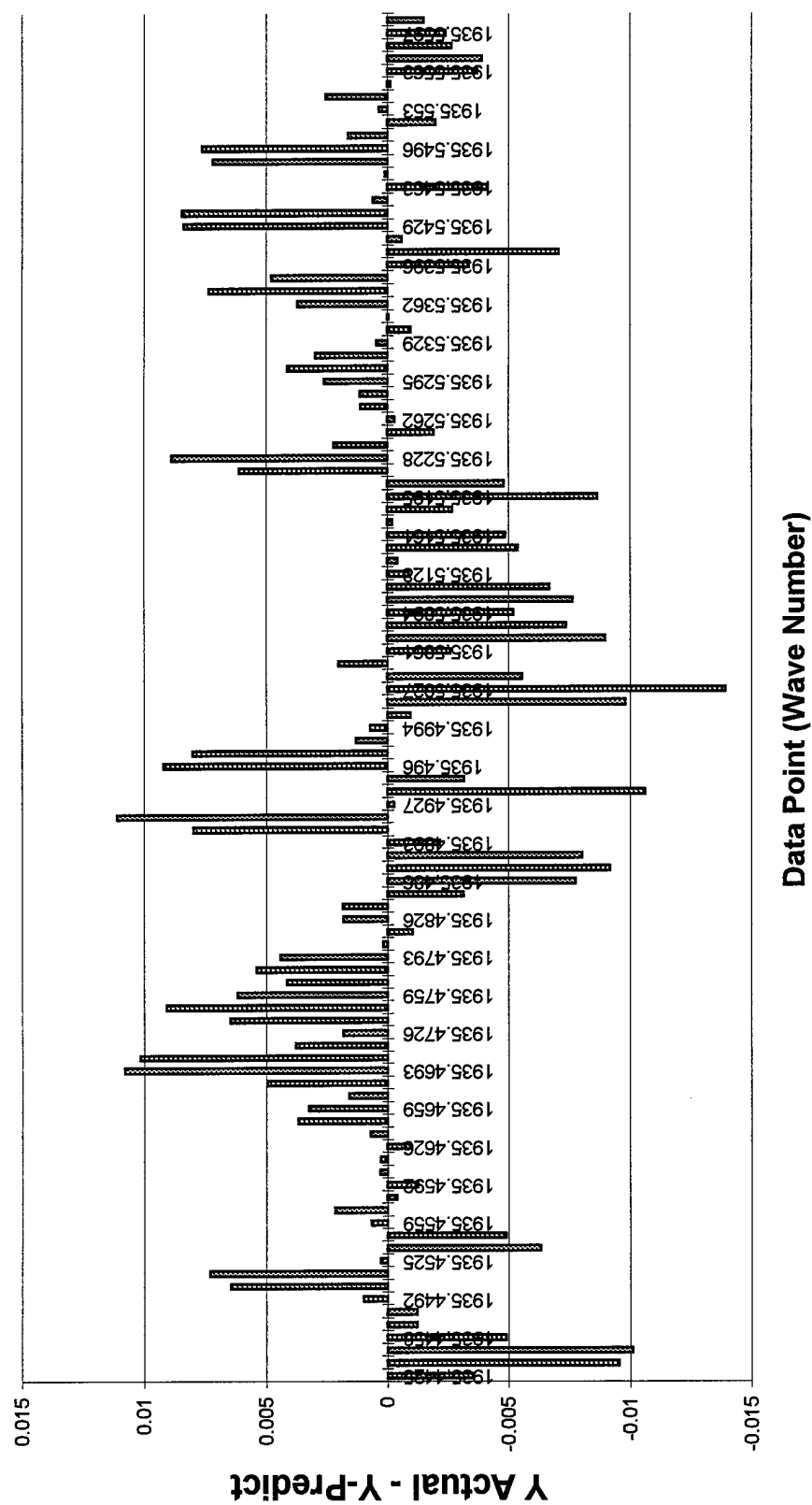


Figure 3-11: Curve fit of an unresolved 3/2 state  $\Lambda$ -doublet of NO at  $J'' = 18.5$  in the R-branch (500 mTorr NO, 55 Torr Kr).



**Table 3-3: Numeric output for curve fit of 3/2 state NO line at J'' = 18.5 in the R-branch (500 mTorr NO, 55 Torr Kr).**

Description: C:\Cornice\Nokr004a.prn

File Source: c:\cornice\nokr004a.prn

#### Fitted Parameters

r<sup>2</sup> Coef Det DF Adj r<sup>2</sup> Fit Std Err F-value  
 0.92792494 0.92435687 0.00542198 328.297840

Peak Type	a0	a1	a2	a3
1 Voigt Area G/L	0.00099319	1935.49422	0.00089596	0.00298624
B Linear Bg	40.6595230	-0.0209995		

#### Measured Values

Peak Type	Amplitude	Center	FWHM
1 Voigt Area G/L	0.09817163	1935.49422	0.00668381

Peak Type	Anlytc Area	% Area	Int Area	% Area	Centroid
1 Voigt Area G/L	0.00099319	100.000000	0.00096078	100.000000	1935.49447
Total	0.00099319	100.000000	0.00096078	100.000000	

#### Parameter Statistics

Peak 1 Voigt Area G/L

Parm	Value	Std Error	t-value	95% Confidence Limits	
Area	0.00099319	1.7311e-05	57.3732070	0.00095885	0.00102752
Ctr	1935.49422	4.6875e-05	4.1291e+07	1935.49413	1935.49431
Wid	0.00089596				
Wid2	0.00298624	7.4152e-05	40.2720367	0.00283916	0.00313332

#### Baseline Linear Bg

Parm	Value	Std Error	t-value	95% Confidence Limits	
a0	40.6595230	11.7582276	3.45796360	17.3371343	63.9819117
a1	-0.0209995	0.00607502	-3.4567025	-0.0330493	-0.0089498

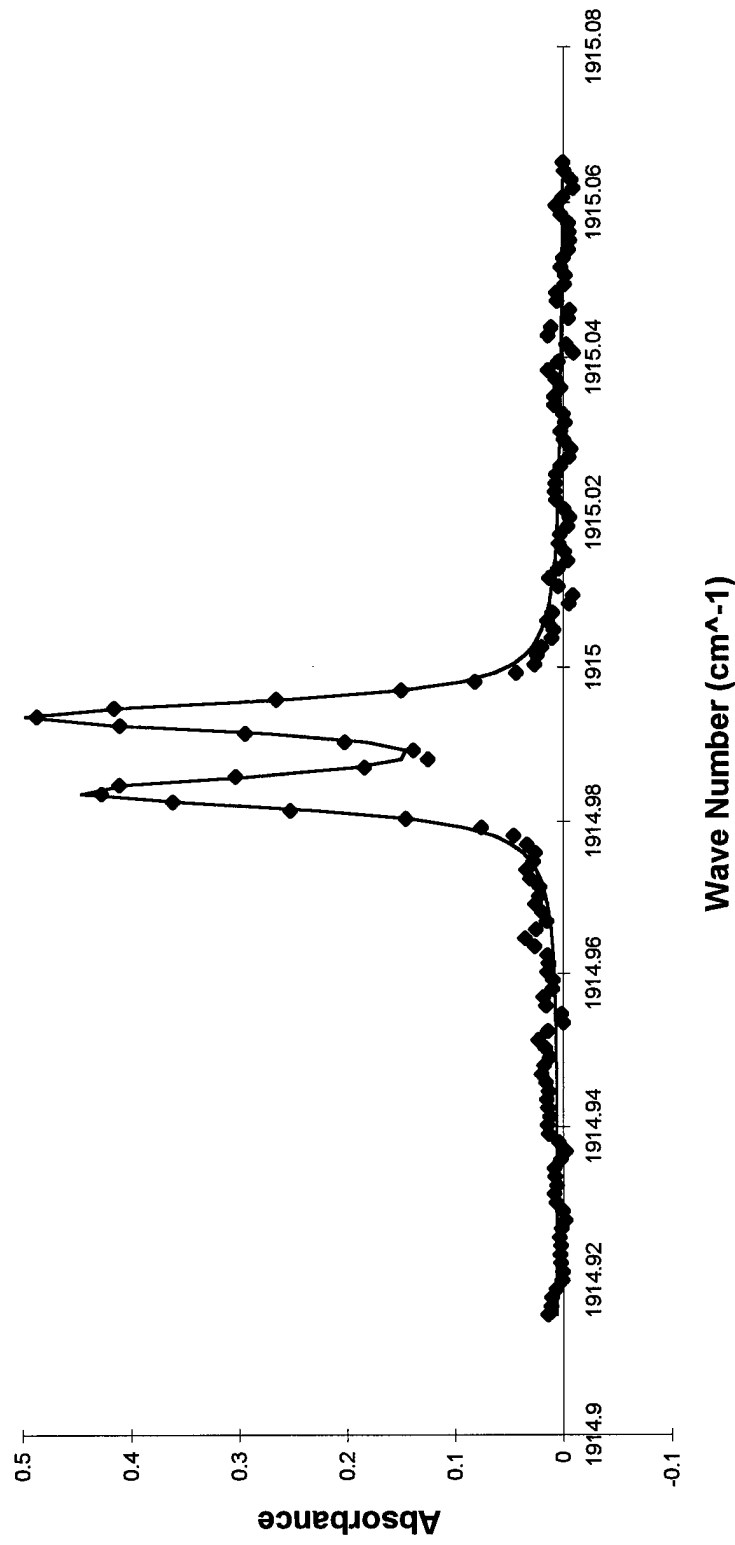


Figure 3-13: Curve fit of 1/2 state  $\Lambda$ -doublet of NO at  $J'' = 11.5$  in the R-branch (500 mTorr NO, 40 Torr Xe).

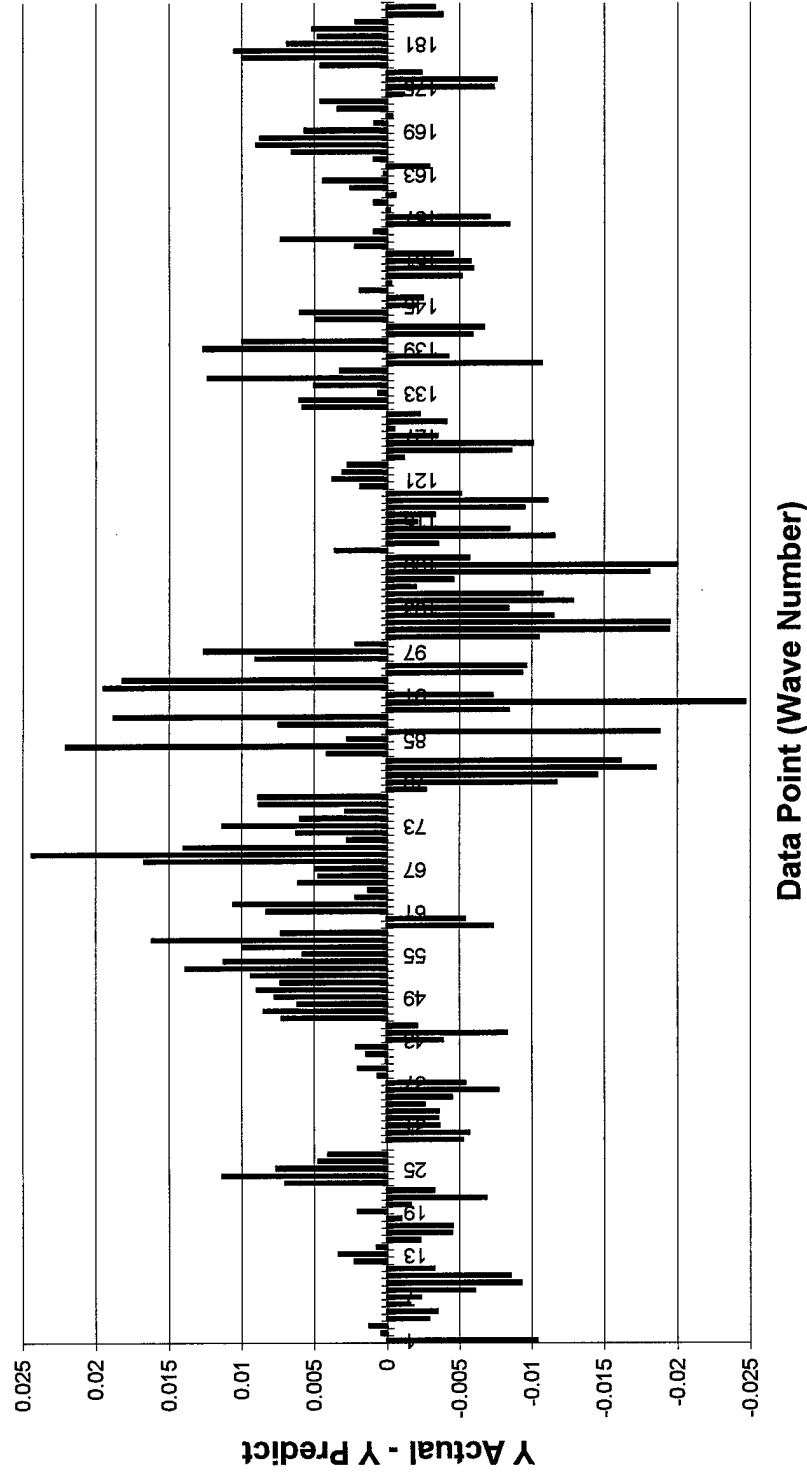


Figure 3-14: Residuals for Figure 3-13.

**Table 3-4: Numeric output for curve fit of 1/2 state NO line at J'' = 11.5 in the R-branch (500 mTorr NO, 40 Torr Xe).**

<u>Fitted Parameters</u>					
r <sup>2</sup>	Coef Det	DF	Adj r <sup>2</sup>	Fit Std Err	F-value
0.99069350		0.99027286		0.00849623	2706.91583
Peak	Type	a0	a1	a2	a3
1	Voigt Area G/L	0.00305848	1914.98390	0.00089596	0.00195231
2	Voigt Area G/L	0.00309749	1914.99375	0.00089596	0.00173255
B	Linear Bg	85.7730886	-0.0447891		
<u>Measured Values</u>					
Peak	Type	Amplitude	Center	FWHM	Asym50
FW Base					
1	Voigt Area G/L	0.42902518	1914.98390	0.00487265	1.00630255
1.00234583					
2	Voigt Area G/L	0.47542920	1914.99375	0.00450853	1.00218328
1.00082939					
Peak	Type	Anlytc Area	% Area	Int Area	% Area
Centroid					
1	Voigt Area G/L	0.00305848	49.6831294	0.00302143	49.6470078
0.00012771					
2	Voigt Area G/L	0.00309749	50.3168706	0.00306439	50.3529922
0.00011288					
Total		0.00615598	100.000000	0.00608582	100.000000
<u>Parameter Statistics</u>					
Peak 1 Voigt Area G/L					
Parm	Value	Std Error	t-value	95% Confidence Limits	
Area	0.00305848	2.3062e-05	132.618776	0.00301297	0.00310399
Ctr	1914.98390	1.4457e-05	1.3246e+08	1914.98388	1914.98393
Wid	0.00089596				
Wid2	0.00195231	2.3527e-05	82.9813428	0.00190588	0.00199874
Peak 2 Voigt Area G/L					
Parm	Value	Std Error	t-value	95% Confidence Limits	
Area	0.00309749	2.1937e-05	141.197793	0.00305420	0.00314079
Ctr	1914.99375	1.2457e-05	1.5373e+08	1914.99373	1914.99378
Wid	0.00089596				
Wid2	0.00173255	2.0314e-05	85.2881380	0.00169246	0.00177264
<u>Baseline Linear Bg</u>					
Parm	Value	Std Error	t-value	95% Confidence Limits	

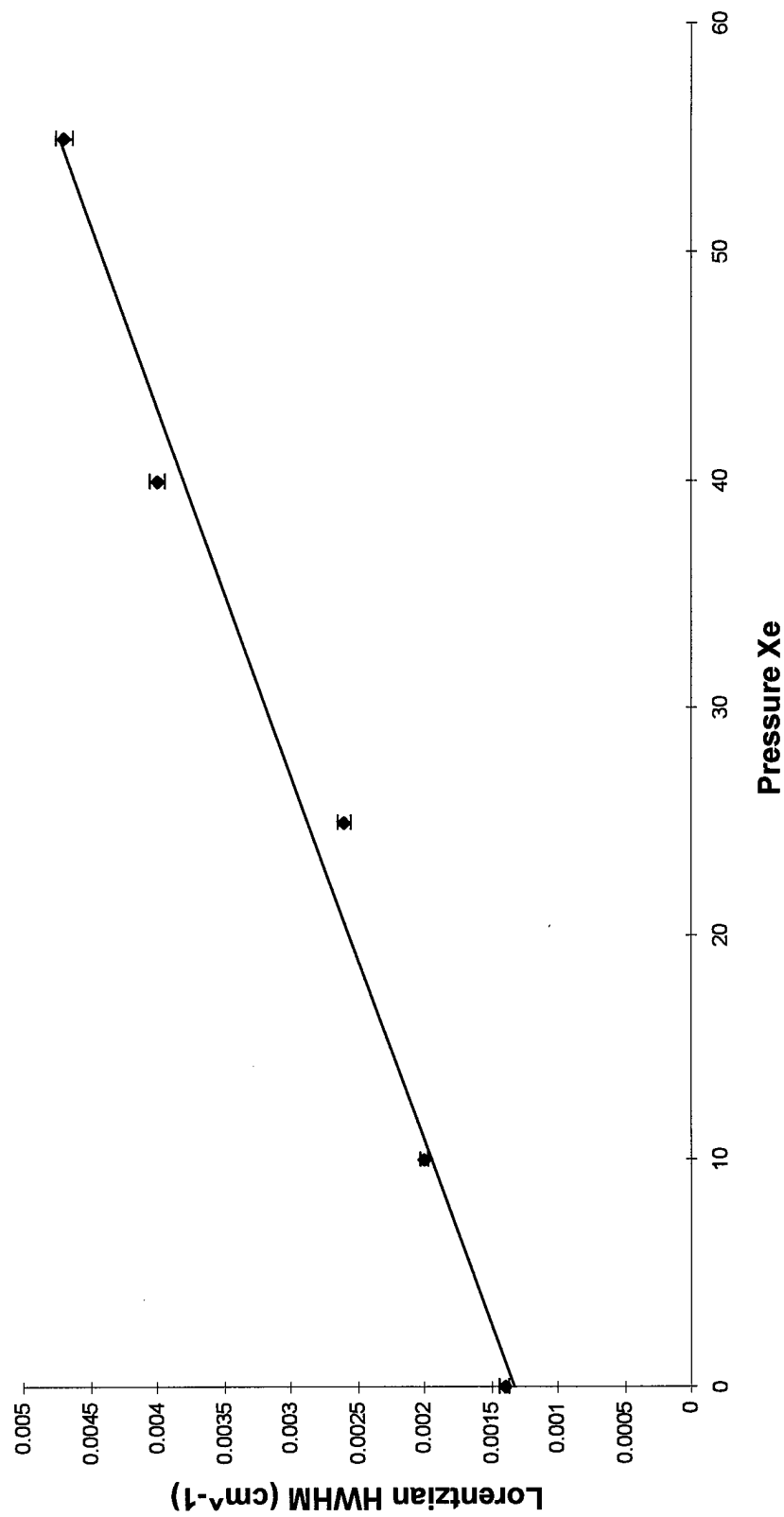


Figure 3-15: Example of Pressure Broadening Coefficient determination for the  $J''=6.5$  e line of NO in the P-branch (500 mTorr NO, 40 Torr Xe).

**Table 3-5: Numerical output accompanying NO Presure Broadening Coefficient determination.**

Description: NO Broadened with Xenon J6.5e (P-Branch)						
Rank 1 Eqn 8160 [Line Robust None, Gaussian Errors] y=a+bx						
XY *	X Value	Y Value	Y Predict	Residual	Residual%	Weights
1	0	0.0014	0.0014753	-7.53e-05	-5.376212	3.2e-05
2	10	0.0018	0.0019425	-0.000142	-7.916277	2.9e-05
3	25	0.0029	0.0026433	0.0002567	8.8506194	4.6e-05
4	40	0.0033	0.0033442	-4.42e-05	-1.338518	5.4e-05
5	55	0.004	0.004045	-4.5e-05	-1.125253	6.4e-05
r^2	Coef Det	DF	Adj r^2	Fit Std Err	F-value	
0.9790382962	0.9580765923		0.0001728954		140.1181369	
Parm	Value	Std Error	t-value	95% Confidence Limits		P> t
a	0.001475267	0.0001469	10.04265301	0.001007765	0.001942769	
0.00210						
b	4.67226e-05	3.94712e-06	11.83715071	3.41611e-05	5.92841e-05	
0.00130						
Area Xmin-Xmax Area Precision						
0.15180762 1.828339e-16						
Function min	X-Value	Function max	X-Value			
0.001475267	1.954254e-10	0.0040450101	55			
1st Deriv min	X-Value	1st Deriv max	X-Value			
4.67226e-05	30.259750649	4.67226e-05	33.975567574			
2nd Deriv min	X-Value	2nd Deriv max	X-Value			
-3.58414e-11	27.499946953	3.584144e-11	38.385123631			
Procedure	Minimization	Iterations				
LevMarqdt	Least Squares	6				
r^2	Coef Det	DF	Adj r^2	Fit Std Err		
0.9790382962	0.9580765923		0.0001728954			
Source	Sum of Squares	DF	Mean Square	F Statistic	P>F	
Regr	4.1885279e-06	1	4.1885279e-06	140.118	0.00130	
Error	8.9678496e-08	3	2.9892832e-08			
Total	4.2782064e-06	4				
Date	Time	File Source				
Sep 16, 1997	9:33:04 AM	c:\cornice\analysis\noxe\p-branch\noxep6.5e.prn				

### $\gamma_0$ vs. $J''$ Pattern Study

Here is where we were able to see direct evidence of our problem with NO. We had no actual experimental data to compare our noble gas broadening to and no researcher has calculated theoretical values like Ritter's with O<sub>2</sub>. When we plotted  $\gamma_0$  vs.  $J''$ , we compared our data to Spencer's 1994 N<sub>2</sub> experimental broadening data for an idea of how our pattern should look. We expected NO to follow a similar pattern as with O<sub>2</sub> and Spencer's N<sub>2</sub> broadening data in that  $\gamma_0$  should increase with decreasing  $J''$ . We expected a trend of increasing  $\gamma_0$  with increasing mass of broadener just like with our O<sub>2</sub> experiment and we expected helium to buck the trend. Since Spencer's N<sub>2</sub> data showed similar values for the e and f  $\Lambda$ -double lines, we expected the same trend with our noble gas broadening.

Our  $\gamma_0$  data did not have similar values for the e and f  $\Lambda$ -doubles in the P-branch, which was our first deviation from what was expected, but the values were close in the R-branch. In the R-branch, the e and f lines were separated by more than the separation of the P-branch lines and this helped the fitting algorithm treat them separately in most cases. The P-branch f lines always had a greater value of  $\gamma_0$  than the e lines, and the difference decreased to almost zero, but never quite consistently zero, in the lower 5 or 6  $J''$  doublets. In the R-branch, the doublets were nearly equal, although not as close as Spencer's, with no pattern of either the e or f lines having consistently higher  $\gamma_0$  than the other. This gave us an idea of where the actual  $\gamma_0$  is, although our errors were high. In the R-branch we saw a similar pattern as with O<sub>2</sub> where the higher mass broadeners produced higher  $\gamma_0$ . Since our experimental error was low, we conclude that this trend is

reliable. We were concerned that our experimental error was not consistent with the separation of values in the P-branch. This is understood to be caused by the fitting algorithm itself. It is fitting the peaks as it sees them, as two Voigts which are close together, with no restraints on their amplitudes or widths. So the fits are good, although not physically representative, since we know the widths and amplitudes should be similar (Spencer, 1994),

In general, our data is not more than an order of magnitude further from where we expected them to be. A hint of where we expect them to be is shown in Appendix B, where we averaged the e and f values. Although this gives us a ballpark figure to shoot for in further research, this averaging is not valid for determining actual values. We considered this theory, but when we examined the Voigt function, we discovered that the relationship of intensity to Lorentzian width is not quite linear.

We did not convert  $\gamma_0$  to  $\sigma$  for the NO study, nor did we compare  $\sigma$  to polarizability and reduced mass as with O<sub>2</sub>.

#### IV. Conclusion and Recommendation

##### O<sub>2</sub> Study

We were satisfied with our  $\gamma_0$  data and its correlation with Ritter's data. We were satisfied with the performance of both the curve fitting method and the method for determining  $\gamma_0$ . Here is how we would improve the data if given the time: First, we would ensure the spectrometer was better aligned to eliminate the spectral feature discussed in Chapter 3. This requires contractor intervention to determine if in fact it is aligned or not, and if not, what the problem is. Next, we would repeat the experiment with a filter centered over the R-branch to reduce signal to noise ratio there. We could also increase signal-to-noise ratio by coadding many 100 scan runs. This increases the time required for each data point, but as can be seen by comparing Figures 4-1 and 4-2, the signal to noise ratio seems to increase by about factor of the square root of the number of additional coadds of 100 scan runs.

When we examined our plots of  $\sigma$  vs.  $J''$  (Figure 4-3) we found that the pattern of increasing  $\sigma$  with decreasing  $J''$  followed the same trend as with  $\gamma_0$ . It is not known quantitatively why this pattern should be so, but it is nonetheless understandable that there should be a variation. Using a classical analogy, imagine a collision between a spinning molecule and a hard sphere. The collision will act differently if the molecule is spinning rapidly than if it is spinning slowly with respect to the speed of collision. In the collision between the slow spinning molecule and the sphere, the sphere has more of a chance to

enter deeply into the potential of the molecule and approach the internuclear axis. During the collision process, the sphere will "see" different potentials depending on the direction of approach to the molecule. A collision between a fast-spinning molecule and a hard sphere will approach being a collision between two hard spheres. See Figure 4-3 for an example of a  $\sigma$  vs.  $J$  plot.

When we analyzed our plots of  $\sigma$  vs. polarizability, we found a linear relationship. This is understandable, since collisions are not hard sphere interactions. The collision partners' electron clouds interact during the collision, and depending on the size of the collision partner, there can be large or small changes to the cloud. Polarizability is a representation of the ability to change the cloud significantly enough to induce a dipole moment, and the moment will affect the collision potential. Understandably, the larger collision partners like Xenon had larger polarizabilities and hence, larger cross section,  $\sigma$ . Notice that  $N_2$  did not fit with the linear relationship, it being a diatomic molecule whose polarizability is more complex than the spherical noble gases. See Figure 4-4 for an example of a  $\sigma$  vs. polarizability plot. This kind of relationship will help us understand the collision potentials.

Next we compared  $\sigma$  to reduced mass of the collision pair. Using a classical approach, the linear dependence makes sense. Heavier collision partners will have larger cross sections. Figure 4-5 is an example of such a plot. Notice how  $N_2$  falls more into line with its mass. This, too will move us towards an understanding of the collision potentials.

Further research in this area can be done using  $\text{H}_2\text{O}$  as a broadener with the same pressures of  $\text{O}_2$ . A method of measuring the partial pressure of water vapor in the cell would be needed as well as a method of efficiently removing the water from the cell between measurements.

Another interesting experiment would be to do a study of temperature variation on collisional broadening of  $\text{O}_2$  using the noble gases as collision partners. Using materials available at present, we can cool the cell to temperatures of liquid nitrogen (77K), liquid helium (23K), the freezing point of water (273K), and room temperature (295K) (Wolf, private conversations). We would use these four temperature points and keep the pressure constant. We could then determine the temperature dependence of the collisional broadening of the  $\text{O}_2$  lines. Other methods of cooling the cell exist, including immersion in a liquid nitrogen bath and regulating the temperature with heating elements (Spencer, 1997). Heating the cell above room temperature is possible using either a heating element installed in the cell or by exciting the vibrational states of  $\text{H}_2\text{O}$  using microwave radiation. What is useful to the Air Force here is that the temperature range we would use spans the atmospheric temperature range, leading us to a method of temperature sounding the atmosphere remotely from space or ground.

## NO Study

Here, we have not sufficiently satisfied our goal of the determination pressure broadening coefficients for the two states of NO. If we had time here's what we planned to do to improve our results: First, we would eliminate the spectrometer feature discussed in Chapter 3. Again, this requires contractor intervention. We think our method of producing the spectra is sound, and can only be improved with higher resolution, which requires a spectrometer with a longer path length for the movable mirror (See Appendix A). We can improve signal to noise ratio next time by doing longer runs (greater than 100 scans per run) for each measurement, or by using the method of coadding many 100 scan runs discussed in the O<sub>2</sub> section. Since this requires much more time, this would require improving the gas handling system to eliminate leaks over the long term. The best idea is to pre-fill a glass cell with a rubber-seal-on-glass valve and place it in the spectrometer by itself each time with no gas handling system. We tried this once using CO as a broadening gas and got our highest signal to noise ratio so far and better resolution on the far lines in each branch. See Figures 4-1 and 4-2 for a comparison of our CO spectra. Note how the signal to noise ratio increases by a factor of the square root of the number of additional coadds in both the wing of the R-branch (Figure 4-6) and in the Q-branch (Figure 4-7).

Clearly, we are not fitting the peaks well. We need to modify the curve fitting algorithm to better handle the split peaks of the 1/2 state and the unresolved doublets of the 3/2 state. The Voigt profile should work, but we must reduce the number of free parameters in the fitting algorithm. With a single peak, we have three. But with a double

peak, we have six. If we lock the distance between the peak centers (Spencer, 1994) we will reduce the parameters by one. Our Peak Fit software does not have this feature. Next would be to try to hold the Lorentzian widths and/or the amplitudes of the two peaks constant (Liou and Torbert, 1987). This is physically acceptable, given that the populations in the two states should be equal at a given temperature (Burggraf, private conversations). This would further reduce the number of free parameters to four.

If that does not work, we could try fitting the peaks with a Galatry profile or a speed-dependent Voigt profile (Ritter, 1987). These were compared by Ritter, et. al. for their oxygen spectroscopy experiment in 1987, and they had the lowest residuals using the Galatry profile.

We are satisfied with the table Curve software for determining  $\gamma_0$  from the Lorentzian widths, since it works well with what it's fed. Future researchers are welcome to use our data and it has been archived in the Physics Department for this reason. Since, in general, NO collisional broadening is new research, the next step would be to explore molecular gas broadening of NO.

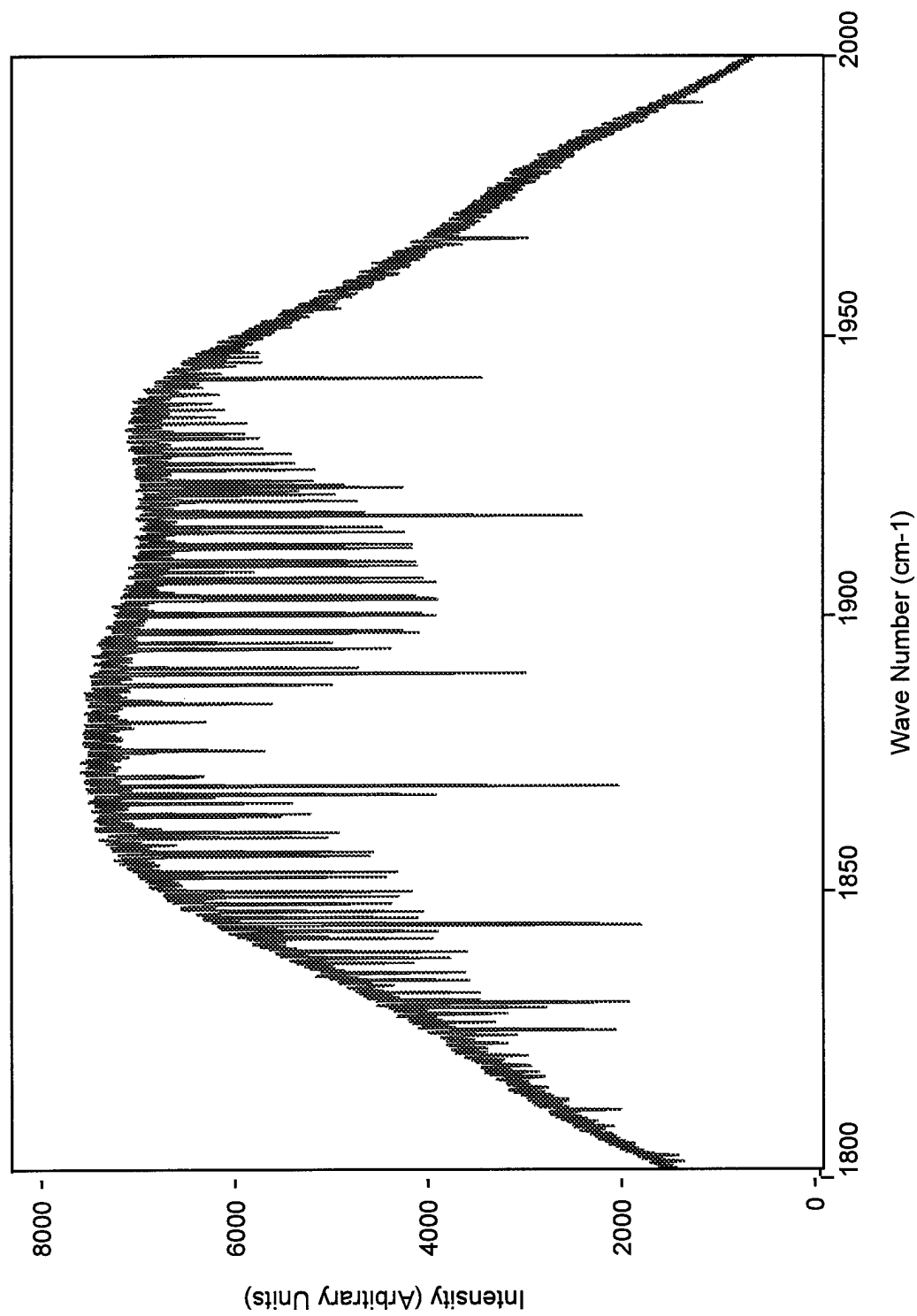


Figure 4-1: NO broadened by CO spectrum, 20Torr CO, 500m Torr NO, 100scans (coads).

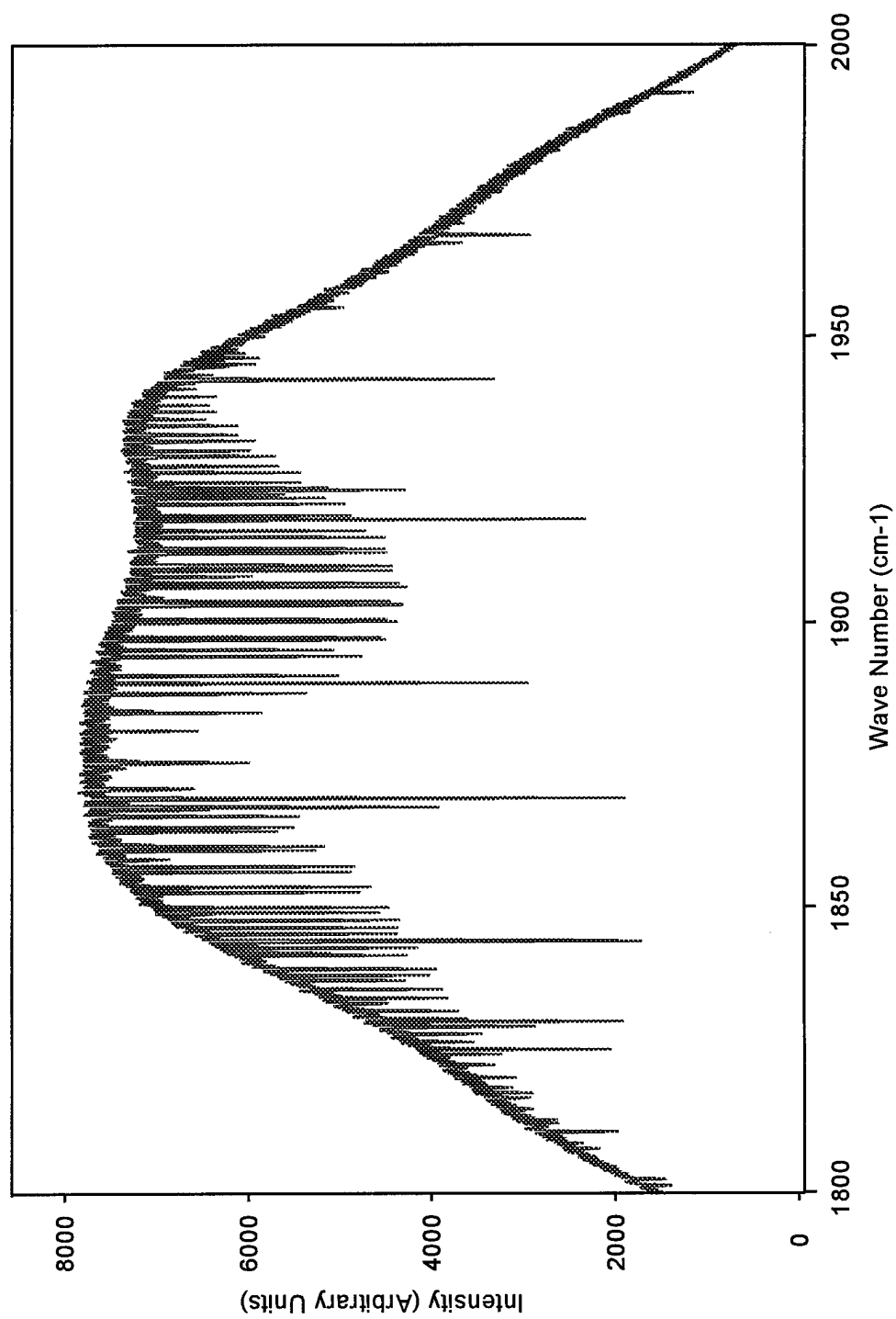


Figure 4-2: NO broadened by CO spectrum, 20Torr CO, 500m Torr NO, 3 coadded spectra of 100 coadds each.

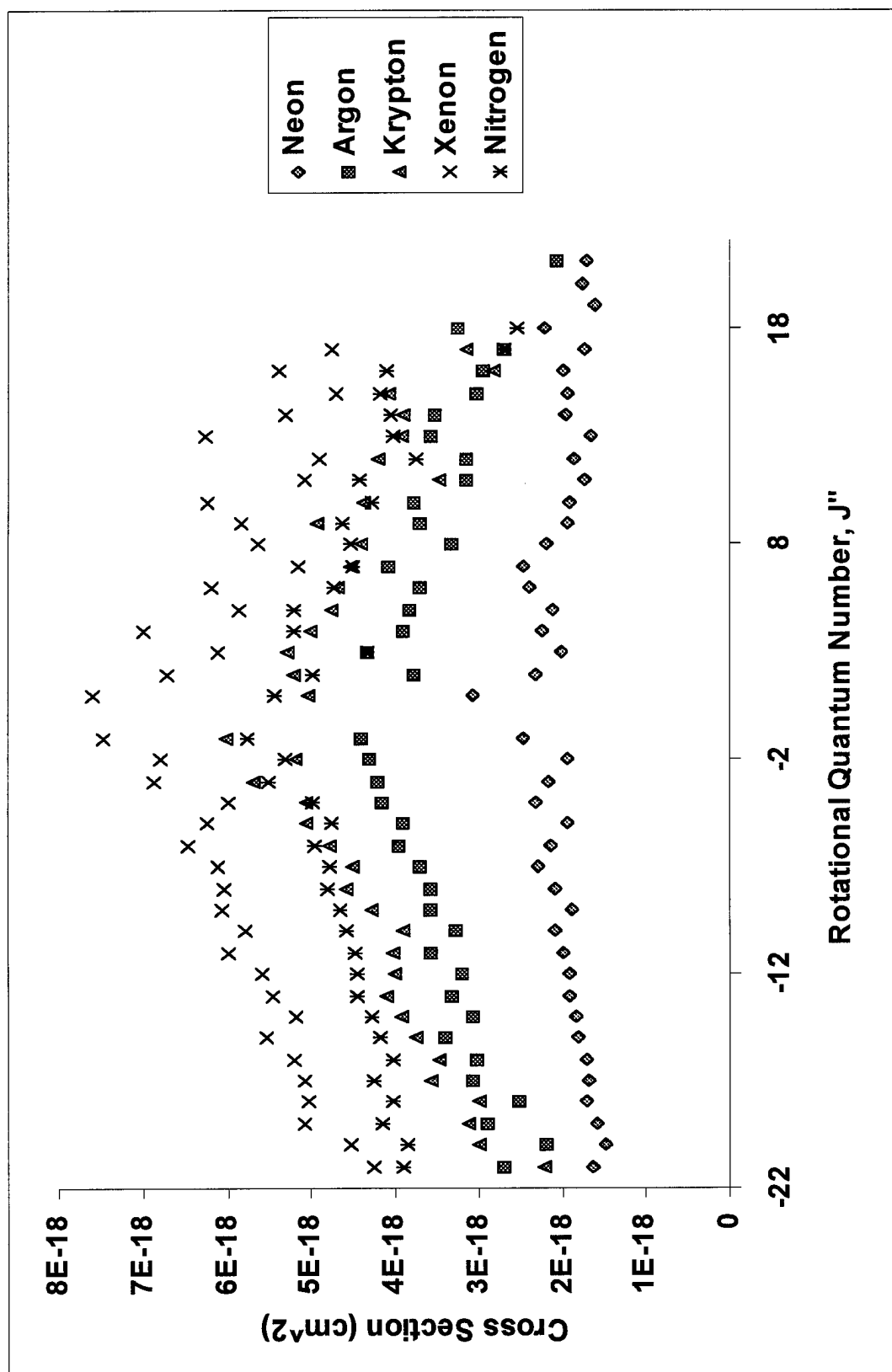


Figure 4-3:  $\sigma$  vs.  $J''$  plot for O<sub>2</sub> noble gas broadening.

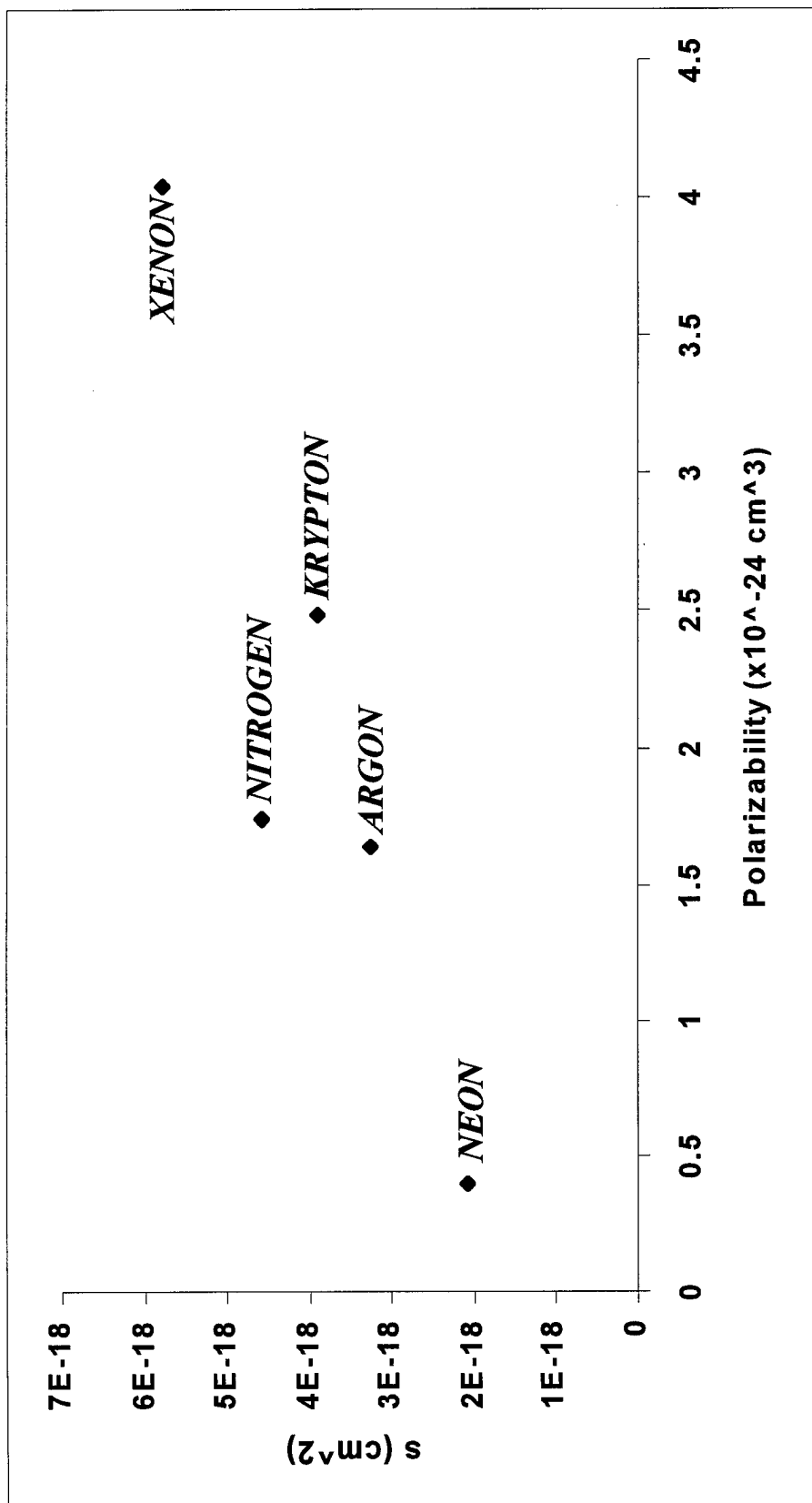


Figure 4-4:  $\sigma$  vs. polarizability for the  $J''=9$  line of  $\text{O}_2$  broadening.

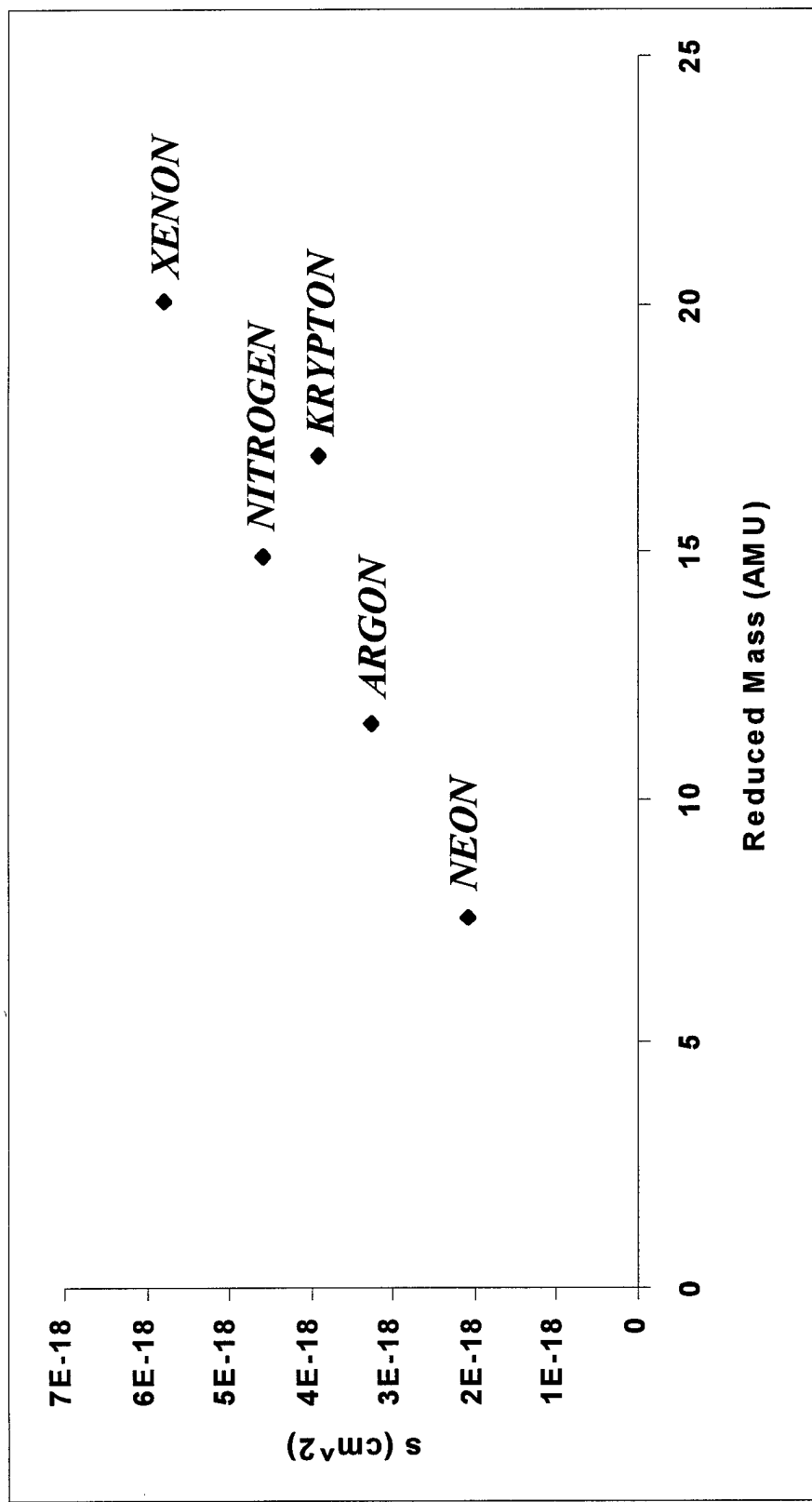


Figure 4-5:  $\sigma$  vs. reduced mass of collision pair,  $\text{O}_2$  broadening  $J''=9$  line.

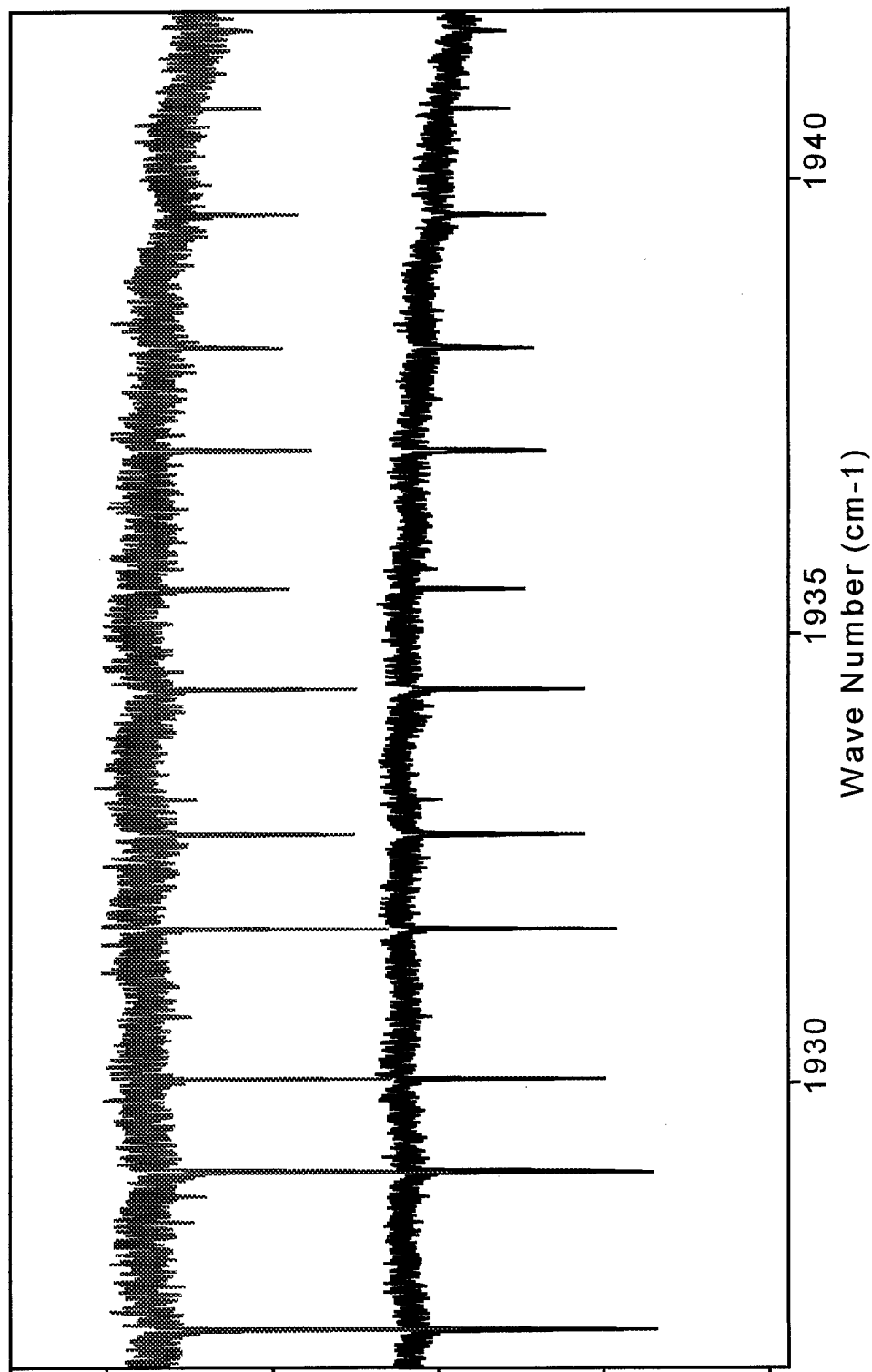


Figure 4-6: Comparison of single 100 scan spectrum and 3 coadded spectra, all at 20 Torr CO and 500mTorr NO. Top trace is single spectrum, bottom is 3 coadded spectra, both are the region around  $J'' = 18.5$  in the R-branch.

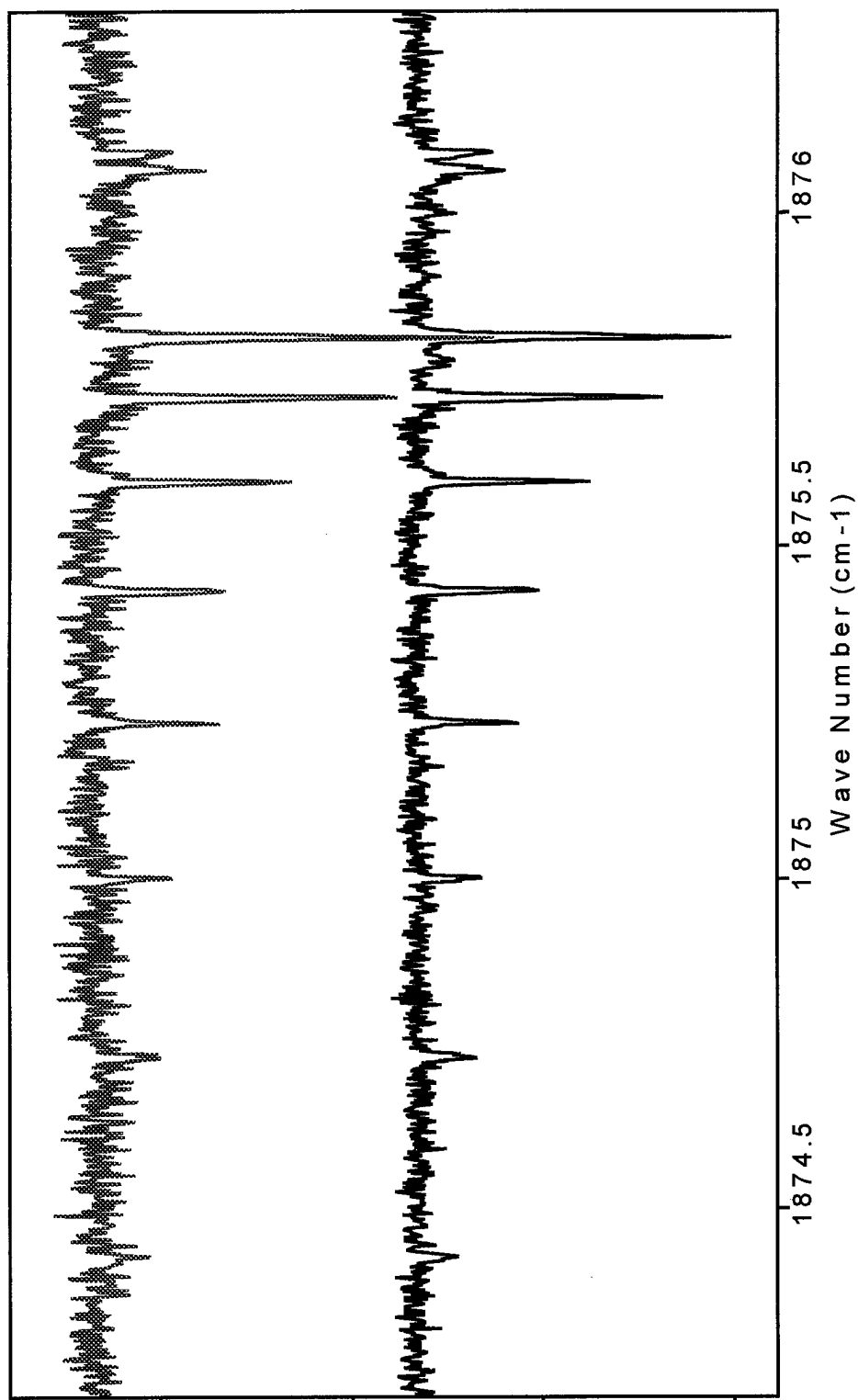
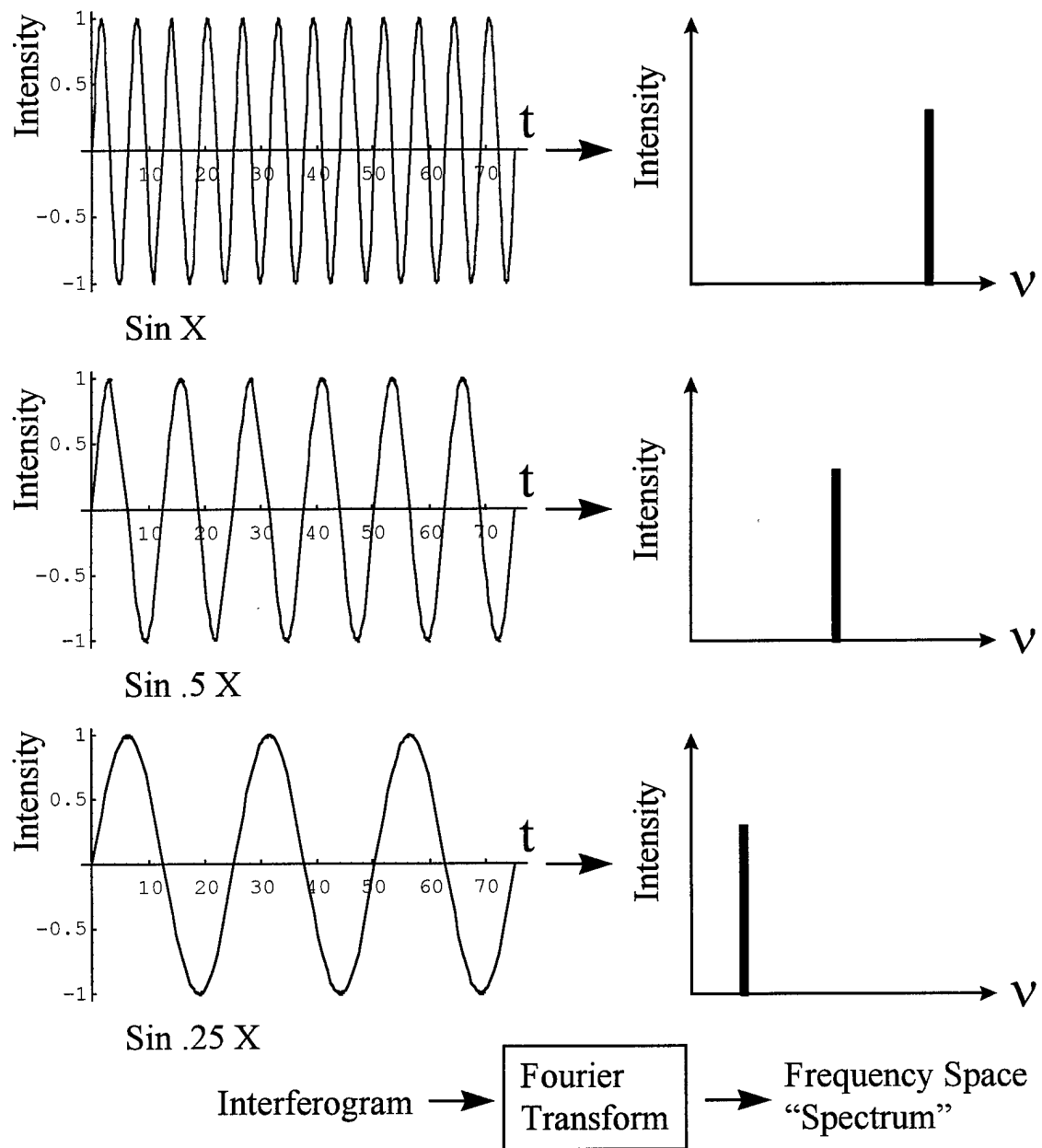


Figure 4-7: Comparison of single 100 scan spectrum and 3 coadded spectra, all at 20 Torr CO and 500mTorr NO. Top trace is single spectrum, bottom is 3 coadded spectra, both are the Q-branch.

## Appendix A: Fourier Transform Spectroscopy Theory

The Bomem DA-8 200 Fourier transform spectrometer is basically a Michelson interferometer where one mirror arm is mounted on a movable track. (Bomem spectrometer manual). See Figure 2-1 for a diagram of the apparatus. Imagine an interferometer with a monochromatic source. If the mirrors are exactly the same distance from the beam splitter the beams recombine at the detector and interfere constructively (add) to give a detector output at maximum. Likewise with an integral number of wavelengths difference. If the mirrors are off by exactly  $\frac{1}{2}$  wavelength distance, destructive interference occurs and the detector senses a minimum. In between  $\frac{1}{2}$  integral and integral wavelength differences, the detector output will be in between minimum and maximum output (Sears, 1984). Now if we smoothly move the mirror from its zero point out, we will see alternating intensity with a sinusoidal variation. If we record the intensity vs. time, this is our "interferogram" which is shown for three different frequencies in Figure A-1 (Goodman, 1989). Different monochromatic sources will produce sinusoidal interferograms with different frequencies. A Fourier transform of a perfect sine wave is a delta function in frequency space (Kreyszig, 1996). This frequency space representation *IS* our spectrum. So looking at Figure A-1, the spectra of the three monochromatic sources are to the right and display *one* frequency at *one* intensity. This is the basis of the FT spectrometer's operation (Goodman, 1989). Now, demonstrate with the use of three frequencies as if we had three monochromatic sources. See Figure A-2. The interferograms show constructive and destructive addition of the three frequencies (here we have equal intensities of frequencies in the source). The Fourier transform of this

gives us a spectrum with three delta functions at the locations of each frequency of the source.



**Figure A-1: Fourier transform spectrum production process using individual monochromatic sources.**

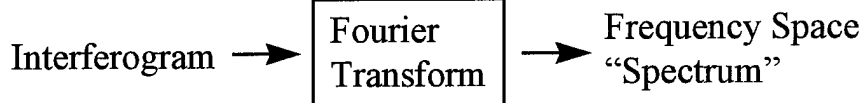
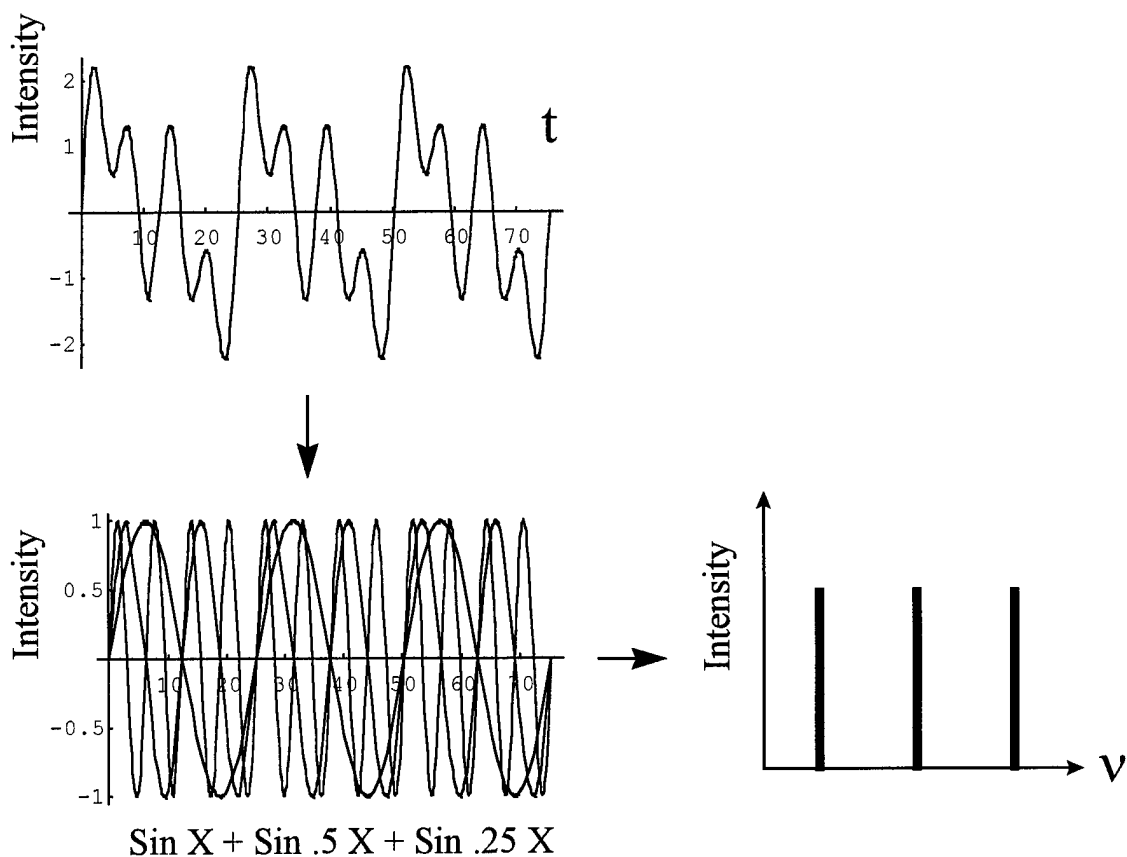
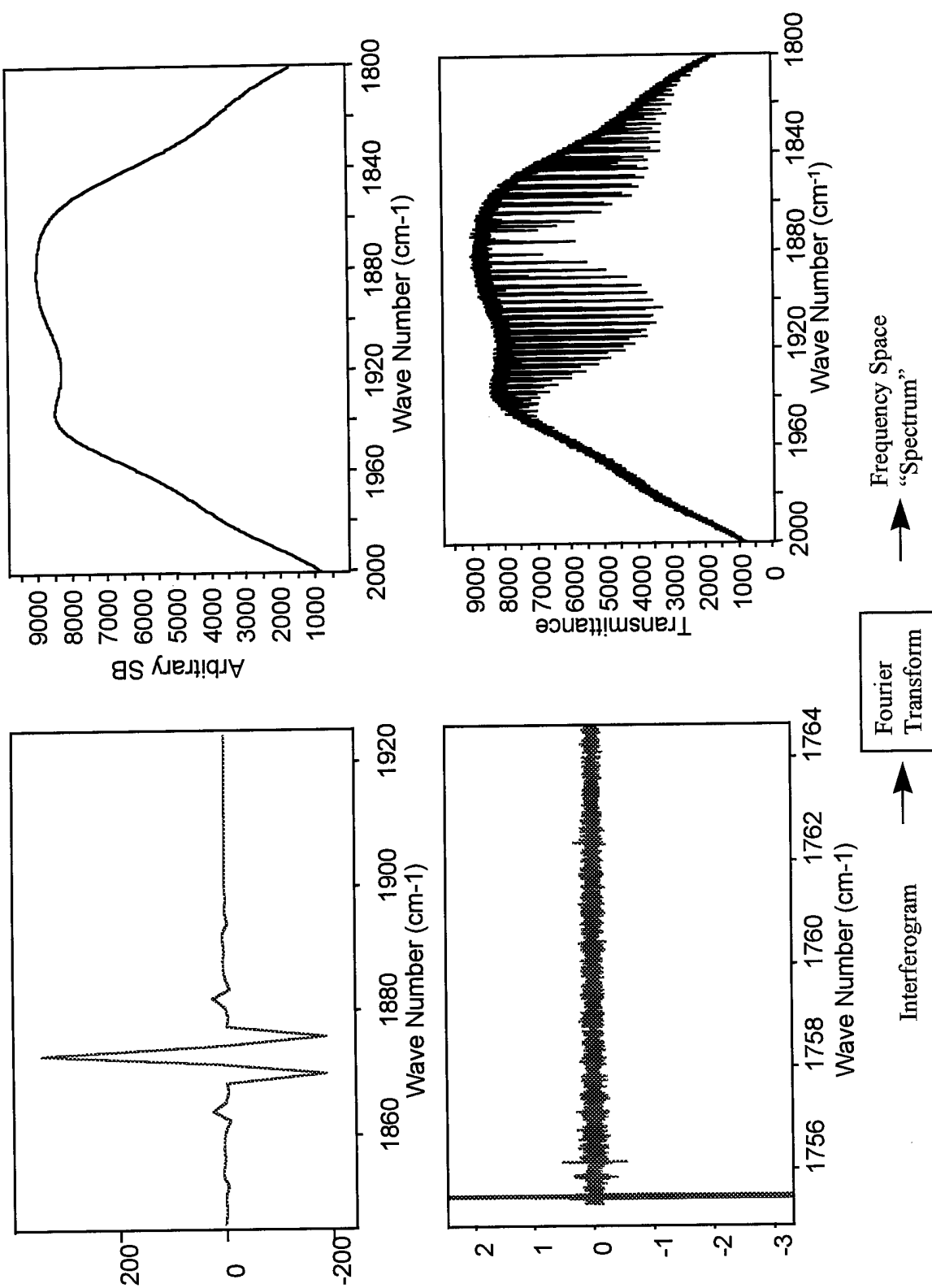


**Figure A-2: Fourier transform spectrum production process using three monochromatic sources at once.**

Remember, we use a continuum source in our spectrometer, in the visible range for the  $O_2$  experiment and infrared for NO. The interferogram will contain many added sine waves of many frequencies. What you would see then, after the Fourier transform, is a spectrum with an infinite number of delta functions with intensities proportional to the intensity of the individual source frequency "parts" (Goodman, 1989). This will look like our background trace, which is exactly what it is. The background trace is the spectrum

of the SOURCE (Goodman, 1989). Figure A-3 shows the interferogram and spectrum for the source (Banwell, 1972).

Now, add a cell of absorbing gas which completely *removes* certain frequencies from the source (or a filter!). This will be represented in the interferogram as missing sine waves at the frequencies where the sample absorbs. That is how we get our spectrum. The Fourier transform will not see those frequencies and will not place "delta functions" where the absorption takes place. It will display zero intensity there. If only partial absorption takes place at a certain frequency, the interferogram will display a sine wave at that frequency, but at decreased intensity (amplitude). The Fourier transform will show partial absorption in the spectrum. Figure A-3 shows an interferogram and spectrum with absorbing gas in the beam path (Banwell, 1972).



## Appendix B: Results Graphs

### Pressure broadening coefficient vs. rotational quantum number, m for O<sub>2</sub> study

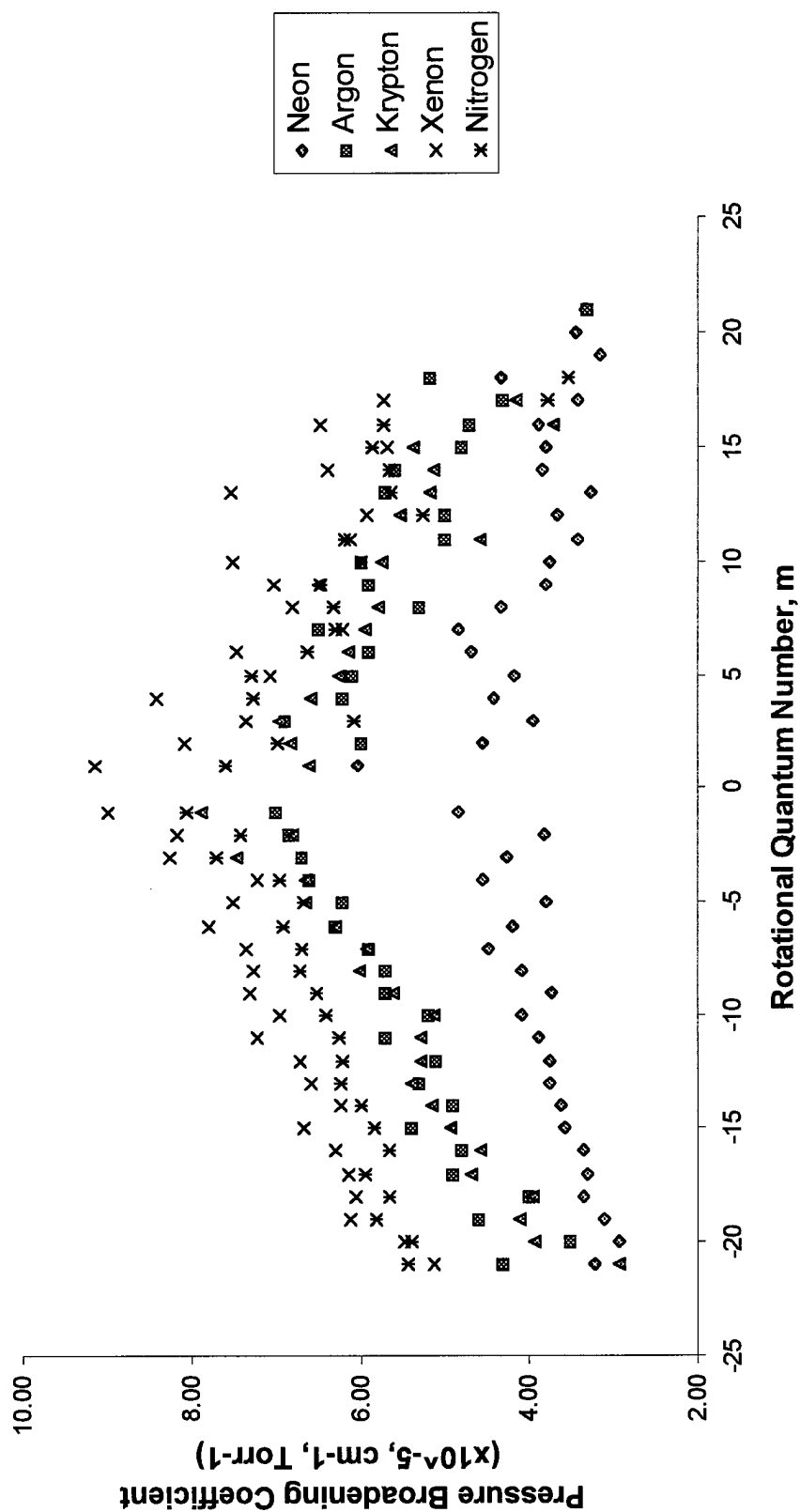
O2 Pressure Broadening, N2 and all Noble gases (No Comparisons)	94
O2 - N2 Broadening: Cornicelli 1997 (with error bars)	95
O2 - Ne Broadening: Cornicelli 1997 (with error bars) vs. Ritter 1987	96
O2 - Ar Broadening: Cornicelli 1997 (with error bars) vs. Ritter 1987	97
O2 - Kr Broadening: Cornicelli 1997 (with error bars) vs. Ritter 1987	98
O2 - Xe Broadening: Cornicelli 1997 (with error bars) vs. Ritter 1987	99

### Pressure broadening coefficient vs. rotational quantum number, m for NO study

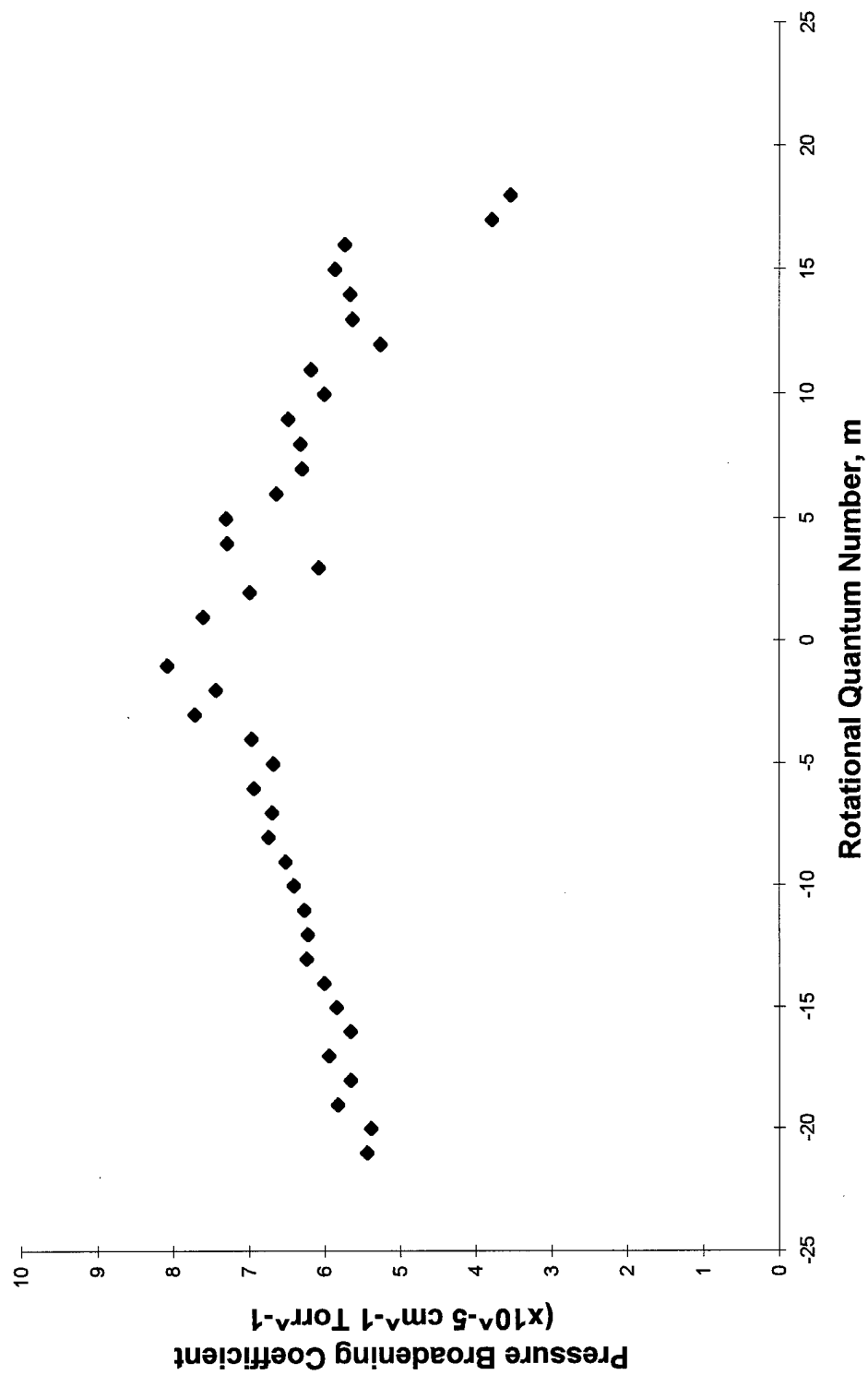
NO - He Broadening, e and f $\Lambda$ -doubles: Cornicelli 1997 vs. Spencer 1994	100
NO - He Broadening, f state: Cornicelli 1997 (with error bars)	101
NO - He Broadening, e state: Cornicelli 1997 (with error bars)	102
NO - Ne Broadening, e and f $\Lambda$ -doubles: Cornicelli 1997 vs. Spencer 1994	103
NO - Ne Broadening, f state: Cornicelli 1997 (with error bars)	104
NO - Ne Broadening, e state: Cornicelli 1997 (with error bars)	105
NO - Ar Broadening, e and f $\Lambda$ -doubles: Cornicelli 1997 vs. Spencer 1994	106
NO - Ar Broadening, f state: Cornicelli 1997 (with error bars)	107
NO - Ar Broadening, e state: Cornicelli 1997 (with error bars)	108
NO - Kr Broadening, e and f $\Lambda$ -doubles: Cornicelli 1997 vs. Spencer 1994	109
NO - Kr Broadening, f state: Cornicelli 1997 (with error bars)	110
NO - Kr Broadening, e state: Cornicelli 1997 (with error bars)	111

NO - Xe Broadening, e and f $\Lambda$ -doubles: Cornicelli 1997 vs. Spencer 1994	112
NO - Xe Broadening, f state: Cornicelli 1997 (with error bars)	113
NO - Xe Broadening, e state: Cornicelli 1997 (with error bars)	114
NO - All theoretical PBCs Using Averaging Between e and f states	115

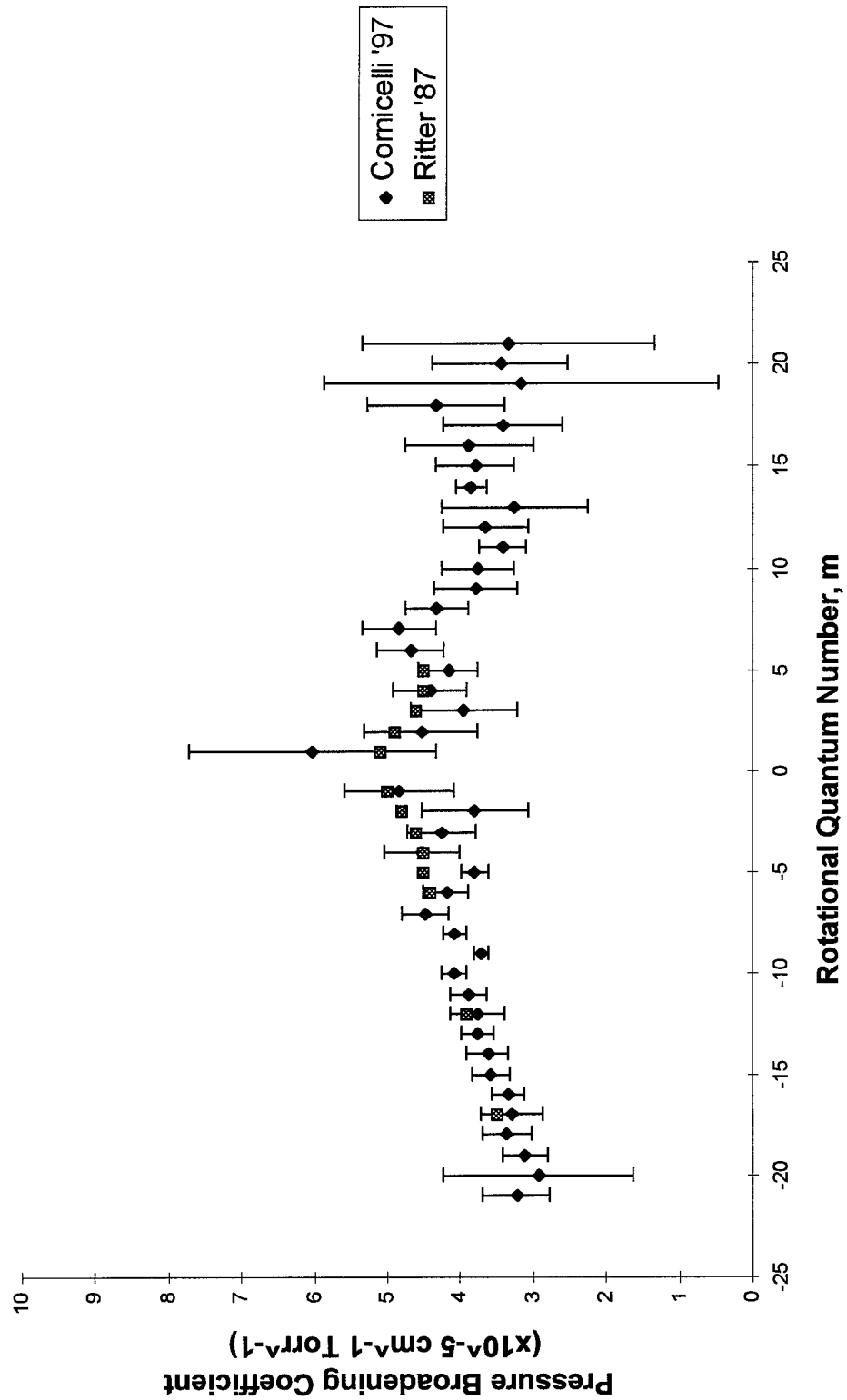
# Noble Gas Broadening of Oxygen Cornicelli '97



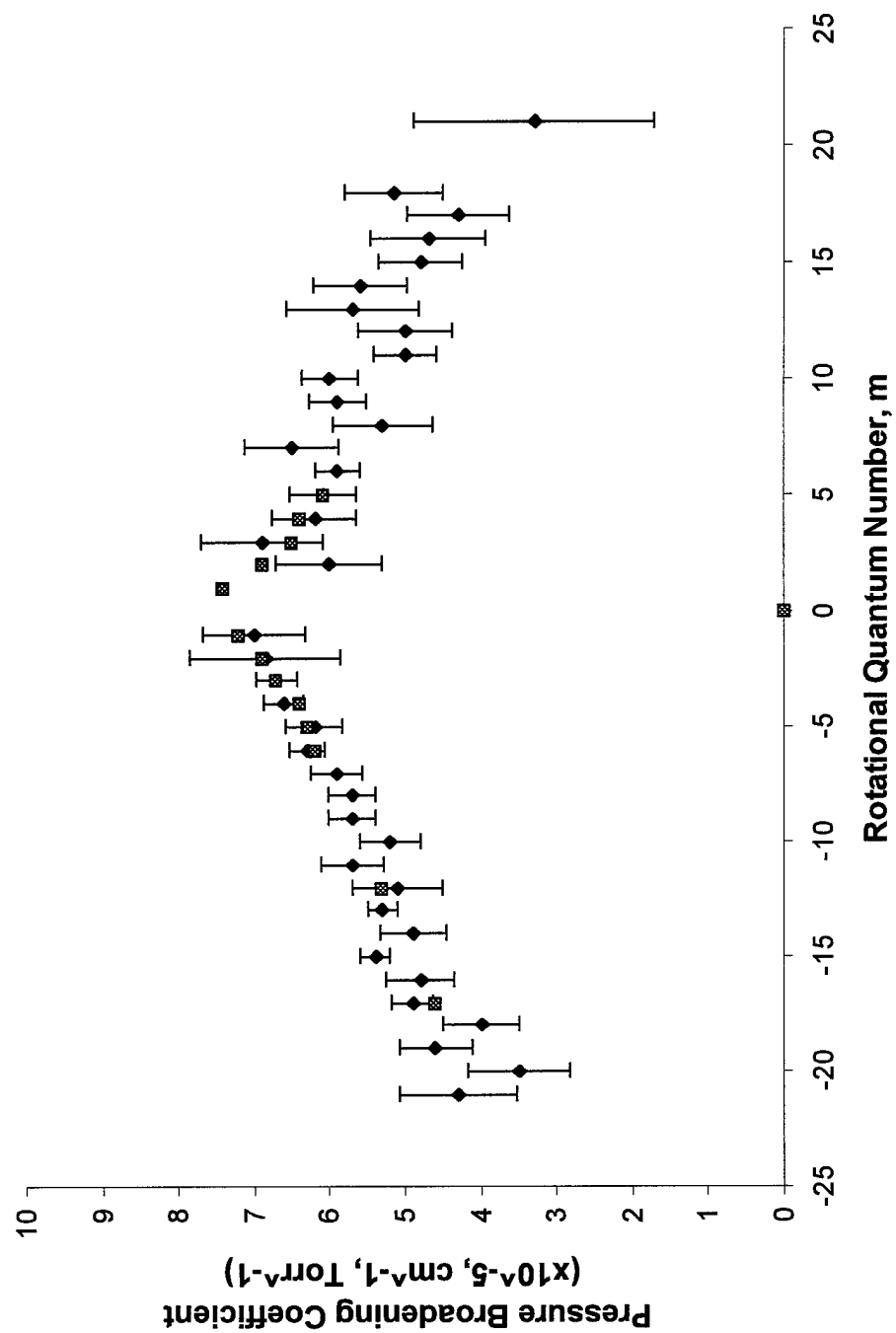
# O2 Broadened With N2



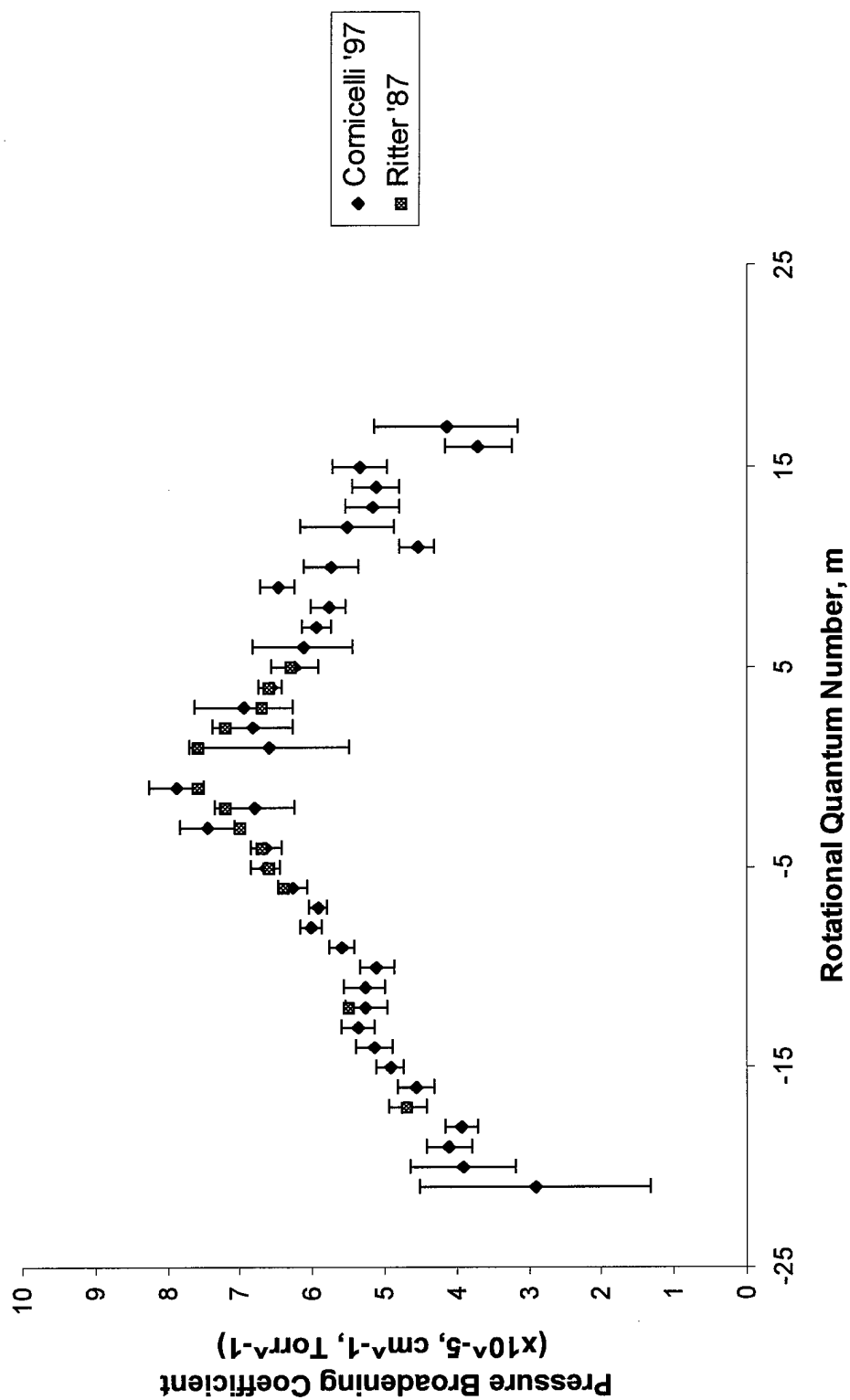
# O2 Broadened With Neon



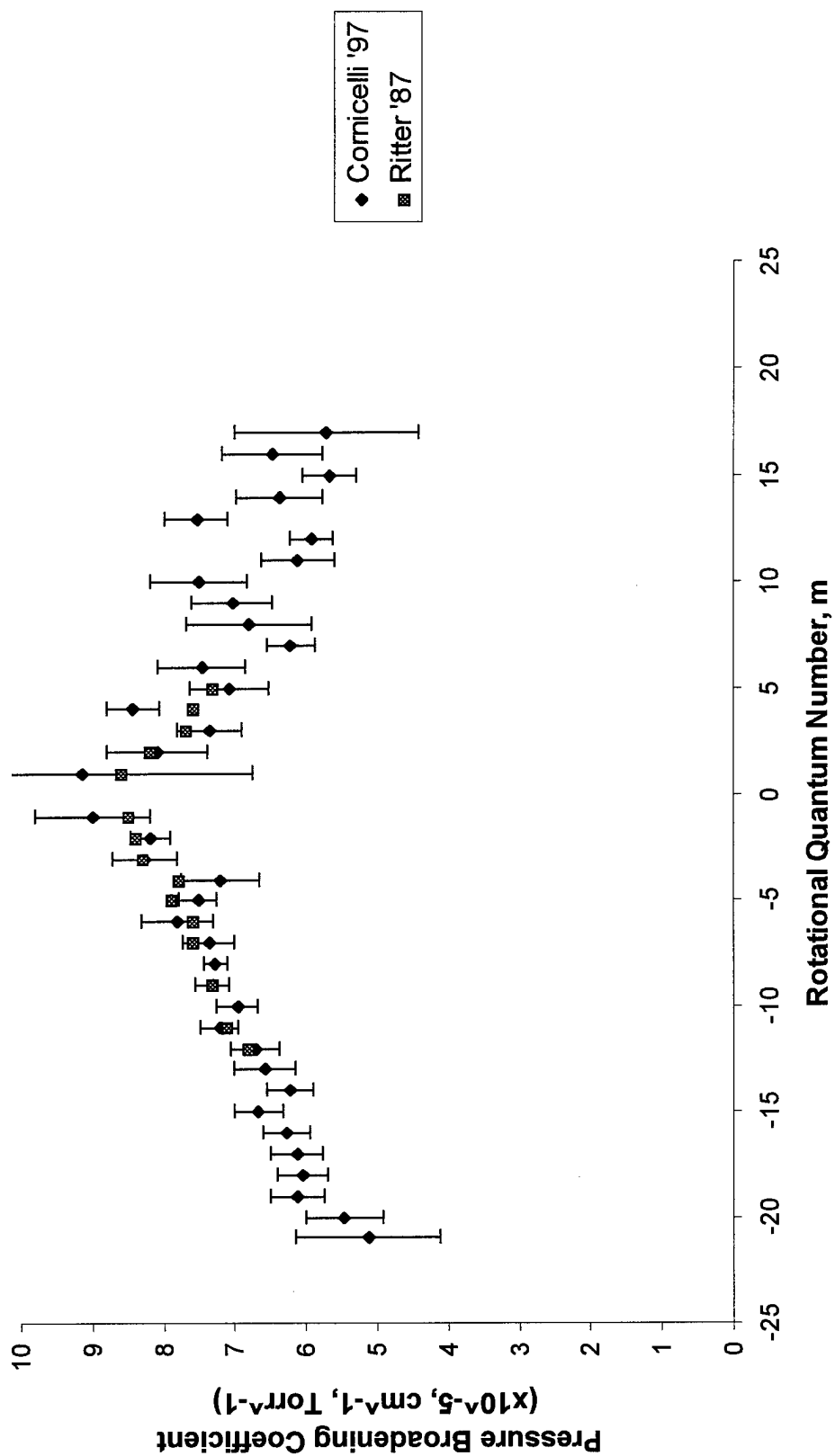
# Oxygen Broadened With Argon



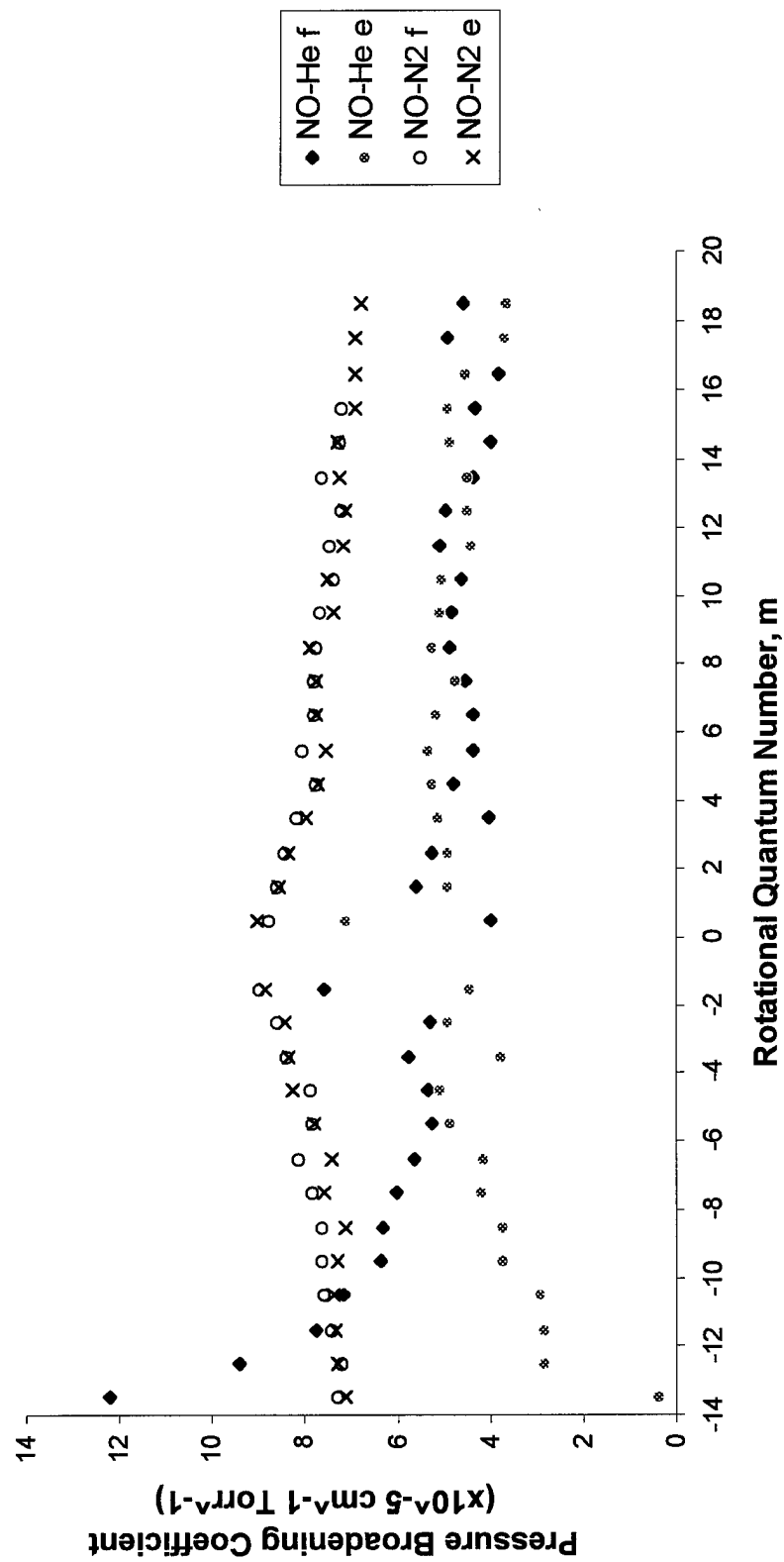
# Oxygen Broadened With Krypton



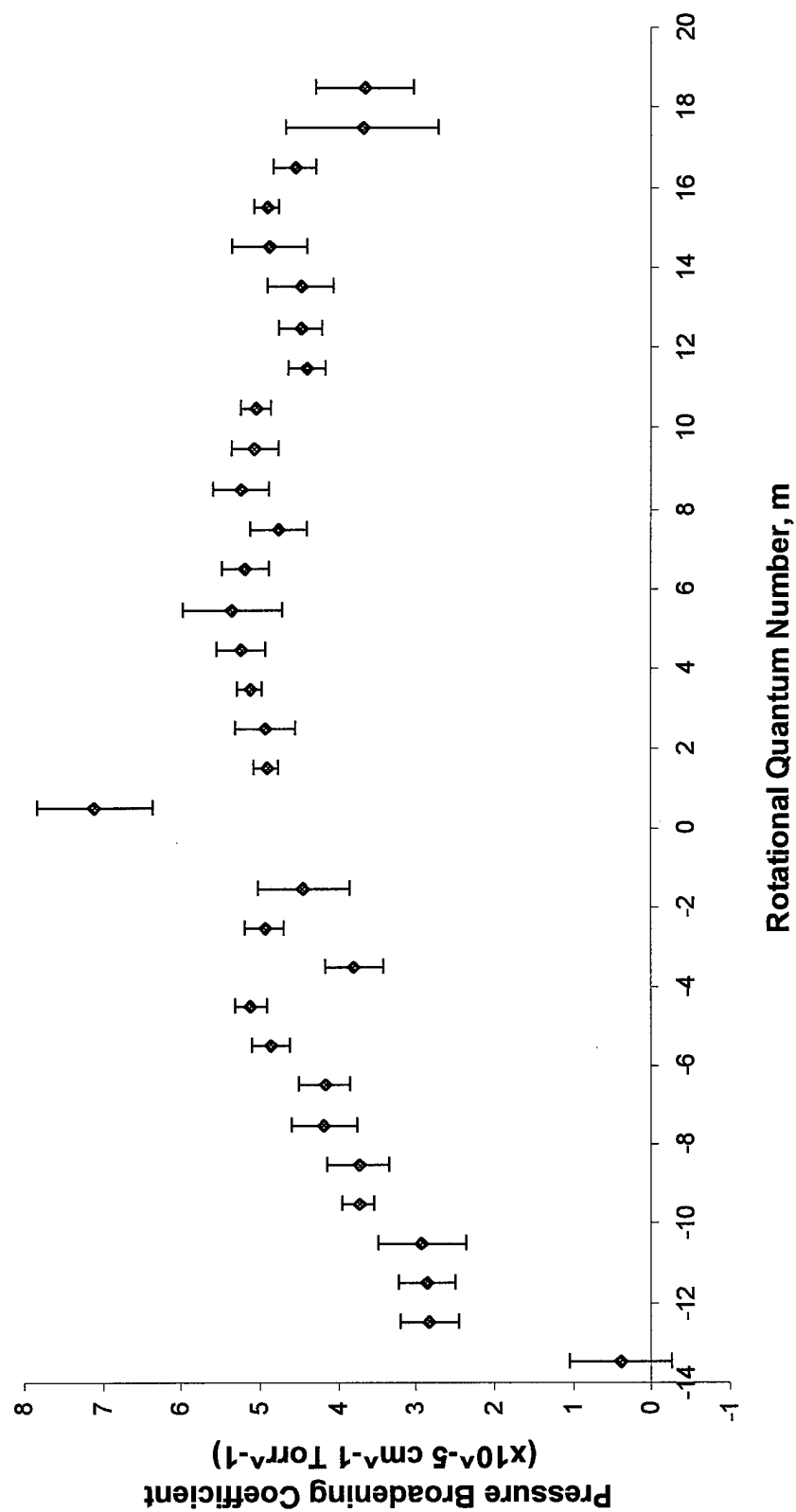
# Oxygen Broadened With Xenon



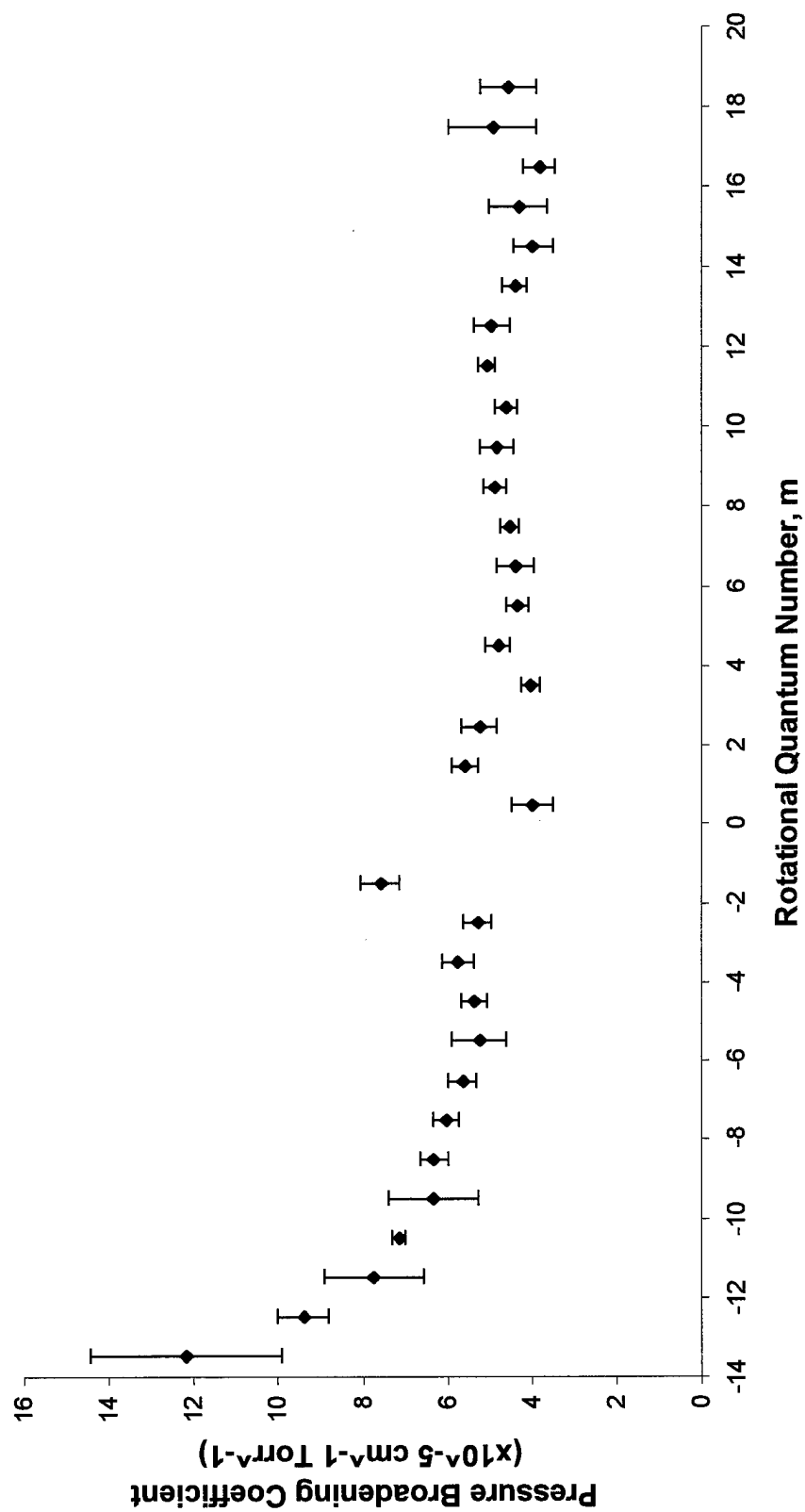
NO - He, Cornicelli 1997  
vs NO - N2, Spencer 1994



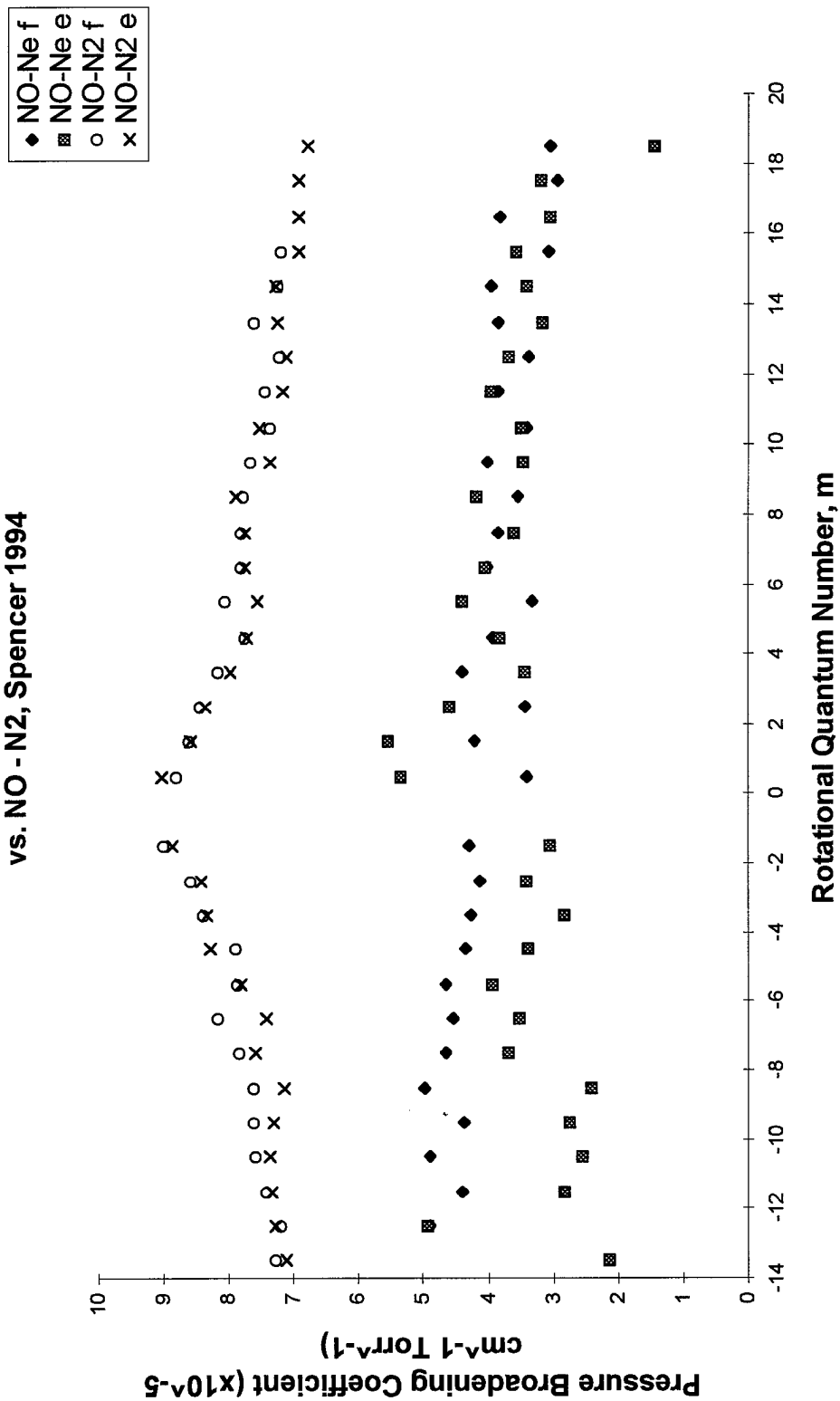
NO Broadened With He (e-state)



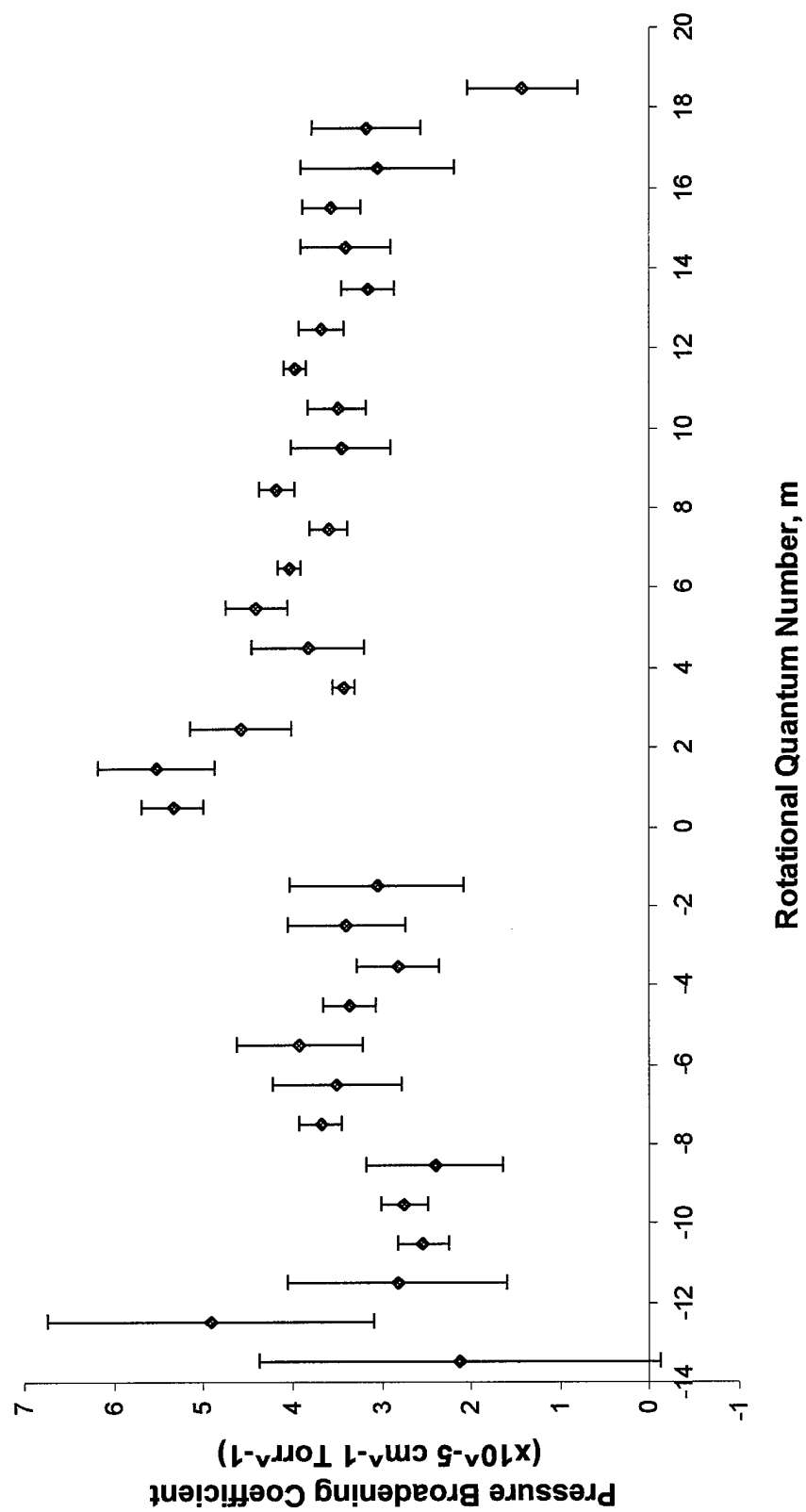
# NO Broadened With He (f-state)



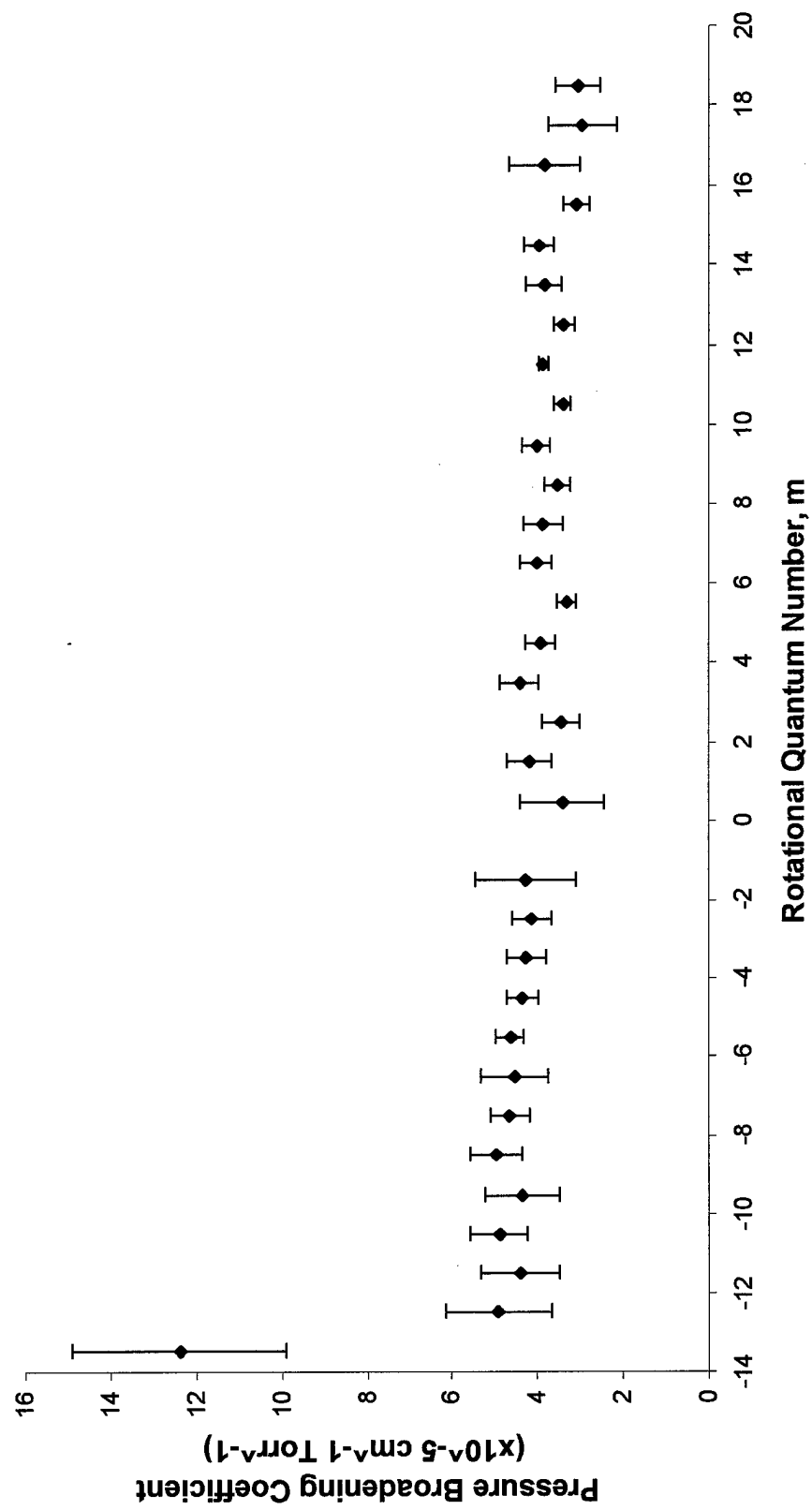
NO - Ne, Cornicelli 1997  
vs. NO - N2, Spencer 1994



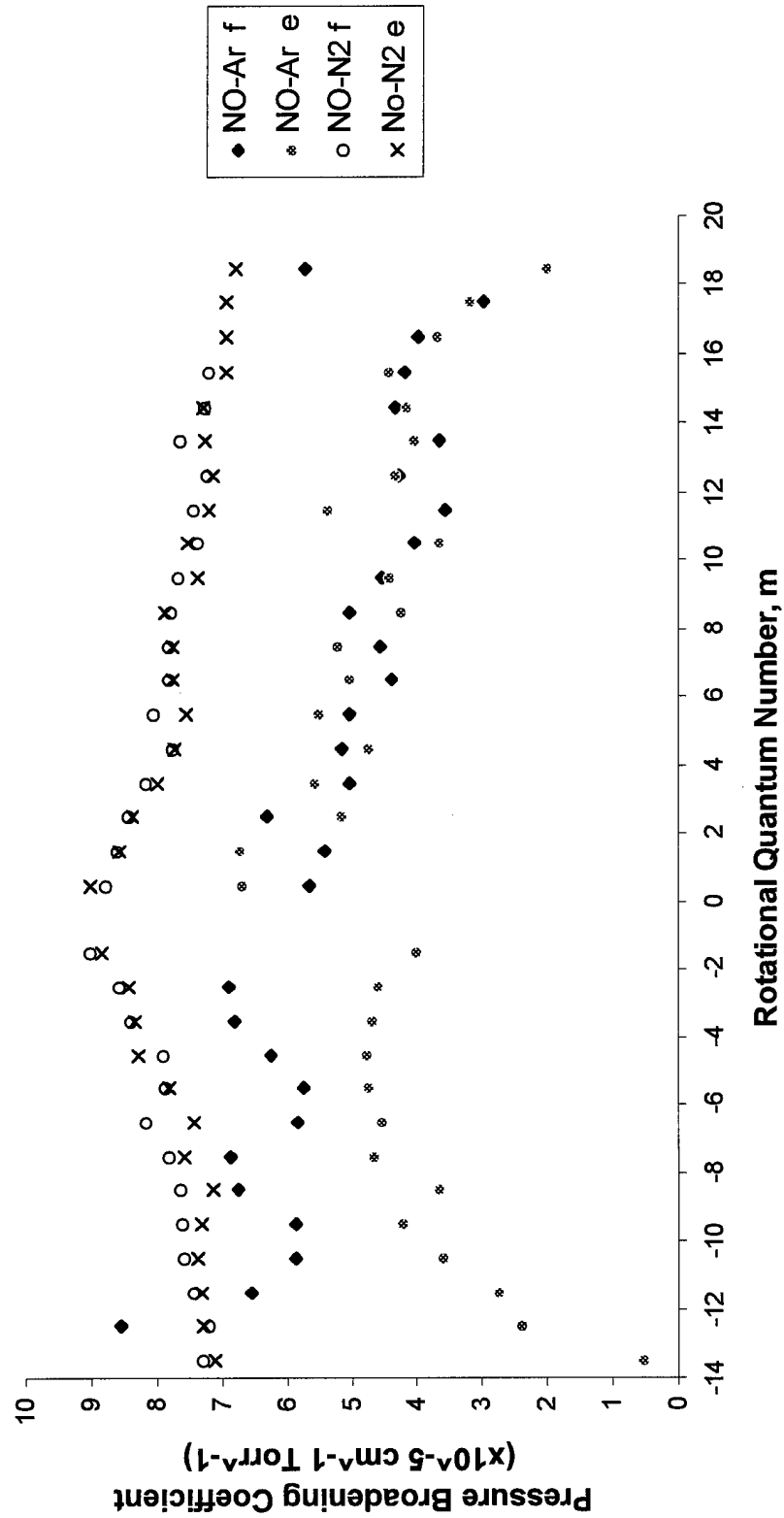
NO Broadened With Ne (e-state)



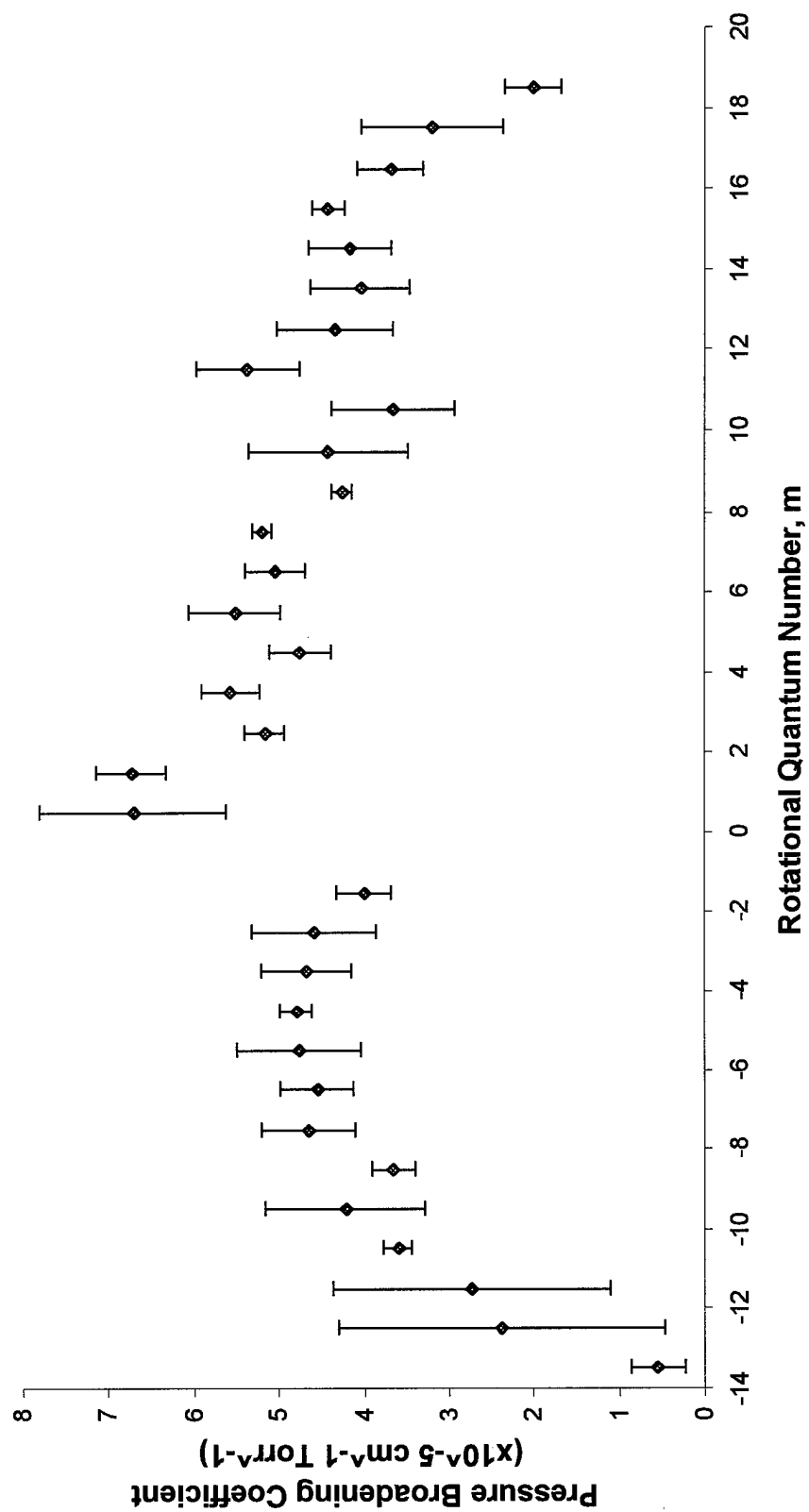
# NO Broadened With Ne (f-state)



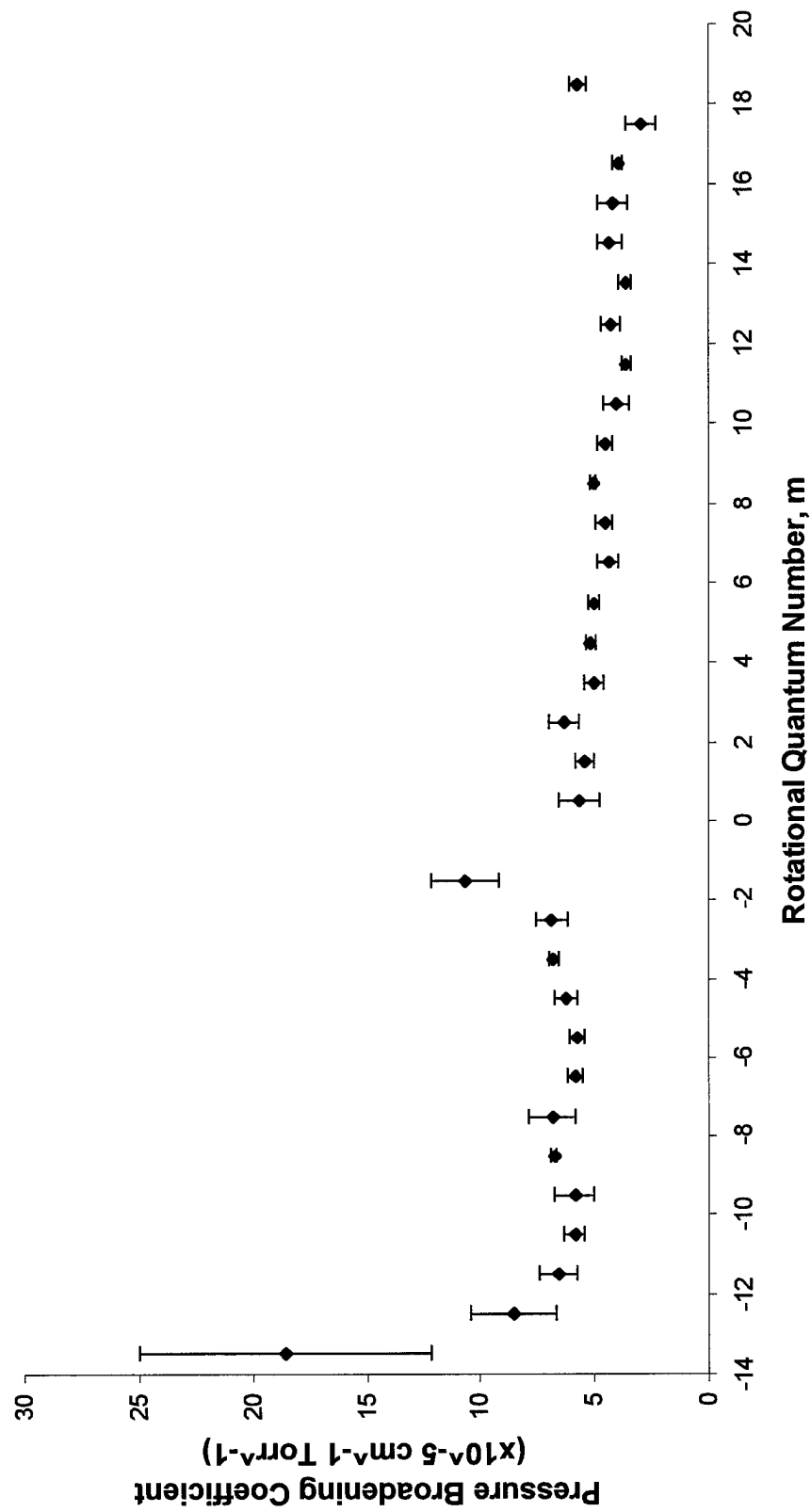
NO - Ar, Cornicelli 1997  
vs NO - N<sub>2</sub>, Spencer 1994



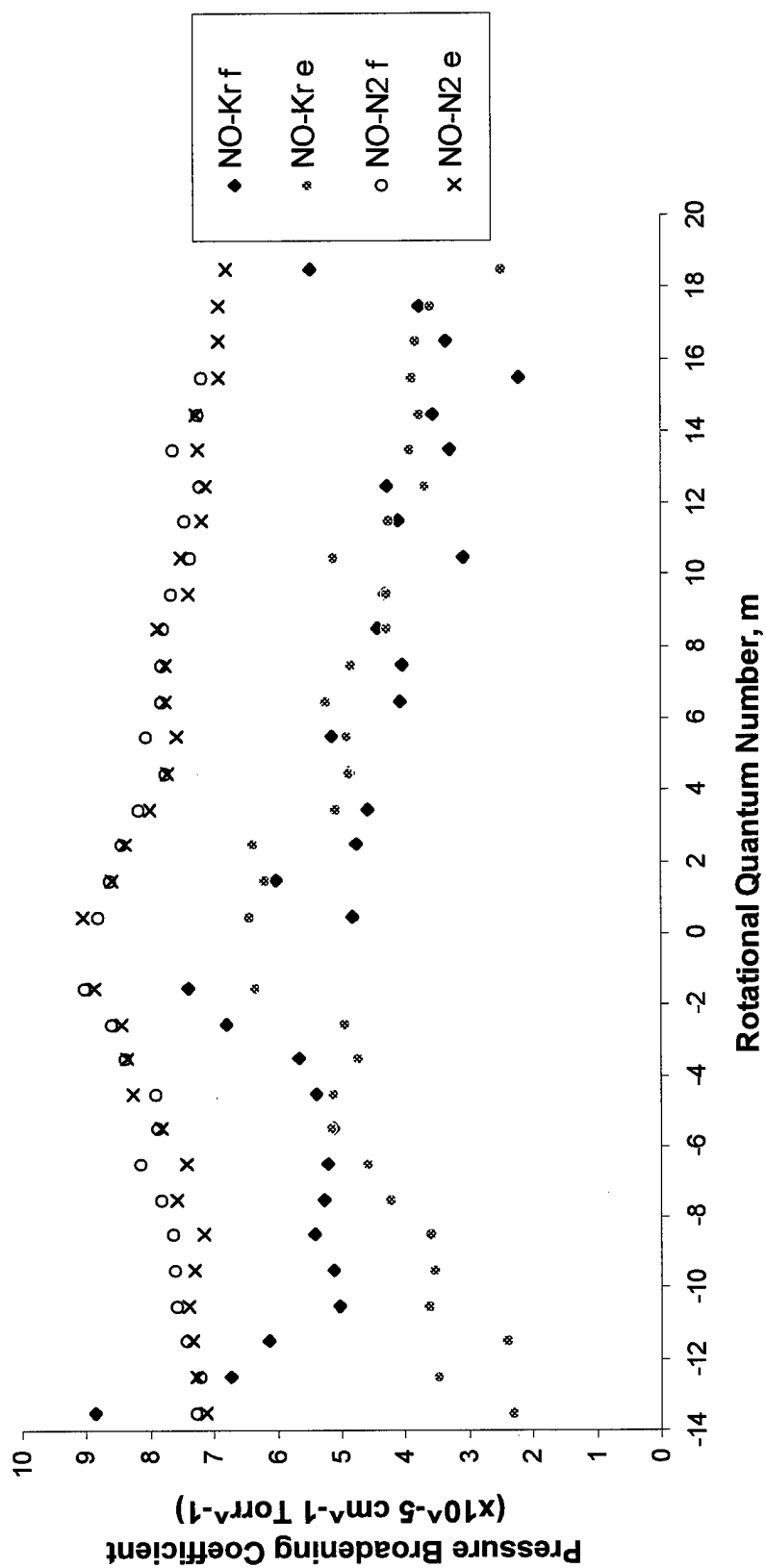
# NO Broadened With Ar (e-state)



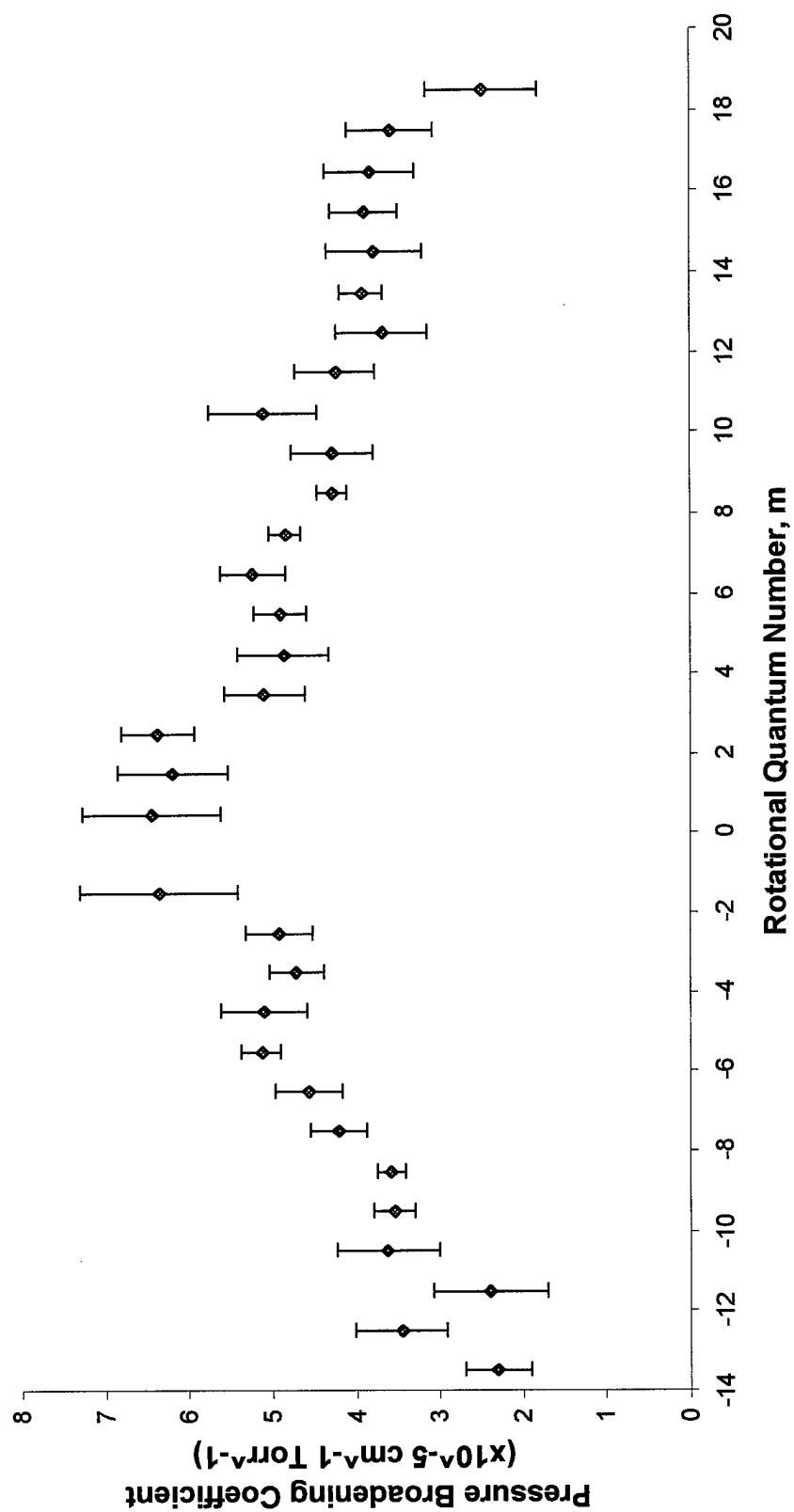
# NO Broadened With Ar (f-state)



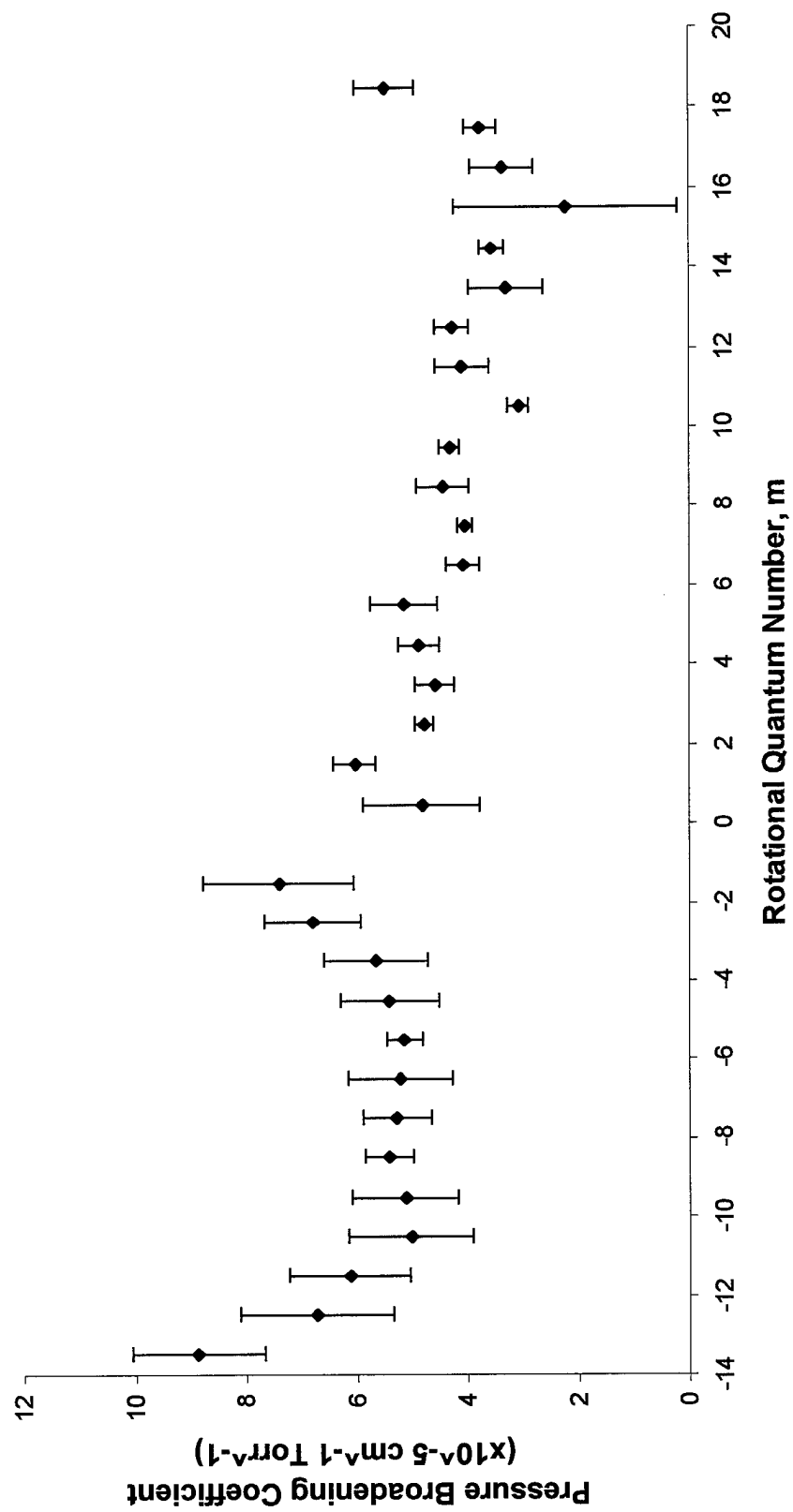
NO - Kr, Comicelli 1997  
vs NO - N<sub>2</sub>, Spencer 1994



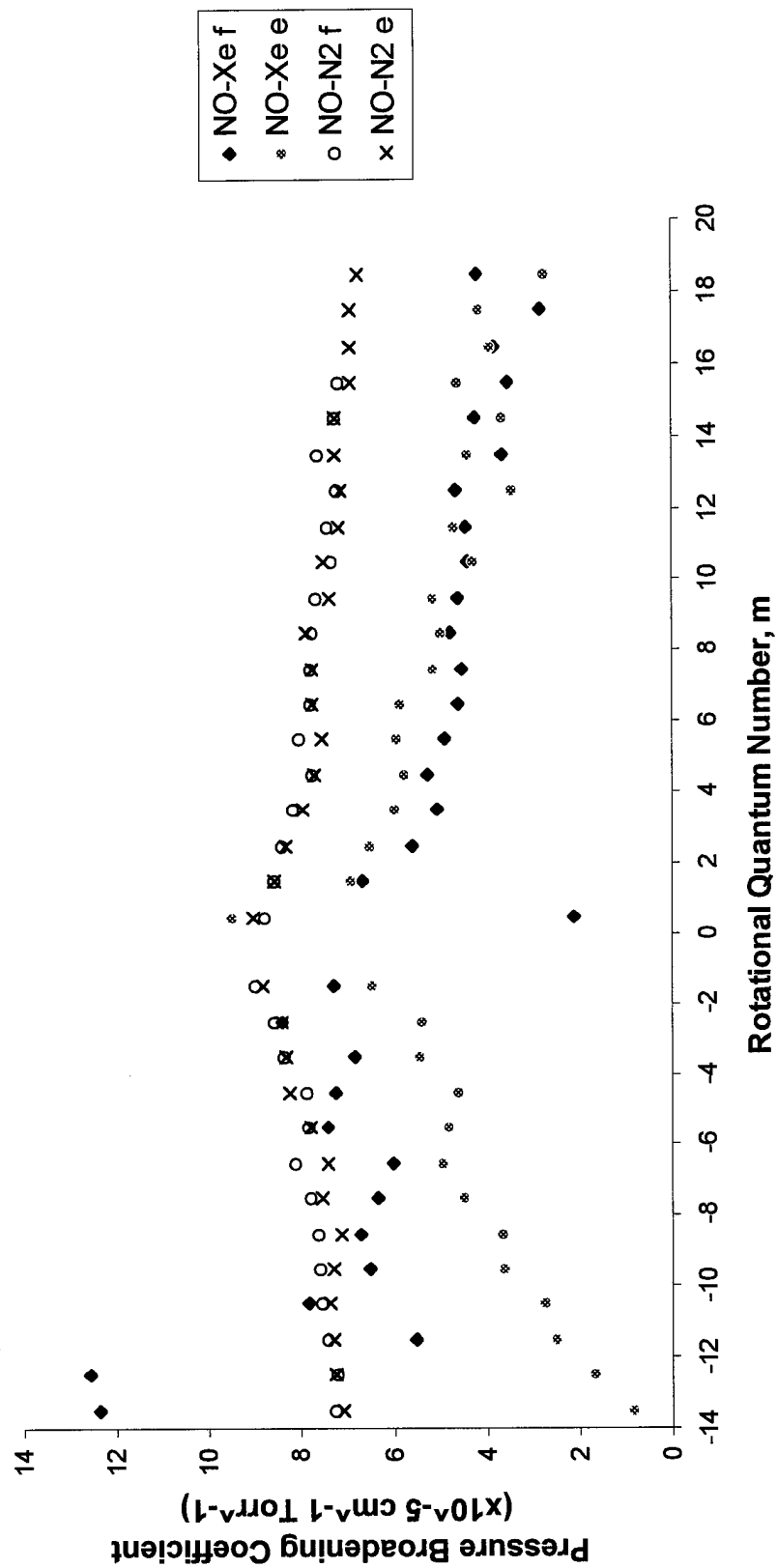
NO Broadened With Kr (e-state)



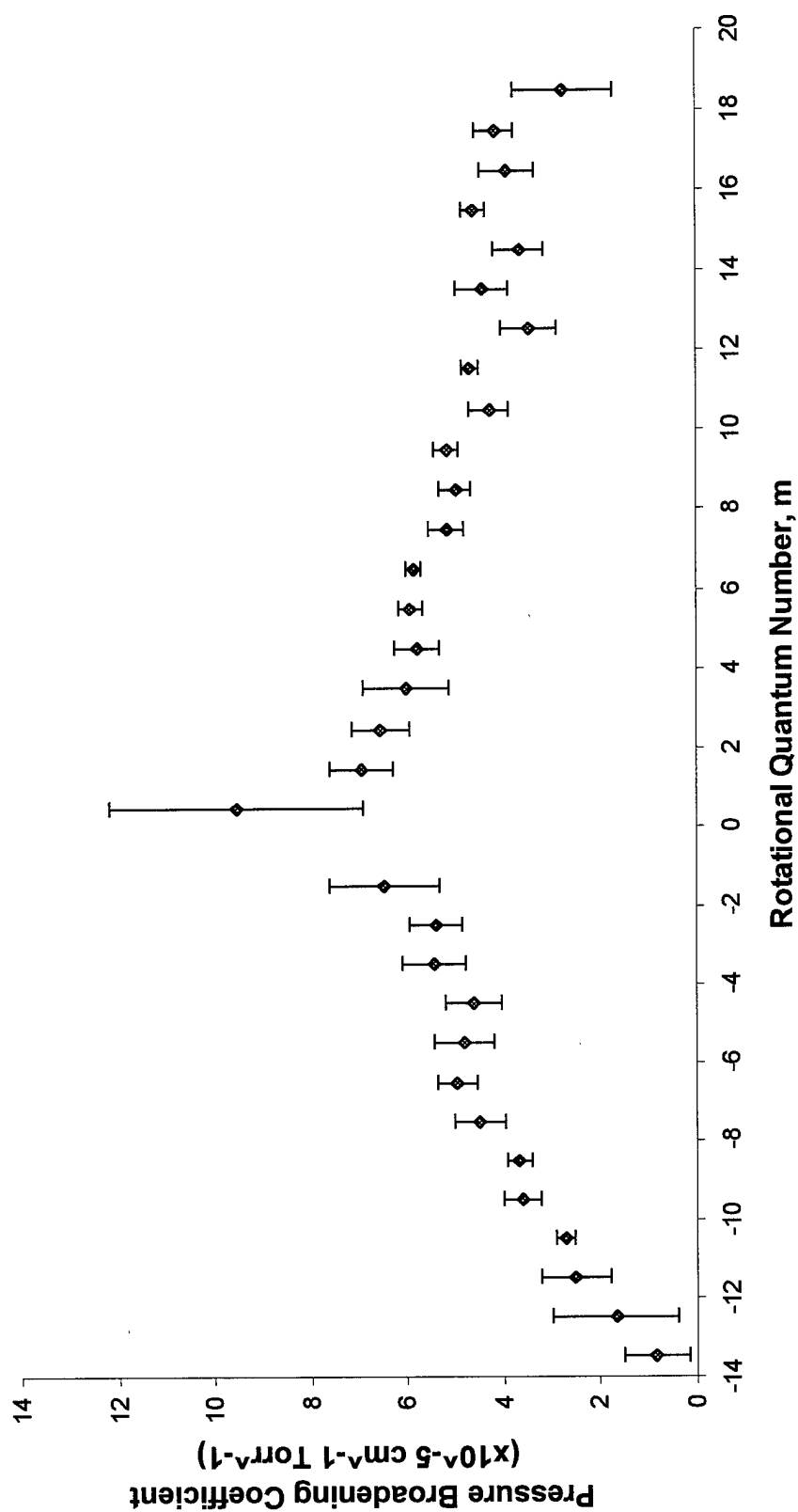
NO Broadened With Kr (f-state)



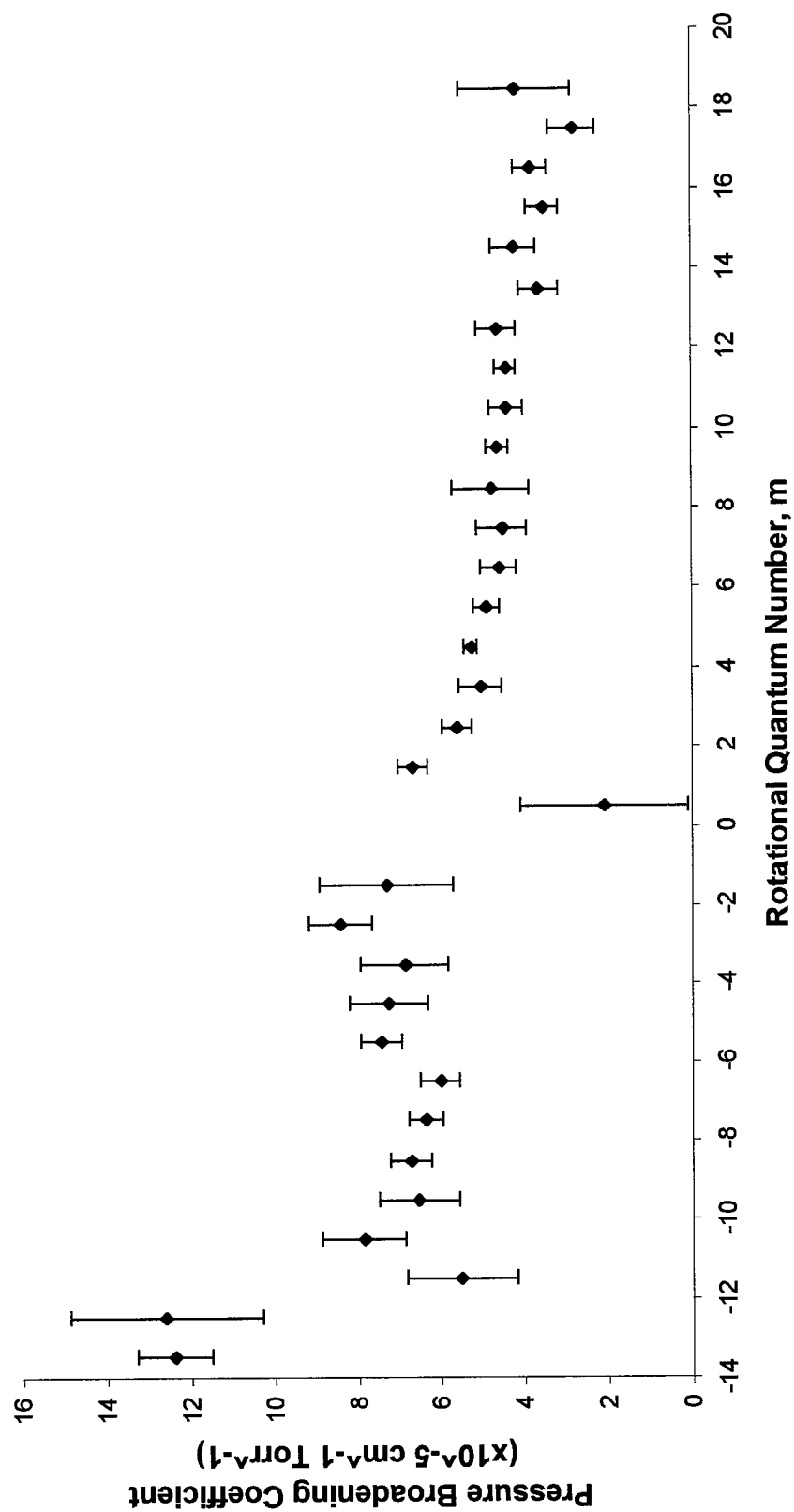
NO - Xe, Cornicelli 1997  
vs NO - N2, Spencer 1994

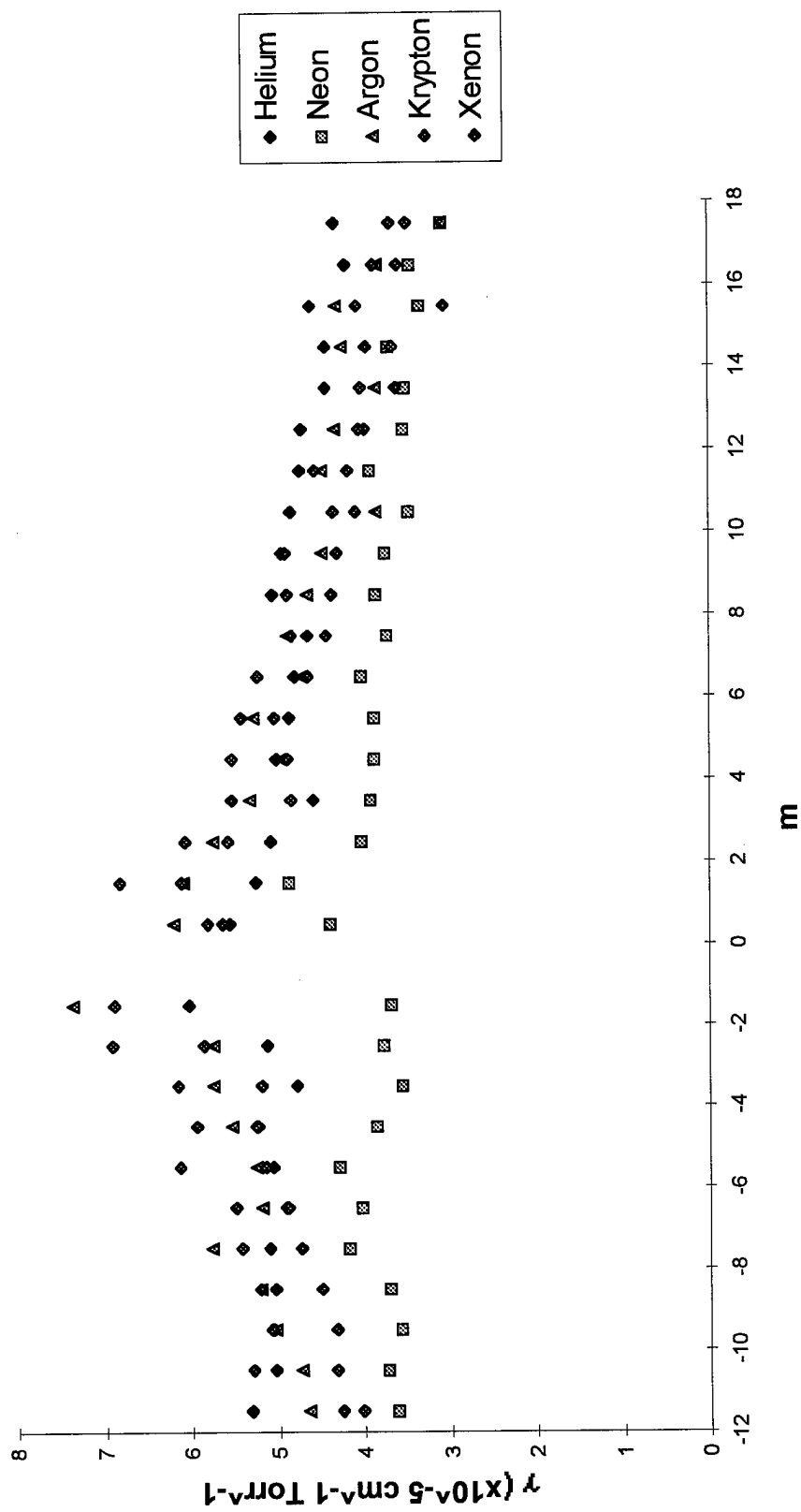


NO Broadened With Xe (e-state)



# NO Broadened With Xe (f-state)





### **Bibliography**

- Abels, L. L., and Shaw, J. H., "Widths and Strengths of Vibrational-Rotational Lines in the Fundamental Band of Nitric Oxide," Journal of Molecular Spectroscopy, Vol 20, 11-28, 1966.
- Amiot, C., Bacis, R. and Guelachvili, G., "Infrared Study of the  $X^2\Pi$   $v=0, 1, 2$  levels of  $^{14}\text{N}^{16}\text{O}$ , Preliminary Results on the  $v=0,1$  levels of  $^{14}\text{N}^{17}\text{O}$ ,  $^{14}\text{N}^{18}\text{O}$  and  $^{15}\text{N}^{16}\text{O}$ ," Canadian Journal of Physics, Vol 56, 1978.
- Ballard, J. and W. B. Johnston, "Experimental Spectral Line parameters in the 1-0 Band of Nitric Oxide," Journal of Molecular Spectroscopy, Vol 127, 83-96, May 1988.
- Banwell, C. N., Fundamentals of Molecular Spectroscopy. New York: McGraw-Hill, Inc., 1972.
- Bevington, Philip, R., Data Reduction and Error Analysis for the Physical Sciences. New York: McGraw-Hill, Inc., 1992.
- Billingsley, F. P., "Calculated Vibration - Rotation Intensities for NO ( $X^2\Pi$ )," Journal of Molecular Spectroscopy, Vol. 61, 53-70, 1976.
- Burch, D. E. and. Gryvnak, D. A. "Strengths, Widths and Shapes of the Oxygen Lines Near  $13100\text{ cm}^{-1}$  (7620 Å)," Applied Optics: Vol. 8 No. 7, 1493-1499, July 1969.
- De Angelis, Gianfrani M. L., Pavone F., Sasso, A and. Tino G. M, "Temperature Dependence of Self Broadening in Molecular Oxygen Spectrum," Il Nuovo Cimento, Vol. 18 D, No. 5, May 1996.
- Di Rosa, M. D. and Hanson R. K., "Collision Broadening and Shift of NO Absorption Lines by  $\text{H}_2\text{O}$ ,  $\text{O}_2$ , and NO at 295K," Journal of Molecular Spectroscopy, Vol. 164, 97-117, 1994.
- Galkin, V. D. "Line Shifts in the Oxygen A-Band as a Function of the Pressure," Optical Spectroscopy: Vol. 35 No. 4, 367-369, October 1973.
- Gillette, R. H., and Eyser, E. H., "The Fundamental Rotation-Vibration Band of NO," Physical Review, Vol 56, December, 1939.
- Goodman, Joseph W., Statistical Optics. New York: John Wiley and Sons, 1989.
- Hastings, N.A.J., Statistical Distributions. London: Butterworth and Co., 1975.

Herzberg, G. Molecular Spectra and Molecular Structure, Vol. III, Electronic Spectra and Electronic Structure of Polyatomic Molecules. Princeton, New Jersey: D. Van Nostrand Company, 1966.

Jansson, Peter A. Deconvolution and Applications in Spectroscopy. Orlando: Academic Press, Inc., 1984.

Kearns, D. R., "Physical and Chemical Properties of Singlet Molecular Oxygen," Chemical Reviews: Vol. 71, No. 4, December 1971

Kreyszig, E., Advanced Engineering Mathematics. New York: John Wiley and Sons, 1993.

Miller, J. H., Boese, R. W., and Giver, L. P., "Intensity Measurement and Rotational Intensity Distribution for the Oxygen A-Band," Journal of Quantitative Spectroscopy and Radiative Transfer: Vol 9, pp. 1507-1517, 1974.

Sears, F. W., Zemansky M. W. and Young, H. D., University Physics. London: Addison Wesley Publishing, 1984.

Rees, M. H. Physics and Chemistry of the Upper Atmosphere. Great Britain: Cambridge University Press, 1989.

Ritter, K. J., and Wilkerson, T. D., "High Resolution of the Oxygen A-Band," Journal of Molecular Spectroscopy: Vol 121, pp. 1-19, 1987.

Ritter, K. J., Ph. D. Dissertation, University of Maryland., 1986.

Perram, G. A., Private conversations with advisory committee member.

Pine, A. S. and Maki, A. G., "Pressure Broadening, Lineshapes and Intensity Measurements in the 2-0 Band of NO," Journal of Molecular Spectroscopy, Vol 114, pp. 132-147, 1985.

Pope, R. S. et. al., "Collision Broadening of Spectral Lines in the X to b System of O<sub>2</sub>," Conference Paper: International Conference on Fourier Transform Spectroscopy.

Pope, R. S., Private conversations.

Spencer, M. N., C. Chackerian, L. P. Giver, and L. R. Brown, "The Nitric Oxide Fundamental Band: Frequency and Shape Parameters for Rovibrational Lines," Journal of Molecular Spectroscopy, Vol. 165, 506-524, 1994.

Spencer, M. N., C. Chackerian, L. P. Giver, and L. R. Brown, "Temperature Dependence of Nitrogen Broadening of the NO Fundamental Vibrational Band," Journal of Molecular Spectroscopy, Vol. 181, 307-315, 1997.

Steinfeld, J. I., Introduction to Modern Molecular Spectroscopy. Great Britain: Cambridge University press, 1993  
Verdeyen,

Vyrodov, A. O., J. Heinze, and U. E. Meier, "Collisional Broadening of Spectral Lines in the A-X (0-0) System of NO by N<sub>2</sub>, Ar, and He at Elevated Pressures Measured by Laser Induced Fluorescence," Journal of Quantitative Spectroscopy and Radiative Transfer, Vol. 53, 277-287, 1995.

Wolf, P. J., Private conversations with advisory committee chairman.

### Vita

John Joseph Cornicelli was born on 31 December 1966 in Amityville, New York to Salvatore Joseph and Marie Vivian Cornicelli. He graduated from high school in Bethpage, New York in 1984 and attended Duquesne University, Pittsburgh, Pennsylvania, from which he earned the degree of Bachelor of Science in Physics in 1988. Upon graduation, he was employed as a laboratory chemist for Pittsburgh Criminalistics, Pittsburgh, Pennsylvania. He received his commission from the Reserve Officer Training Corps in May 1988 and entered Air Force active duty in December 1988. Through the Air Force Institute of Technology, he attended Texas A & M University, College Station, Texas, from which he earned the degree of Bachelor of Science in Meteorology in 1989. He served as Wing Weather Officer with the 380<sup>th</sup> Bombardment Wing at Plattsburgh AFB, New York, and then as Flight Commander at Shemya AFB, Alaska. He then served as Officer-in-Charge, Weather Department, with the 66<sup>th</sup> Military Intelligence Brigade in Augsburg, Germany, and then on the staff of the Director of Operations, Weather, with Air Force Special Operations Command at Hurlburt Field, Florida. He entered the School of Engineering, Air Force Institute of Technology, in June 1996 and is a member of the American Nuclear Society. He is married to the former Nathalie Murielle Veillette of Repentigny, Quebec and has one daughter, Marianne Lise.

Permanent Address: 5 Laurel Place  
Bethpage, New York 11714

21 Rue Champlain  
Repentigny, Quebec J6A-5L5

REPORT DOCUMENTATION PAGE			Form Approved OMB No. 0704-0188	
Public reporting burden for this collection of information is estimated to average 1 hour per response, including the time for reviewing instructions, searching existing data sources, gathering and maintaining the data needed, and completing and reviewing the collection of information. Send comments regarding this burden estimate or any other aspect of this collection of information, including suggestions for reducing this burden, to Washington Headquarters Services, Directorate for Information Operations and Reports, 1215 Jefferson Davis Highway, Suite 1204, Arlington, VA 22202-4302, and to the Office of Management and Budget, Paperwork Reduction Project (0704-0188), Washington, DC 20503.				
1. AGENCY USE ONLY (Leave blank)		2. REPORT DATE		3. REPORT TYPE AND DATES COVERED Maters Thesis May 96-Dec 97
4. TITLE AND SUBTITLE Collisional Broadening of Spectral Lines in the X to b System of O2 and the First Vibrational Band of NO by the Noble Gases			5. FUNDING NUMBERS	
6. AUTHOR(S) John J. Cornicelli, Captain, USAF				
7. PERFORMING ORGANIZATION NAME(S) AND ADDRESS(ES)			8. PERFORMING ORGANIZATION REPORT NUMBER  AFIT/ENP/GAP/97D-01	
9. SPONSORING/MONITORING AGENCY NAME(S) AND ADDRESS(ES) Air Force Research Laboratory AFRL/DELC Kirtland AFB, NM Attn: Matthew Rotondaro DSN: 246-0718			10. SPONSORING/MONITORING AGENCY REPORT NUMBER	
11. SUPPLEMENTARY NOTES Approved for Public Release, Distribution Unlimited				
12a. DISTRIBUTION AVAILABILITY STATEMENT			12b. DISTRIBUTION CODE	
13. ABSTRACT (Maximum 200 words) Collisional broadening of the rotational spectral lines of the X to b system of O2 and the first vibrational band of NO by the noble gases is examined by Fourier transform spectroscopy. Peaks of the individual rotational lines are modeled with a Voigt function, from which Lorentzian half widths are extracted. Lorentzian widths are plotted vs. pressure of foreign gas, from which the pressure broadening coefficients and pressure broadening cross sections are calculated. The pressure broadening coefficients are compared to theoretical values determined by past research for O2. NO coefficients are compared to similar research using N2 as collision partner. O2 broadening coefficients/cross sections were found to increase with decreasing rotational quantum number. Also, a linear dependence is found between cross section and both polarizability of the collision partner and reduced mass of the collision pair				
14. SUBJECT TERMS Collisional broadening, line broadening, rotational spectrum, vibrational transition, electronic transition, Fourier transform spectroscopy, Voigt function, pressure broadening coefficients			15. NUMBER OF PAGES	
			16. PRICE CODE	
17. SECURITY CLASSIFICATION OF REPORT  Unclassified	18. SECURITY CLASSIFICATION OF THIS PAGE  Unclassified	19. SECURITY CLASSIFICATION OF ABSTRACT  Unclassified	20. LIMITATION OF ABSTRACT  UL	